2010

Induction of p53 Dependent Cellular Senescence Through HdmX Inhibition or YPEL3 Expression

Kelly Lynn Robbins Miller
Wright State University

INDUCTION OF P53 DEPENDENT CELLULAR SENESCENCE

THROUGH HDMX INHIBITION OR YPEL3 EXPRESSION

A dissertation submitted in partial fulfillment
of the requirements for the degree of
Doctor of Philosophy

By

KELLY LYNN ROBBINS MILLER
B.A., Denison University, 2002
M.S., Wright State University, 2006

WRIGHT STATE UNIVERSITY

SCHOOL OF GRADUATE STUDIES

June 9, 2010

I HEREBY RECOMMEND THAT THE DISSERTATION PREPARED UNDER MY SUPERVISION BY Kelly Lynn Robbins Miller ENTITLED Induction of p53 Dependent Cellular Senescence Through HdmX Inhibition or YPEL3 Expression BE ACCEPTED IN PARTIAL FULFILLMENT OF THE REQUIREMENTS FOR THE DEGREE OF Doctor of Philosophy.

Steven J. Berberich, Ph.D.
Dissertation Director

Gerald M. Alter, Ph.D.
Ph.D. Program Director

Jack A. Bantle, Ph.D.
Vice President for Research and
Graduate Studies and Interim Dean
of Graduate Studies

Committee on
Final Examination

Steven J. Berberich, Ph.D.

Paula Bubulya, Ph.D.

Madhavi Kadakia, Ph.D.

Michael Leffak, Ph.D.

Robert Putnam, Ph.D.

Abstract

Miller, Kelly Lynn Robbins. Ph.D., Biomedical Sciences Ph.D. Program, Wright State University, 2010. Induction of p53 Dependent Cellular Senescence through HdmX Inhibition or YPEL3 Expression.

Mutations in p53 that compromise its function have been reported in approximately half of all human cancers (Vousden *et al*., 2002). The other half of human tumors that retain wild-type p53 have a dysfunctional p53 pathway through other mechanisms (Wade *et al*., 2009). Activation of p53 leads to cell cycle arrest, DNA repair, apoptosis and senescence, however, the pathway leading to cellular senescence is the focus of this study. Cellular senescence is a process leading to irreversible arrest of cell division. Under normal physiologic conditions, the activity of p53 is kept in check by its negative regulators, Mdm2 and MdmX. While MdmX overexpression has been linked to human tumor formation, the mechanism has yet to be elucidated. The first part of this thesis describes the ability of HdmX to block oncogenic Ras mediated senescence in human diploid fibroblasts (HDFs) through interactions with Hdm2 and p53, elucidating a potential mechanism for HdmX's contribution to tumor formation. Furthermore, senescence induction was demonstrated when HdmX was reduced in prostate adenocarcinoma cells (mutant Ras, wild-type p53, high HdmX), suggesting that targeting HdmX in tumor cells with this genotype may be a useful anti-cancer therapeutic approach.

In part two of this thesis, a novel-p53 target, YPEL3, was described as a senescence inducer in non-transformed and human tumor cell lines. YPEL3, acting downstream of p53, was shown to be required for oncogenic Ras mediated senescence

but functions as a senescence inducer independent of p16 or p21 expression in HDFs, suggesting its critical nature to senescence signaling. In accordance with its potential activity as a tumor suppressor protein, YPEL3 expression was found to be differentially regulated in breast tumor versus normal tissue. In the third part of this thesis, I discovered that YPEL3 is down-regulated by ERα signaling in a p53 independent manner. Estrogen depletion of MCF7 cells led to activation of YPEL3 and induction of cellular senescence of this breast carcinoma cell line, suggesting that YPEL3 may be a valid therapeutic target for treating ER+ breast tumors. This study describes novel mechanisms that are involved in the activation of p53 and subsequent downstream targets leading to cellular senescence.

Table of Contents

List of Figures

List of Tables

Acknowledgements

I would like to thank advisor Dr. Steven J. Berberich for allowing me to work in his lab and for all the mentoring, support and scientific conversation throughout my dissertation work. I would also like to thank my committee members, Dr. Paula Bubulya, Dr. Michael Leffak, Dr. Madhavi Kadakia and Dr. Robert Putnam for their time and thoughtful suggestions in all of our meetings together. In addition, I would like to thank the BMS Program, Dr. Gerald Alter, Diane Ponder and Karen Luchin for their assistance throughout my dissertation work, especially for their extra attention and time during my transitions from WSU Boonshoft School of Medicine to the BMS Program and back again. I very much appreciate their genuine concern. I would like to thank WSU Boonshoft School of Medicine for the opportunity to train as a member of the MD/PhD Program and a special thank you to Dr. Russell for being a constant source of encouragement during my academic endeavors.

I would like to specially thank my family, Mom, Dad, Chris, Kim, Rob and the rest of the gang for their unconditional love and support during my entire academic training career. I would also like to thank my nephew Blake for being a constant source of energy and inspiration. I am blessed to have them in my life and I would not be on this journey without them!

I. Introduction and Purpose

Cancer is the second leading cause of all deaths in the United States, accounting for 23% of those occurring in 2006 (Jemal *et al*., 2009). Although second to heart disease in overall deaths per year, cancer accounts for the highest number of deaths in persons younger than 85 years of age. A total of 1,479,350 new cancer cases were projected to occur in the United States in 2009 (Jemal *et al*., 2009). The good news is that through advances in prevention, early detection and treatment, the overall cancer death rate is on the decline. However, there are many types of cancer, including but not limited to ovarian, lung or pancreatic cancers, that still have no tools for early detection and few, if any, treatment options which leaves patients and their families with little hope. In order to keep the death rate on the decline and obtain treatments options for all forms of cancer, researchers must continue to provide information that aids in effective early detection and treatment development.

Common to all tumor formation is inactivation of the p53 pathway. Due in large part to this finding, the tumor suppressor protein, p53, has become one of the most widely studied genes in cancer research today. Determining the precise mechanisms involved in p53 pathway functioning may elucidate promising early detection and anti-cancer treatment targets. The goal of this study is to highlight novel discoveries in p53 pathway regulation and function with the intent of providing insight into potential anti-cancer drug

targets. To this end, it is first necessary to review pertinent findings related to p53 structure and function.

p53 Structure and Function

Encoded by the TP53 gene residing on the short arm of chromosome 17, the tumor suppressor protein p53 was initially discovered by two labs in 1979, Lane and Crawford along with Linzer and Levine, whose results are published in Nature and Cell, respectively (Lane *et al*., 1979; Linzer *et al*., 1979). Discovered for its ability to bind Large T antigen from Simian Virus 40, p53 was initially described as an oncogene (Crawford *et al*., 1981). It was not until years later that p53 was correctly defined as a tumor suppressor protein (Baker *et al*., 1989; Finlay *et al*., 1989). p53 has since been famously coined the "guardian of the genome" for its role in preventing genome mutation and conserving stability.

This 393 amino acid protein can be divided into five functional domains: a transactivation domain, proline rich domain, DNA binding domain, oligomerization domain and a regulatory domain (reviewed by Balint *et al.*, 2001; Figure 1). The transactivation domain (1-63) binds regulatory proteins like Mdm2, which is a negative regulator of p53 (Momand *et al*., 2000) and p300/CBP, which functions as a histone acetyltransferase acting to increase the expression of p53 target genes (Grossman, 2001). The proline rich domain (64-92) is considered a regulatory region and has been indicated to have a role in signal transduction through its SH3 domain binding activity (Walker *et al*., 1996).

Figure 1: Domain Structure of p53 Protein. Schematic representation of the five functional domains of p53. The transactivation domain contains amino acids 1-63, proline rich domain 64-92, sequence specific DNA binding domain 94-292, oligomerization domain 326-355 and regulatory domain 363-393. NLS = nuclear localization sequence, NES = nuclear export sequence (Balint *et al.*, 2001).

The majority of tumor-derived p53 mutations occur in the sequence specific DNA binding domain or central region of the protein (94-292), which is the region that directly contacts DNA. The oligomerization domain (326-355) is responsible for the tetramerization of p53, which is the active form of this transcription factor. Assuming that a mutation that occurs in the central domain of p53 renders the protein non-functional but it retains its ability to oligomerize, then the presence of a single mutant within the p53 tetramer might disturb the overall function of p53. Essentially, mutant forms of p53 can function as dominant negatives or gain-of-function proteins in this manner. The remaining carboxy-terminus of the protein (363-393) contains a negative auto-regulatory domain with acetylation and phosphorylation sites that help to regulate the DNA binding activity of p53 (Prives *et al*., 2001).

p53 transactivation is increased following genotoxic (DNA-damaging) stress and activates target genes involved in cell cycle arrest, apoptosis, DNA repair and senescence (Ashcroft *et al*., 1999). Additionally, knock-out studies in mice demonstrated that loss of p53 led to a shortened life span (6 months) where most mice died from lymphomas and sarcomas (Donehower *et al*., 1992). Mutations in p53 that compromise its function have also been reported in approximately half of all human cancers (Vousden *et al*., 2002). The other half of human tumors that retain wild-type p53 have a dysfunctional p53 pathway through other mechanisms (Wade *et al*., 2009). Taken together these results support that p53 functions as a tumor suppressor protein limiting or blocking the development of cancer. It is the necessity for a tumor to inactivate the p53 pathway that makes understanding how p53 is activated and what genes it controls essential to advancement of cancer treatment.

Cellular Senescence

Activation of p53 leads to cell cycle arrest, DNA repair, apoptosis and senescence as mentioned previously. While all end-points are important, the pathway leading to cellular senescence is the primary focus of this study. Cellular senescence is a process leading to irreversible arrest of cell division. Cells that undergo senescence cannot divide upon mitogen stimulation, but they remain metabolically and synthetically active. There are two types of senescence, accelerated and replicative. Replicative senescence was first described in 1965 by L. Hayflick when he noticed that human diploid cells have a limited in vitro lifetime (Hayflick, 1965). Replicative senescence has further been demonstrated to be a function of telomere shortening with age and demonstrated in tissues and *in vivo*. Accelerated senescence prevents the uncontrolled growth of cells that have undergone some insult, like oncogenic Ras mutation (Ferbeyre *et al*., 2002). Both of these processes require functional p53 and are considered protective mechanisms against tumor formation.

Senescent cells undergo characteristic changes in morphology that are utilized to measure senescence in the laboratory. They show an enlarged and flattened shape, have increased beta-Galactosidase activity at pH 6, and develop a distinct chromatin structure referred to as senescence associated heterochromatin foci (SAHF) (Figure 2 a and b) (Dimri *et al*., 1995; Narita *et al*., 2003). In addition, senescent cells have also been indicated to characteristically alter expression patterns of certain genes including, but not limited to, p16, p21 and PAI-1. It appears that the expression of "senescence markers" is cell type and senescence inducer specific making their utility as a measure of senescence

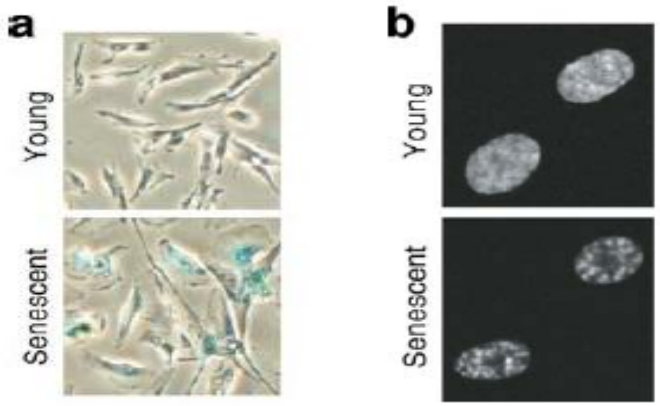

Figure 2: Senescent Phenotype. (a) and (b) proliferating (upper) and Ras infected senescent (lower) WI-38 fibroblasts stained with SA-β-gal (a) or DAPI (b). Senescent cells show increased SA-β-gal activity (blue, a) and chromatin condensation (b) (Narita *et al*., 2003).

limited. However, the aforementioned morphological changes specific to a senescent cell give us the tools necessary to study the pathways leading to senescence.

There are two tumor suppressor protein networks, p53 and the Retinoblastoma protein family (Rb/p107/p130), that control the central activating pathways leading to senescence (Ben-Porath *et al*., 2005; Figure 3). Both p53 and the Rb family have been shown to be activated in senescent cells with p53 being implicated in the induction and the Rb family in the maintenance of senescence. p53 serves to activate its transcriptional targets such as p21, while Rb is active during senescence in its hypophosphorylated form and binds the E2F protein family members to repress their transcriptional targets. Many targets of E2F proteins, upon transcription, play a role in cell-cycle progression. While the Rb family is important to senescence, the focus of this proposal will be on the p53 pathway.

There are two major pathways that act upstream to induce p53 during the induction of senescence. The DNA damage response mediated by ATM/ATR and Chk1/Chk2 causes post-translational stabilization of p53 through its phosphorylation and p19/p14/Arf (Alternative Reading Frame, $p19^{Arf}$ in mouse cells and $p14^{Arf}$ in human cells) activates p53 by sequestration of Mdm2, a negative regulator of p53 (Ben-Porath *et al*., 2005). The Arf protein, encoded at the INK4a locus with p16, is induced in situations of stress like the presence of oncogenic Ras or myc. Once p53 is activated, there are downstream targets that have been implicated in the senescence pathway, including p21, which is a cyclin dependent kinase inhibitor that inhibits the activity of cyclin-CDK2 and

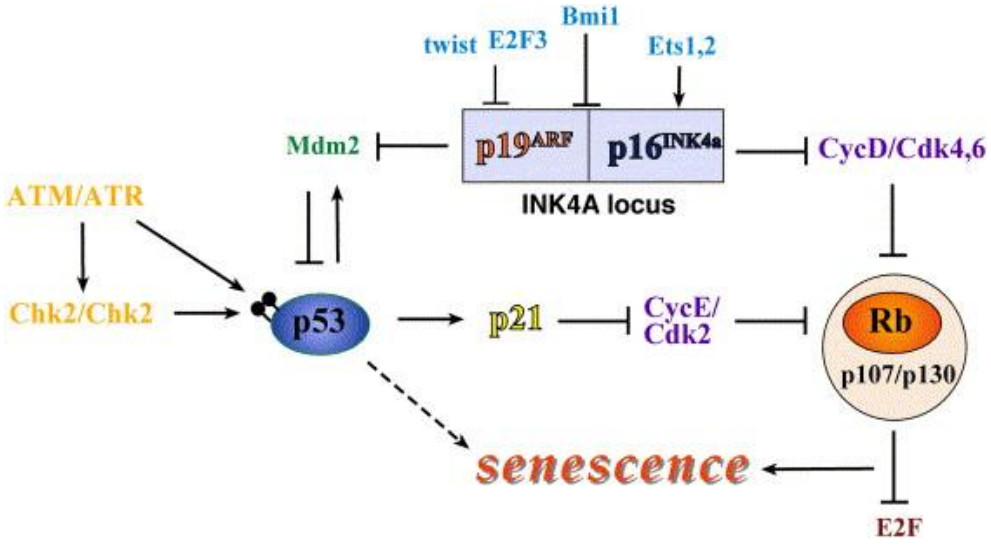

Figure 3: p53 and Rb are the Main Activators of Senescence Schematic representation of known key players of the senescence pathway (Ben-Porath *et al.*, 2005).

CDK4 complexes to regulate cell cycle progression at G1. While activation of p21 is required for senescence induction in most situations, other p53 targets that are critical to the senescence pathway is an active area of research. It is clear, however, that the induction of senescence happens through a dynamic mechanism where key regulators are turned on and off in a specific manner.

The studies of senescence are further confounded by differences in the senescence pathway that exist between human and mouse fibroblasts cell culture systems where most of the senescence pathway discoveries have been made. While it appears that p53 and the Rb family are the critical mediators of senescence induction and maintenance, other regulators of the senescence pathway are not as clearly defined. For example, the inactivation of p21 is sufficient to prevent senescence in human cells (Brown *et al.*, 1997) while p21-null MEFs undergo replicative and oncogenic Ras induced senescence normally (Pantoja *et al*., 1999). This implies that there is a missing link between the p53 and the Rb family pathways or that other proteins can compensate for p21 in the mouse system.

It is unclear in the literature whether there is a linear activation of p53 through p21 to Rb or a parallel activation of p53 and Rb during cellular senescence. It seems that both models may be correct and the function of $p16^{INK4a}$, a direct input line to Rb, may determine which model is carried out in various cell types. p16 is not normally expressed in human adult tissue, but is induced during senescence in MEFs and HDFs. Its inactivation blocks senescence in human but not mouse cells, suggesting that the relevance of the p16 arm of the senescence pathway is enhanced in human cells (Brookes

et al., 2002; Duan *et al*., 2001). Interestingly, ARF, the other protein encoded at the INK4a locus with p16 (Figure 3), is not up regulated to the same extent during senescence in humans as in mouse cells and is required for senescence in mouse but not human cells. In any case, it is clear that p53 and the Rb family function as a complex, stress-signal integration and processing unit that detects various stress stimuli and activates the appropriate proteins to carry out the necessary cellular response.

Interestingly, tumor cells have been indicated to undergo accelerated senescence by genetic manipulation or treatment with chemotherapeutic drugs, radiation, or differentiating agents (Roninson 2003). Clinical data also indicates that expression of different biological classes of senescence-associated growth-regulatory genes, like p53, in tumor cells has significant prognostic implications (Roninson 2003). Additionally, the discovery that a brief reactivation of p53 in a mouse liver carcinoma model leads to cellular senescence followed by tumor regression through clearance of these cells by the innate immune system has provided a foundation for senescence as a favorable outcome for anti-tumor drug discovery (Xue *et al*., 2007). Uncovering the specific genes and regulatory mechanisms responsible for the induction and maintenance of tumor cell senescence will aid in the design of new anti-cancer therapeutics.

Hdm2 and HdmX

Under normal physiologic conditions, when programs like senescence are not initiated, the activity of p53 is kept in check by its negative regulators, Mdm2 (Hdm2) and MdmX (Mdm4, HdmX). Mdm2 physically associates with p53 targeting it for degradation and inhibits p53-mediated transcriptional activation (Marine *et al*., 2007).

Mdm2 over expression is a known mechanism for promoting tumor formation, especially in human sarcomas (Oliner *et al*., 1992). MdmX inhibits only the transcriptional activation of p53 and is over expressed in several human tumors, the majority of which contain wild-type p53 (Table 1). For example, MdmX has been demonstrated to be over expressed in approximately 19% of breast carcinomas and targeting MdmX using RNAi technology in MCF7 breast carcinoma cells led to a G1/S cell cycle arrest accompanied by an increase in p53 and p21 (Danovi *et al*., 2004; Heminger et al., 2009). These and several other similar studies have suggested roles for MdmX in human tumor formation.

Mdm2 and MdmX are structurally related proteins that have similar p53 binding domains at the N-terminus and a RING-finger domain at the C-terminus (Figure 4). Contrary to Mdm2, MdmX is a more stable protein and is thought to be regulated primarily by post-translational modifications, making protein-protein interaction and subcellular localization studies important in determining roles for and regulation of MdmX (Tanimura *et al*., 1999; Marine *et al*., 2007). MdmX not only interacts with p53, but also heterodimerizes with Mdm2. Most transfection studies indicate that this interaction regulates Mdm2 and MdmX protein stability (Marine *et al*., 2007). It is known that Mdm2 and MdmX carry out non-redundant functions to keep p53 levels low throughout development. There are two main models for why MdmX and Mdm2 cannot compensate for each other *in vivo,* suggested by the fact that too little Mdm2 or MdmX elicits lethality whereas an excess of either can be oncogenic. The first view is that MdmX and Mdm2 contribute to the regulation of p53 independently (Danovi *et al*., 2004; Laurie *et al*., 2006). The second is that Mdm2 and MdmX form a complex that is more

Tumor Type	% of Cases	Reference
Retinoblastoma	60%	(42)
Glioblastoma	4%	(41)
Colon	19%	(13)
Lung	18%	(13)
Breast	19%	(13)
Melanoma	14%	(13)
Hepatocellular carcinoma	50%	(104)
Head and neck	50%	(105)
Sarcoma	22%	(43)
Bladder cancer	25%	(106)
All cell lines	40%	(107)

NOTE: Percentages indicate the overall frequency of changes, irrespective of mechanism.

Table 1 : Tumors with Either Increased Mdmx Copy Number or Increased Mdmx mRNA. Various human tumor tissue samples or cell lines were evaluated for MdmX expression and this table was compiled in a review by Wade and Wahl, (2009).

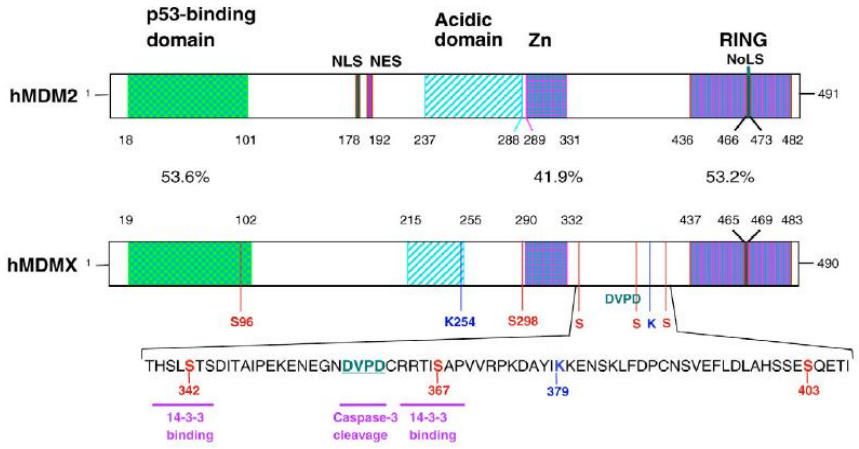

Figure 4: Comparison of Mdm2 and MdmX Structural Domains. Mdm2 and MdmX contain p53-binding, acidic, zinc (Zn) and ring finger domains (Marine *et al*., 2007). NLS = nuclear localization sequence, NES = nuclear export sequence, hMDM2 = human version of Mdm2, hMDMX = human version of MdmX, NoLS = nucleolar localization sequence, RING = ring finger domain.

effective at inhibiting p53 transactivation or enhancing p53 turnover than either alone (Wade *et al*., 2009). Evidence exists to support each view, so exactly how MdmX functions to inhibit p53 and the regulation of this interaction remains to be determined.

While probing the direct contribution of MdmX to tumor formation, Danovi and colleagues (2004) noticed that MdmX could cooperate with oncogenic Ras (H-Ras^{V12,} constitutively activated) in the neoplastic transformation of MEFs (mouse embryonic fibroblasts) and that MdmX/H-Ras^{V12} infected MEFs were no longer contact inhibited and formed tumors within three weeks when subcutaneously injected into nude mice (Figure 5). Tumors were confirmed to retain p19^{Arf}, p53, and MdmX. It is important to note that infection of H-Ras^{V12} alone into MEFs causes accelerated senescence, as previously described.

Additionally, mitogenic signaling has been shown to induce MdmX expression at the transcript level (Gilkes *et al*., 2008). This regulation of MdmX expression may prevent unwanted p53 activation during normal cellular proliferation; however, when inappropriately activated, this pathway may block the tumor suppressive functions of p53 during abnormal cellular proliferation leading to initial tumor formation. Together with the over expression of MdmX in MEFs blocking oncogene induced senescence, these activities of MdmX represent potential mechanisms for how HdmX over expression contributes to human tumor formation.

The pathways leading to senescence in murine and human cells have similarities and differences, as described previously. While it has been demonstrated that MdmX can block oncogene induced senescence in mouse cells, the question remains as to whether

Figure 5: MdmX Bypasses HRas^{V12} Induced Senescence and Cooperates with HRas^{V12} in Neoplastic Transformation. Animals were injected with MEFs expressing Ras^{V12} (not pictured, no tumor), MdmX, MdmX/Ras^{V12} or E1A/Ras^{V12} at 6-8 weeks of age and were inspected for appearance of tumors 3 weeks later (Danovi *et al*., 2004; Figure 3). Numbers represent # of mice positive for tumor formation/total number of mice examined. E1A+Ras infection was used as a positive control and MdmX infection alone as a negative control.

HdmX retains this ability in human cells and the mechanism through which this outcome is achieved.

Mdm2 (Hdm2) has been implicated in the senescence pathway through its well-established interaction with Arf (Pomerantz *et al*., 1998). In response to a variety of oncogenic stimuli, Arf expression causes a rapid increase in p53 levels through its ability to bind Mdm2 and inhibits Mdm2's action on p53. Specifically, Arf functions by sequestering Mdm2 in the nucleolus, away from p53. In many human tumors, inactivation of the INK4a locus can be demonstrated representing another mechanism for deregulation of the p53 pathway.

YPEL3

Once p53 has been activated, it acts as a transcription factor to regulate genes that are involved in mechanisms like cell cycle arrest and senescence. In order to study novel p53 regulated genes, a microarray experiment was completed where the negative regulators of p53 (Hdm2 and HdmX) were silenced in MCF7 breast carcinoma cells using siRNA technology (Heminger *et al*., 2009). MCF7 cells contain wild-type p53, therefore, knocking down Hdm2 and HdmX allowed for the non-genotoxic stress induction of p53. This led to a G1 phase cell cycle arrest along with sensitization of the arrested MCF7 cells to DNA damage (Heminger *et al.*, 2009). From analysis of the microarray data, a novel p53 target was discovered named YPEL3 (yippee-like protein 3). Further validation studies, including chromatin immunoprecipitation (ChIP), confirmed that YPEL3 is a direct p53 target gene (Kelley *et al*., 2010).

The Yippee gene was first identified in *Drosophila* through a yeast interaction trap screen for proteins that interact with Hemolin, a member of the immunoglobulin superfamily (Roxstrom-Lindquist *et al*., 2001). Hemolin is known to be up regulated during development and also binds bacteria and lipopolysaccharide during bacterial infection. The biological role for this interaction has not been elucidated. Later, five human Yippee-like genes, including YPEL3, were described in human and mouse tissues (Hosono *et al*., 2004; Figure 6) YPEL3 was found to be ubiquitously expressed in human fetal tissues (Figure 6) and to have high sequence conservation between a wide range of species (Roxstrom-Lindquist *et al*., 2001). Interestingly, human and mouse YPEL3 have 100% sequence identity (Hosono *et al*., 2004).

Although no further experiments have been reported that describe the interaction of *Drosophila* YPEL3 with Hemolin, S.J Baker (2003) described the biology of a small unstable apoptotic protein (SUAP) which was subsequently determined to be YPEL3. Using a murine myeloid precursor cell line, apoptosis was induced by IL-3 deprivation and granulocyte colony stimulating factor treatment followed by RNA analysis. YPEL3 was induced in the apoptotic myeloid precursor cells compared to normal, growing cells with IL-3 present (Baker, 2003). Additionally, YPEL3 was also found to be rapidly degraded by the proteasome which led to the descriptive name of small unstable apoptotic protein. It is undetermined whether YPEL3 acts as a growth suppressor in human cells, and if so, through what mechanism.

As a direct p53 target and potential growth suppressor, our lab investigated whether YPEL3 expression was decreased in various human tumor tissues versus normal

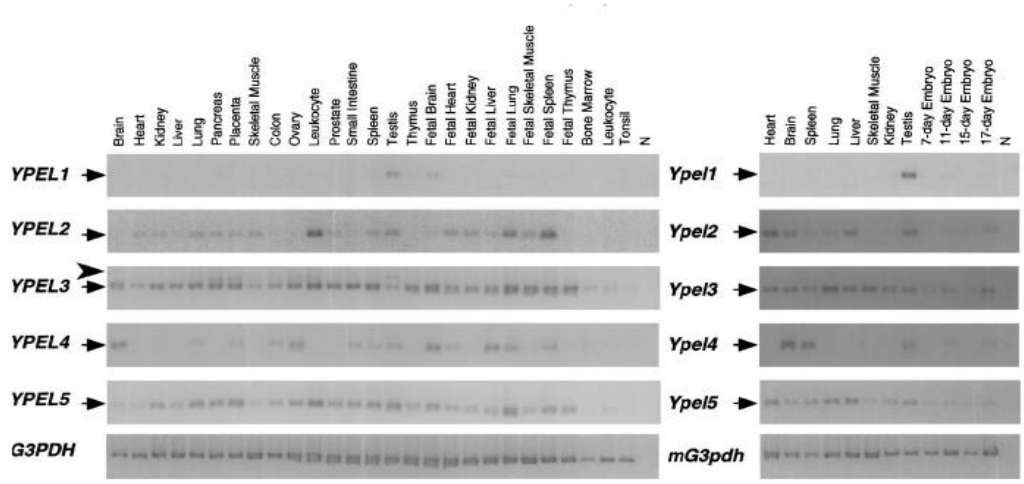

Figure 6: Expression Profiles of Human and Mouse YPEL Genes in Various Tissues. RT-PCR was carried out using cDNA's derived from various organs and tissues from mouse (left panel) and human (right panel). Expression profiles for mouse and human are similar. The arrow head of YPEL3 indicates an extra band seen in pancreas, placenta and testis considered to be a product of alternative splicing (Hosono *et al*., 2004; Figure 3).

control. In a screen of eight different tumor types, it was noted that YPEL3 expression correlated with estrogen receptor status in breast tumor samples (personal communication, Rebecca Tuttle MD). YPEL3 was also uncovered during a microarray study in a list of genes that do not contain an estrogen response element that are down regulated by estrogen in an ER+ breast tumor cell line (Cicatiello *et al*., 2010). These findings led to the investigation of YPEL3 regulation by the estrogen receptor.

Estrogen Receptor

As mentioned previously, inactivation of the p53 pathway is one of the most frequent events in cancer formation. Breast cancers are unique in that mutations in p53 itself occur in only about 20% of breast tumors (Liu *et al*., 2008). For most breast cancers, wild-type p53 is inactivated by other mechanisms, which are largely unknown. It has been reported recently that ERα directly binds to p53 and represses its function providing a mechanism for p53 deregulation in ER+ breast cancers (Liu *et al*., 2006). Additionally, ER- breast tumors have a higher incidence of p53 mutations compared to ER+ tumors (Troester *et al*., 2006), making the reactivation of wild-type p53 an attractive anti-cancer therapeutic goal for ER+ tumors.

Estrogens function through ER's to regulate many physiological processes in a p53-independent manner including but not limited to normal cell growth, development and tissue specific gene regulation in the reproductive organs, bones, brain and other tissues (Matthews *et al*., 2003). The biological activities of estrogen are mediated by two estrogen receptors, namely ERα and ERβ, as reviewed by Matthews *et al*. (2003). As members of the nuclear receptor superfamily, ERα and ERβ serve as ligand-regulated

transcription factors. Ligand binding to either estrogen receptor causes conformational changes in the receptor leading to dimerization, protein-DNA interaction and recruitment of other co-regulators and transcription factors. It is also known that ER's regulate gene expression through their own response element and interactions with other transcription factors, as mentioned previously with p53 (Matthews *et al.*, 2003). Some mechanisms of estrogen signaling are independent of DNA binding, referred to as non-genomic regulation. While the focus for this study is on ERα, it should be mentioned that ERβ is known to antagonize ERα mediated transcriptional activity and is gaining attention as an important ER family member.

Recent advances in breast cancer treatment have been focused on hormone receptor status determination of the tumor. The current standard of treatment for breast cancer patients includes assessment of human epidermal growth factor receptor-2 (Her-2), estrogen receptor (ER), specifically the α subtype, and progesterone receptor (PR) status of the tumor by immunohistochemistry. The hormone receptor status has implications for which therapeutic options will be utilized. For example, Tamoxifen is used in women to treat ER+ breast tumors for its specific ability to inhibit the binding of estrogen to the estrogen receptor (reviewed by Osborne, 1998). This drug is not useful for the treatment of ER- tumors.

Some drugs in current use have rather large side effect profiles making their use difficult at times. For example, the adverse events reported for Tamoxifen include menopausal symptoms (hot flashes, vaginal discharge), ocular toxicity, thromboembolic events and most seriously an increase in endometrial cancer at a relative risk of 2.2 as

compared with population-based rates (Osborne, 1998). Although these adverse effects were only reported in a small percentage of those treated with Tamoxifen, they are still a risk that some patients will not take. Additionally, almost half of the women with ER+ breast tumors treated with Tamoxifen demonstrate resistance (Ring *et al*., 2004). If new anti-cancer drugs are developed that have more specific, down-stream targets then the side effect profiles will be reduced, which is an ongoing research goal. For example, targeting the downstream targets of the ER that are critical for growth suppression in breast tumors would be more specific and potentially reduce the adverse effects noticed when all ER signaling is blocked.

Purpose for Study

The goal of this study is to uncover precise, novel mechanisms that are involved in the activation of the tumor suppressor protein p53 and subsequent downstream targets leading to cellular senescence. While it has been demonstrated that p53 activation is critical to senescence induction, the downstream p53 targets that are essential for this process have not been fully elucidated. Therefore, this dissertation is designed to investigate p53 activation and critical downstream targets that lead to senescence induction in human cells. First, the activation of p53 leading to senescence will be detailed by targeting a known p53 negative regulator, HdmX. Second, the novel p53 target YPEL3 will be described for its role as an inducer of growth suppression through the induction of cellular senescence and I will begin to describe YPEL3's location within the current senescence pathway model. Third, the regulation of YPEL3 by the estrogen receptor will be described for its impact on senescence in a breast carcinoma cell line.

Together the results provided by these studies are intended to aid in the design of effective anti-cancer therapeutics with the goal of tumor cell senescence leading to tumor regression.

II. Materials and Methods

Cell lines, Antibodies and Reagents

Human tumor cell lines, MCF7 (breast carcinoma), U2OS (osteosarcoma), H1299 (non-small cell lung carcinoma), LNCaP (prostate adenocarcinoma) were grown in Dulbecco's Modified Eagle's Medium (DMEM; Cellgro) supplemented with 10% fetal bovine serum (FBS) or newborn calf serum (NCS) and 10 μg/mL gentamycin unless otherwise specified. The human diploid fibroblast cell line IMR90 (ATCC) and mouse embryonic fibroblasts (MEF) were also grown in DMEM supplemented with 10% FBS and 10 μg/mL gentamycin unless otherwise specified.

HdmX (Bethyl Laboratories, Inc.), p21 (C-19; Santa Cruz Biotechnology, Inc.), p16 (C20; Delta Biolabs), Hdm2 (H221; Santa Cruz Biotechnology, Inc.), p53 (FL393; Santa Cruz Biotechnology, Inc.), Estrogen Receptor (Ab-16; Thermo Scientific) and YPEL3 (Proteintech) polyclonal antibodies were used as indicated. Hdm2 (SMP14;), p53 (Ab-4, Ab-6; Calbiochem), V5 (Invitrogen), GFP (Invitrogen), Estrogen Receptor (Ab-10; NeoMarkers) and β-actin (Sigma) monoclonal antibodies were used as indicated. Horseradish peroxidase (HRP)-conjugated anti-mouse or anti-rabbit secondary antibodies (Promega) were utilized along with Super Signal substrate (Pierce) for chemi-luminescence detection of proteins.

β-estradiol and Tamoxifen was purchased from MP Biomedicals, LLC. β-estradiol was dissolved in ethanol and added to serum free DMEM for storage at -20°C. Tamoxifen was dissolved in ethanol and stored at -20°C.

Lentivirus Generation, Titering and Infection

The ViraPower™ Lentiviral Expression System available from Invitrogen was utilized to generate replication incompetent, HIV-1 based lentivirus used to deliver and express genes of interest in either dividing or non-dividing mammalian cells. Lentivirus was generated following instructions supplied with the kit with only minor modifications. Briefly, approximately 8 million 293FT cells were reverse-transfected using Lipofectamine 2000 (Invitrogen) overnight with ViraPower™ packaging mix along with the gene of interest cloned into either the pLenti4, pLenti6 or pLKO.1 plasmid. All pLenti plasmids used are listed in Table 2. This transfection mixture was removed the following morning and 5.5 mL of complete media (DMEM containing 10% NCS and 10 µg/mL gentamycin) added. Lentivirus containing supernatant was harvested approximately 48 hours post-transfection. Remaining cells and debris were removed from the lentiviral containing supernatant by centrifugation at 1500 rpm for 3-5 minutes. Lentiviral supernatant was stored in 1 mL aliquots at -80°C until further use.

Concentration of infectious lentiviral particles in the supernatant was determined by transducing H1299 cells with 10 fold dilutions of lentivirus, selecting for stably transduced cells using the appropriate selecting agent (pLenti4-Zeocin, pLenti6-Blasticidin, pLKO.1-Puromycin) for approximately 7 days and then staining the cells with 1% crystal violet in 70% methanol. The number of antibiotic resistant colonies was

Lentiviral Plasmid	Antibiotic Resistance	Company or Person Responsible for Cloning
pLenti6-GFP	Blasticidin	Steven Berberich
pLenti6-Hdm2	Blasticidin	Steven Berberich
pLenti6-HdmX	Blasticidin	Steven Berberich
pLenti6-HdmXC437G	Blasticidin	Kelly Miller
pLenti6-HdmXG57A	Blasticidin	Kelly Miller
pLenti6-H-Ras^{G12V}	Blasticidin	Steven Berberich
pLenti6-RescueHdmX	Blasticidin	Nick Maiorano
pLenti4-shHdmX	Zeocin	Kate Heminger, BMS Thesis
pLenti4-shLacZ	Zeocin	Kate Heminger, BMS Thesis
pLenti4-YPEL3	Zeocin	Kevin Kelley, BMS Thesis
pLKO.1-shcon	Puromycin	Addgene; Plasmid 1864
pLKO.1-shERα	Puromycin	Sigma; NM_000125
pLKO.1-shp16	Puromycin	Sigma; NM_058197
pLKO.1-shp21	Puromycin	Sigma; NM_000389
pLKO.1-shp53	Puromycin	Addgene; Plasmid 19119
pLKO.1-shYPEL3(A)	Puromycin	Open Biosystems; RMM3981-99225223
pLKO.1-shYPEL3(B)	Puromycin	Sigma; NM_031477

Table 2: Lentiviral Plasmid Name, Antibiotic Resistance and Company or Person Responsible for Cloning.

counted for each dilution and a viral titer calculated indicating the number of infectious viral particles per mL (IVP/mL). Titers generally ranged from 10^5-10^6 IVP/mL. For lentivirus that we were unable to use in this colony formation type assay for biological reasons (YPEL3 for example) the QuickTiter™ Lentivirus Quantitation Kit (Cell Biolabs, Inc.) was utilized to determine lentivirus physical titer. The physical titer was correlated to a functional titer number through a conversion factor determined by comparison of GFP physical titer and infectious titer numbers.

To infect tumor and non-transformed adherent cells, lentiviral supernatant was thawed and diluted in complete media plus 6 µg/mL Polybrene. Lentivirus was used at a multiplicity of infection (MOI) of 5 or a volume equal to or less than half of the total volume of the infection cocktail. Cells were incubated with infection cocktail overnight (at least 18 hours) and then removed and replaced with complete media. The appropriate antibiotic selection was added 24 hours later and continued for 6-14 days until the control plate of uninfected cells were dead. Kill curves were previously determined by Kate Heminger (BMS Thesis; Table 3) to determine the lowest effective dose for selection of some of the tumor cell lines used. Additional kill curves were completed for other cell lines not previously studied (Table 3).

Quantitative RT-PCR

Cells were rinsed once in Dulbecco's Phosphate Buffered Saline (DPBS) and lysed on the culture dish with TRK Lysis Buffer supplemented with β-mercaptoethanol (20 µL of β-mercaptoethanol per 1 mL of TRK Lysis Buffer) and total RNA was isolated per the manufacturer's instructions (e.Z.N.A. Total RNA kit; Omega Bio-Tek). The

Cell Line	Zeocin (µg/mL)	Blasticidin (µg/mL)	Puromycin (µg/mL)
MCF7*	750*	6*	1
U2OS*	500*	6*	1
IMR90	100	5	0.5-1
LNCaP	250	5	n/a

Table 3: Antibiotic Concentrations Used for Selection. *Generated by Kate Heminger, BMS Thesis.

RNA was quantified using the NanoDrop DN-1000 spectrophotometer. The purity of the RNA was estimated by the ratio of the absorbance at 260 nm and 280 nm (A_{260}/A_{280}), with pure RNA having a ratio of 1.8-2.1. One µg of each RNA sample was reverse transcribed with random hexamers to create cDNA using the TaqMan Reverse Transcription Kit (Applied Biosystems) per the manufacturer's instructions. The reverse transcription (RT) reaction was performed in an Applied Biosystems Gene Amp PCR System 2700 programmed to sequentially cycle as follows: initial 10 minute incubation at 25°C, 30 minute RT step at 48°C, 5 minute inactivation step at 95°C, and an infinite hold at 4°C. After RT was complete the cDNA was diluted in 120 µL of sterile DNAse-free water.

Quantitative real-time PCR was performed in a 96-well microtiter plate format on an ABI 7900HT sequence detection system. A 20 µL reaction was prepared by mixing 9 µL of cDNA/water mix, 10 µL of 2X TaqMan Universal PCR master mix and 1 µL of Assay-on-Demand Gene Expression product (Applied Biosystems; contains primers and a fluorescent Taqman probe) designed for the gene of interest, to each well on the 96 well plate. The PCR conditions include a 2 minute hold at 50°C, a 10 minute hold at 95°C followed by 40 cycles of a 15 second 95°C denaturing step and a 1 minute 60°C anneal and elongation step. Each cDNA sample was separately analyzed in triplicate for target gene expression normalized to the internal control of GAPDH. The fold change (RQ) relative to the control sample was calculated which is normalized to GAPDH control RNA levels using SDS 2.0 software (ABI). The mean RQ values are plotted and the error bars represent 95% confidence intervals.

Western Blot Analysis

Cells were harvested by removing media, washing once with cold DPBS and scraping the cells into 1 mL of DPBS. This cell mixture was transferred to a 1.7 mL Eppendorf tube, spun in a refrigerated microfuge at 10,000 rpm (8,161 x g) for 2 minutes to pellet cells. Excess DPBS was removed without disturbing the pellet then tubes were stored at -80°C until further use. Total cell lysates were prepared by thawing the cell pellet on ice in 25-100 µL RIPA buffer (25 mM Tris-HCl pH7.6, 150 mM NaCl, 0.1% SDS, 1% NP-40, 1% sodium deoxycholate) supplemented with protease inhibitor cocktail (PIC) and pipetting up and down to lyse the cells. The cell suspension was incubated on ice for 15 minutes followed by centrifugation in a refrigerated microfuge at 14,000 rpm (15,996 x g) for 10 minutes and then the soluble protein fraction was transferred to a new 1.7 mL Eppendorf tube. Protein concentration was determined using the Bradford method by mixing 1 µL of the whole cell extract with 799 µL of sterile distilled water (SDW) and 200 µL of Bradford reagent (Bio-Rad Inc.). A standard curve was generated using bovine serum albumin (BSA) protein ranging from 2-14 µg in 800 µL SDW and 200 µL Bradford reagent. Mixtures were transferred to a cuvette and the absorbance at 595 nm measured on a Spectronic Genesys 5 spectrophotometer. The standard curve generated was used to determine the protein concentration of each sample from its absorbance value. Then, 100 µg of protein in 1X SDS loading dye (diluted from 6X SDS loading dye; 1X = 60 mM Tris, pH7.6, 2% SDS, 10% glycerol, 5% β-mercaptoethanol and 1% bromophenol blue) was boiled at 100°C for 5 minutes prior to loading on a 12% sodium dodecyl sulfate polyacrylamide gel using a Mini-Protean II Bio-Rad Electrophoresis System. The gel was run at a constant 100 volts for approximately 1

hour in 1X SDS running buffer (25 mM Tris pH 8.3, 250 mM glycine, 0.1% SDS). The proteins were transferred onto a polyvinylidene difluoride (PVDF) membrane (Millipore) (pre-soaked in 100% methanol for 10 seconds followed by SDW for 2 minutes) in a transfer buffer (25 mM Tris, 192 mM glycine, 20% methanol, pH 8.3) using a Bio-Rad transfer system for 40 minutes at a constant 50 mAmps. The membrane was then incubated in 20 mL blocking buffer (1X Tris Buffered Saline (TBS), 5% non-fat dry milk (NFDM), 0.1% Tween-20) on a shaker at room temperature for one hour. The blot was then incubated in the appropriate primary antibody at 1:500-1:5,000 dilution in 1:10 blocking buffer on a shaker overnight at 4°C. The next morning the blot was washed three times for 10 minutes each in 1:10 blocking buffer at room temperature on a shaker, then the blot was shaken in the appropriate secondary antibody (goat anti-mouse or goat anti-rabbit, both from Promega) at 1:5,000 dilution in 1:10 blocking buffer for 45 minutes at room temperature. The blot was again washed three times for 10 minutes each in 1:10 blocking buffer and then exposed to Thermo Scientific SuperSignal West Pico or Femto Detect chemiluminescent reagent (Pierce) for 3-4 minutes and protein visualized on a FUJI FILM LAS 4000 image reader. If necessary, the antibodies were removed from the membrane by shaking the blot in Western strip buffer (25 mM glycine, 1% SDS, pH 2.0) for 20 minutes at room temperature. The membrane was then blocked and immunoblotted using another antibody following the same procedure outlined above.

Colony Formation Assay

MCF7 and U2OS cells containing Tetracycline Repressor (100,000 cells/well) were transduced with Lenti-YPEL3 or left untreated followed by incubation in complete

medium for 24 hours. Following transductions, cells were selected with 750 μg/mL and 500 μg/mL Zeocin, respectively. Tetracycline was used at a concentration of 1 μg/mL for induction of YPEL3-V5. After 15 days, the cells were stained with 1% crystal violet in 70% methanol for five minutes. Plates were washed with DPBS for five minutes, colonies counted and then photographed. The total number of colonies remaining in each well was scored. The experiment was completed in duplicate for U2OS cells and triplicate for MCF7 cells. Average number of colonies remaining with non-Tetracycline treated wells set to 100% was reported +/- standard error of the mean.

Cell Proliferation Assay

At day zero, 50,000 cells (MCF7, MCF7shLacZ, MCF7shYPEL3(A), MCF7shYPEL3(B), U2OS, U2OSshLacZ, U2OSshYPEL3(A) or U2OSshYPEL3(B)) were plated per well in a 6 well dish. Cells were re-fed each day with complete media. On days two, four and six, 3 wells of a 6 well dish were trypsinized for 5 minutes using 1 mL of Trypsin-EDTA 1X (Cellgro). Trypsin was neutralized using 2 mL of complete media and cell suspension was centrifuged at approximately 1700 rpm (250 x g) for 3 minutes to pellet the cells. Excess Trypsin/complete media was removed without disturbing the pellet and cells were resuspended in 1 mL of complete media. This 1 mL cell suspension was analyzed using a Beckman Coulter Vi-Cell™ cell viability analyzer. The total cell count and percent viability of each sample was provided by the Vi-Cell. These numbers were used to graph the average viable cell number per cell type on days 2, 4 and 6.

Nuclear Cytoplasmic Protein Extraction

IMR90 cells were transduced and selected as indicated. After approximately 8 days the cells were rinsed with 2 mL DPBS, scraped in 1 mL DPBS, transferred to a 1.7 mL Eppendorf tube and pelleted in a refrigerated microfuge at 10,000 rpm (8,161 x g) for 2 minutes. Using reagents supplied in the Nuclear/Cytoplasmic Fractionation Kit (Pierce), the pellet was resuspended in 200 µL of cold CER I reagent by vigorously vortexing. The cells were then placed on ice for 10 minutes. 15 µL of CER II reagent was added to each sample and the cytoplasmic extract fraction was prepared. The remaining pellet was resuspended in 90 µL of cold NER reagent and the nuclear fraction was isolated per the instructions supplied with the kit. Protein concentration was determined by Bradford method and SDS polyacrylamide gel and Western blot were completed as previously described.

TNT Reaction

Bluescript plasmids containing HdmX, HdmXG57A, HdmXC437G, Hdm2 or p53 were used to generate protein using a TNT Coupled Reticulocyte Lysate System from Promega. Briefly, biotinlyated lysine containing protein was generated mixing TNT Rabbit Reticulocyte Lysate, TNT Reaction Buffer, TNT RNA Polymerase (T7), Amino Acid mixtures (minus Leucine and minus Methionine), RNasin Ribonuclease Inhibitor, DNA template, Transcend^{TM} tRNA and nuclease free water. These reactions were incubated at 30°C for 90 minutes. Resulting protein was utilized in a co-immunoprecipitation assay as described.

Site-Directed Mutagenesis

The QuikChange XL Site Directed Mutagenesis Kit (Stratagene) was used to generate pLentiHdmXG57A and pLentiHdmXC437G point mutations using the wild-type pLentiHdmX plasmid. Primers used with this kit were designed using Stratagene's Primer Design program available through their website. The sequences for the HdmXG57A primers generated are (sense) 5'-gaggtcatgcactatttagctcagtacataatggtgaag-3' and (antisense) 5'-cttcaccattatgtactgagctaaatagtgcatgacctc-3'. The sequences for the HdmXC437G primers are (sense) 5'-ccagaatctcttgaagccaggtagcttatgtgagaaaag-3' and (antisense) 5'-cttttctcacataagctacctggcttcaagagattctgg-3'. To confirm mutagenesis plasmids were sequenced by Retrogen.

Co-immunoprecipitation

Protein generated from TNT reactions (15 µL of each protein) were incubated per reaction for 1 hour at room temperature. In a separate tube, protein G agarose beads (50 µL per reaction) were rinsed with 500 µL DPBS, pelleted at 10,000 rpm (8,161 x g) for 30 seconds and resuspended in DPBS supplemented with protease inhibitor cocktail (PIC; Sigma) at 100 µL per reaction. Then, 10 µL of anti-p53 (FL393) or anti-Hdm2 (SMP14) antibody was added to 100 µL beads/DPBS mixture per reaction and rotated for 1 hour at room temperature. To the protein mixtures, 100 µL of DPBS/PIC was then added. The bead/antibody mixture was combined with proteins and incubated rotating at 4°C overnight. The next morning the beads were pelleted at 10,000 rpm (8,161 x g) for 30 seconds followed by three wash steps using 500 µL of DPBS and pelleting beads at 10,000 rpm (8,161 x g) for 30 seconds between each wash. Proteins were eluted from beads using 40 µL of 2X SDS loading dye (diluted from 6X SDS loading dye, see

Western Blot for recipe) and heating the beads to 65°C for 2 minutes. Proteins were analyzed by loading input (2.5 microliters of each protein per reaction) and eluted/co-immunoprecipitated material on a 12% SDS-PAGE gel following procedure described under Western Blot.

Senescence Associated β-Galactosidase Assay

A β-galactosidase staining kit was purchased from Cell Signaling Technologies. Cells were stained following the instructions supplied with the kit. Briefly, cells were rinsed with 2 mL DPBS and fixed using 1X Fixation Buffer. Cells were then rinsed two times using 2 mL DPBS. Cells were then stained by applying 1X Staining Solution and incubating the cells at 37° C for 6-18 hours, as indicated. Staining Solution was then removed, cells rinsed with 2 mL DPBS and stored in 70% glycerol at 4°C. Cells were visualized under brightfield on an Olympus 1X70 fluorescence microscope at either 100X or 400X magnification. Images were captured using MagnaFIRE software. The total number of cells and number of blue (β-galactosidase positive) cells were scored for each image, making sure to score at least one hundred cells per treatment condition. Scoring was confirmed by another member of the laboratory in a blinded fashion. The percentage of β-galactosidase positive cells was determined for each treatment condition which was normalized to transduction efficiency based on the percentage of GFP positive cells (each average percentage of β-galactosidase positive cells divided by the percentage of GFP positive cells). This process was completed in biological triplicate and the average percent β-galactosidase positive cells normalized to transduction efficiency +/- standard error of the mean were reported for each treatment condition.

Senescence Associated Heterochromatin Formation (SAHF) Analysis

Cells previously processed with β-galactosidase stain were rinsed with DPBS twice to remove the glycerol storage solution. Cells were then permeabilized with 0.2% TritonX-100 in DPBS for 10 minutes at room temperature. Cells were washed once with 2 mL DPBS and the DNA stained with 25 µg/mL Hoechst dye (bis-Benzimide; Sigma) for 5 minutes at room temperature. The cells were again washed with 2 mL DPBS and stored in 70% glycerol at 4°C. Nuclei were visualized using fluorescence microscopy on an Olympus 1X70 fluorescence microscope at 400X magnification. Images were captured using MagnaFIRE software. The total number of nuclei and number of SAHF containing nuclei were scored for each image, making sure to score at least one hundred nuclei per treatment condition. Scoring was confirmed by another member of the laboratory in a blinded fashion. The percentage of SAHF positive cells was determined for each treatment condition which was normalized to transduction efficiency based on the percentage of GFP positive cells, as described with percent β-galactosidase positive reporting. This process was completed in biological triplicate and the average percent SAHF positive cells normalized to transduction efficiency +/- standard error of the mean were reported for each treatment condition.

III. Results

The p53 and Hdm2 binding domains of HdmX are necessary for HdmX's ability to block oncogene induced senescence.

As previously described, HdmX/Hdm4 (mouse homologue MdmX/Mdm4) negatively regulates p53 through binding and inhibiting p53's transactivation domain (Shvarts et al., 1996). HdmX is found to be over expressed in a significant number of human tumors that express wild type p53, and it was determined that MdmX blocks oncogene induced premature senescence in MEFs (Wade et al., 2009; Danovi et al. 2004). Due to the differences that exist between the murine and human cell culture systems in the study of senescence, it was first necessary to confirm that HdmX can block oncogene induced senescence in human diploid fibroblasts.

Human primary diploid fibroblasts (HDFs), specifically IMR90 cells, at passage 20 or younger were infected with H-Ras^{G12V} (H-Ras) which is a constitutively active (GTP-bound) form of Ras protein previously reported to induce senescence in HDFs (Serrano et al., 1997). The valine substitution in Ras renders the protein always in the GTP-bound active state and allows Ras to function like an oncoprotein. Primary cell lines do not transfect well; therefore, transductions (infections) using various viruses were utilized to deliver genes to these cells. Each gene of interest (oncogenic H-Ras^{G12V}, GFP, Hdm2, and HdmX) was cloned into a lentiviral vector and used for virus

production. Titering of each viral construct was completed using a colony formation assay which provided the number of infectious viral particles per mL (IVP/mL) and the range of titers achieved are indicated in Table 4. IMR90 cells infected at a MOI (multiplicity of infection) of 5 or higher achieved a transduction efficiency of 80% or greater (data not shown), so all viruses were used at an MOI of 5 to ensure equal and optimal infection.

Senescence-associated-β-Galactosidase (SA-β-Gal) activity at a pH of 6.0 is measured by cleavage of an X-gal substrate allowing a blue dyed precipitate to form which can be visualized within cells. This is the most widely used indicator of senescence (Dimri et al., 1995). Acidic β-Galactosidase is a hydrolase located in the lysosome, but the biological role for this enzyme during senescence is unknown. It has been suggested that the increase in acidic β-Galactosidase activity reflects an increase in the lysosomal mass of senescent cells (Kurz et al., 2000). While senescent cells have stopped dividing, they still remain quite metabolically active and the active lysosomal compartment is reflective of this property. Premature senescence measured by β-Galactosidase staining was induced in approximately 50% of wild-type MEFs infected with H-Ras^{G12V} and incubated for 8 days (Ferbeyre et al., 2002). A similar protocol repeated in six independent experiments was used to measure premature senescence in IMR90 cells.

Approximately 55% of the IMR90 cells transduced with H-Ras^{G12V} were senescent (Figure 7). GFP was utilized as a negative control for viral infection and induced senescence in a percentage of cells (7%) similar to no infection (complete media)

Lentivirus	Infectious Viral Particles (IVP)/mL (range)
LGFP	10^4-10^5
LRas (H-Ras^{G12V})	10^5-10^6
LHdmX	10^4-10^5
LHdm2	10^4-10^5

Table 4: Range of Titers for Lentiviral Supernatants. Infectious titers (IVP/mL) were determined using a colony formation assay. The range of titers achieved for each lentivirus is reported. Optimal titers reported by Invitrogen are between 10^5 and 10^6.

(A)

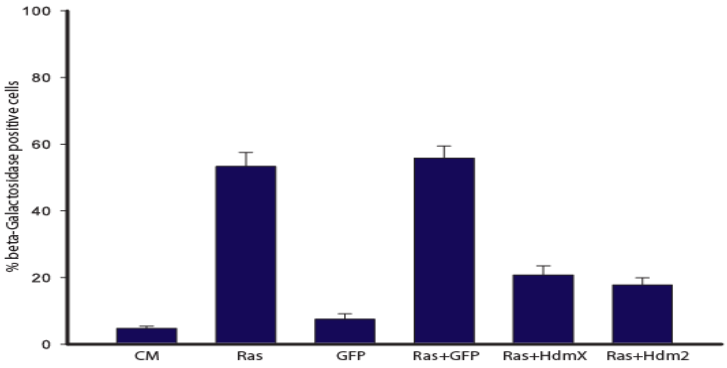

(B)

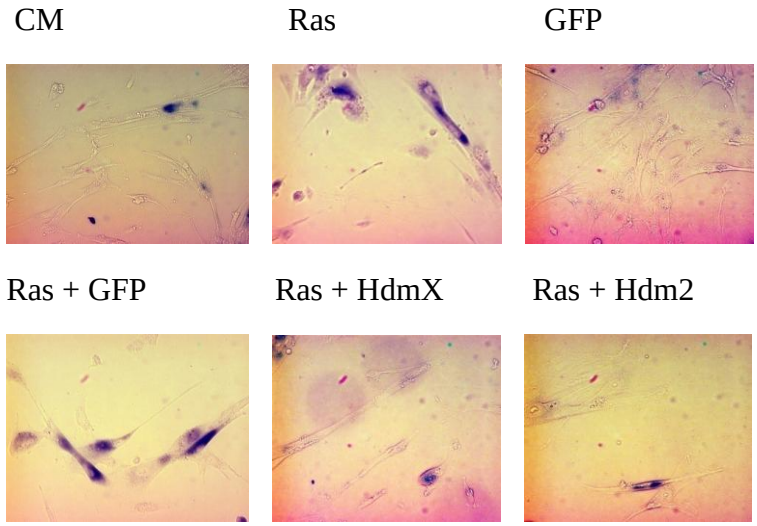

Figure 7: HdmX Blocks H-Ras^{G12V} Induced Premature Senescence in Human Diploid Fibroblasts. (A) Average % β-Galactosidase positive cells from 3 independent experiments +/- SEM per treatment condition normalized to transduction efficiency determined by % GFP positive cells. (CM = complete media, Ras = H-Ras^{G12V}). (B) Representative images from each treatment condition taken at 100X magnification and same exposure time.

treatment. GFP was also used along with H-Ras^{G12V} to compare single infections (H-Ras^{G12V}) to double infections (H-Ras^{G12V} + GFP). The H-Ras^{G12V} + GFP infection is similar to H-Ras^{G12V} alone indicating that infections with two viruses simultaneously can be achieved without affecting senescence levels. The combination infection of H-Ras^{G12V} with Hdm2 was also examined since Mdm2 overexpression has been indicated to overcome growth arrest when co-introduced with other senescence inducers (Carnero et al., 2000). Co-infection of H-Ras^{G12V} with HdmX was the experimental condition and senescence was detected in 25% of these cells compared to GFP and H-Ras^{G12V} co-infection at 55% (Figure 7), suggesting that HdmX overexpression can block H-Ras^{G12V} mediated senescence in HDFs. Hdm2 co-infected with H-Ras^{G12V} also blocked premature senescence as expected. Expression of all constructs used with each treatment was confirmed by Western blotting (Figure 8).

The results represented in Figure 7 indicate that HdmX over expression can block oncogenic Ras induced premature senescence in human diploid fibroblasts, similar to MEFs. Next, I set out to determine if the p53 and/or Hdm2 (Ring finger) binding domains of HdmX are necessary for the ability of HdmX to block H-Ras^{G12V} mediated senescence. In order to address this question, point mutations were created in HdmX that were reported to inhibit its ability to bind p53 or Hdm2. MdmXG57A has been reported by Danovi et al. (2004) to render MdmX unable to bind p53 and this amino acid is conserved in HdmX. MdmXC437G was described by Sharp et al. (1999) as being unable to bind Mdm2 and this residue is also conserved in HdmX. These two point mutations were created using the QuikChange XL Site-Directed Mutagenesis Kit. DNA sequence

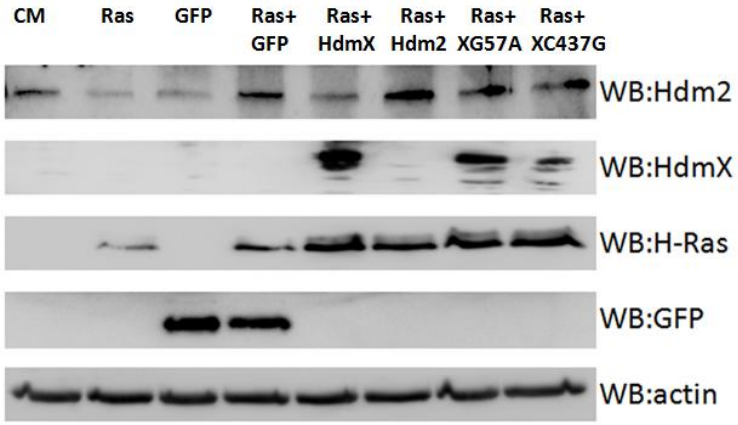

Figure 8: Western Blot Analysis of IMR90 Transductions. IMR90 cells transduced with no virus (CM), H-Ras^{G12V} (Ras), GFP, H-Ras^{G12V} (Ras) + GFP, H-Ras^{G12V} (Ras) + HdmX, H-Ras^{G12V} (Ras) + Hdm2, H-Ras^{G12V} (Ras)+HdmXG57A (XG57A) or H-Ras^{G12V} (Ras) +HdmXC437G (XC437G) as described for Figure 7 and Figure 10. Whole cell lysates were resolved by SDS-PAGE and analyzed by Western blotting for indicated proteins.

analysis was used to confirm successful mutagenesis for both mutations and that the remainder of the HdmX cDNA was wild-type.

The activities of HdmXG57A and HdmXC437G were confirmed by co-immunoprecipitation using TNT generated proteins. Co-immunoprecipitations confirmed that wild-type HdmX and HdmXC437G bound p53 while HdmXG57A was unable to do so and that wild-type HdmX and HdmXG57A bound Hdm2 while HdmXC437G was unable to do so (Figure 9). Together these results confirmed that the mutants were functioning similar to wild-type with the exception of the predicted binding that was disrupted by each single point mutation.

Infection of IMR90 cells with H-Ras^{G12V} induced senescence in approximately 55% of the cells in 7 days (Figure 7). Since binding to p53 is required for HdmX to inhibit p53 transcriptional activity and functional p53 is required for senescence, it was predicted that HdmXG57A would be unable to block H-Ras^{G12V} induced senescence. This was confirmed through the senescence assay using IMR90 cells co-transduced with H-Ras^{G12V} and HdmXG57A (Figure 10). Approximately 55% of IMR90 cells co-transduced with H-Ras^{G12V} and GFP senesced which is similar to cells co-transduced with H-Ras^{G12V} and HdmXG57A. Both of these conditions are different from cells co-transduction of H-Ras^{G12V} and wild-type HdmX where only approximately 25% of the cells senesced. As previously mentioned, HdmX and Hdm2 heterodimerization is also important to p53 regulation. Hdm2, containing a nuclear localization sequence, has been implicated in the shuttling of HdmX to the nucleus where it can interact and negatively regulate p53 (Migliorini et al., 2002). Since HdmXC437G is unable to bind Hdm2, it is

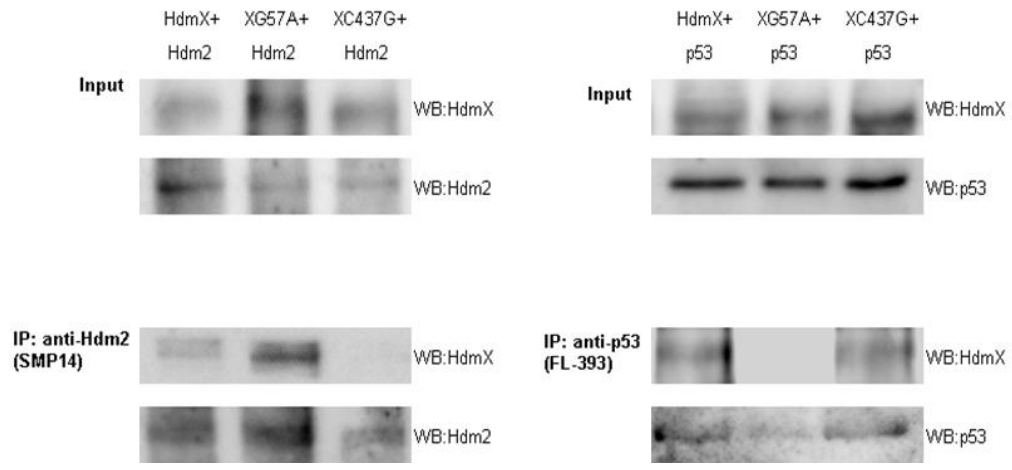

Figure 9: Characterization of HdmXG57A and HdmXC437G Mutants. Co-immunoprecipitations were completed using HdmX, Hdm2, HdmXG57A and HdmXC437G proteins generated using Promega TNT Coupled Reticulocyte Lysate System. Western blots demonstrating input proteins are shown in the top panel (Input). Western blots from co-immunoprecipitated material are shown in the bottom panel (IP).

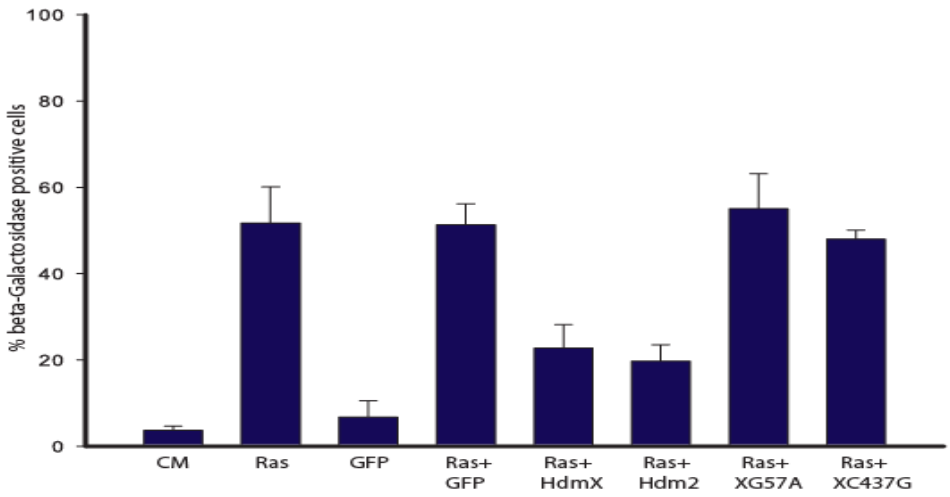

Figure 10: HdmX's p53 and Hdm2 Binding Domains are Essential to Block H-Ras^{G12V} Induced Premature Senescence in Human Diploid Fibroblasts.

Average % β-Galactosidase positive cells from three independent experiments +/- SEM per treatment condition normalized to transduction efficiency determined by % GFP positive cells. (CM = complete media, Ras = H-Ras^{G12V}).

predicted that HdmXC437G will not block H-Ras^{G12V} mediated senescence. This was also confirmed by the senescence assay where IMR90 cells co-transduced with H-Ras^{G12V} and HdmXC437G senesced to a level similar to cells co-transduced with H-Ras^{G12V} and GFP (approximately 50 and 55%, respectively) (Figure 10). Western blot analysis confirmed expression of both HdmXG57A and HdmXC437G (Figure 8). It does appear that HdmXC437G protein is less abundant when infected at the same MOI as wild-type HdmX and HdmXG57A. This suggests that HdmXC437G may be more unstable, which is likely since reports suggest that that MdmX:Mdm2 heterodimer is more stable than either homodimeric form (Tanimura *et al*., 1999). This may, at least in part, explain HdmXC437G's inability to block H-Ras^{G12V} mediated senescence.

To further investigate why HdmXC437G was unable to block H-Ras^{G12V} mediated senescence, a nuclear/cytoplasmic fractionation experiment was completed to determine if HdmXC437G could localize to the nucleus in the presence of Hdm2. Approximately 30% more wild-type HdmX and 25% more HdmXG57A localizes to the nucleus in the presence of additional Hdm2 while HdmXC437G remains predominantly cytoplasmic even with Hdm2 overexpression (Figure 11). These results support the idea that HdmXG57A enters the nucleus but is unable to bind p53, which is reported to be required for HdmX to inhibit p53 transactivation. HdmXC437G , however, appears to be deficient at nuclear localization, which implies that this mutant is not reaching the nucleus where it would interact with p53. Together these results suggest that HdmX binding to p53 and Hdm2 are necessary for its ability to block H-Ras^{G12V} mediated senescence.

(A)

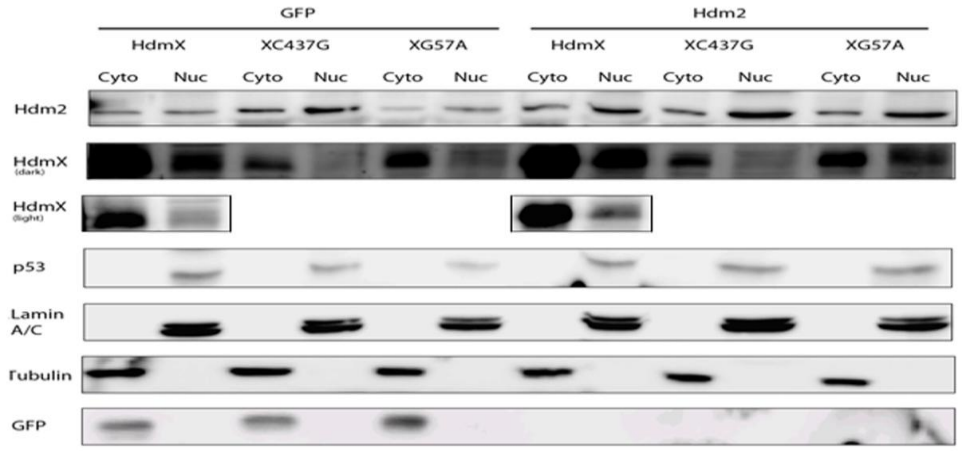

(B)

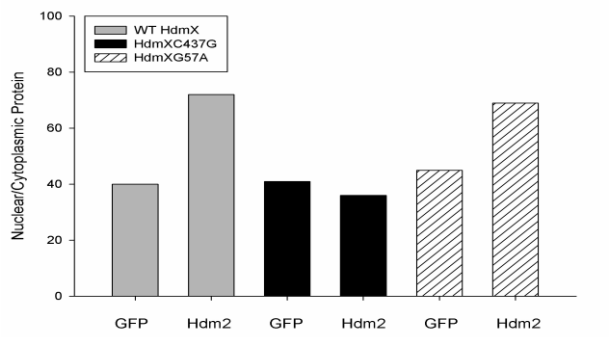

Figure 11: Wild-type HdmX and HdmXG57A Translocate to the Nucleus While HdmXC437G Remains Cytoplasmic. IMR90 cells were transduced with wild-type HdmX, HdmXC437G or HdmXG57A in addition to GFP (left panel) or Hdm2 (right panel). (A) Cells were selected and then nuclear and cytoplasmic protein extracts separated on an SDS-PAGE gel. Localization of Lamin A/C (a nuclear protein) and Tubulin (a cytoplasmic protein) confirm the extract fractionation was effective. (B) Bar graph represents nuclear/cytoplasmic ratios for HdmX proteins in the presence of GFP or Hdm2 as quantified using Multiguage software. *****Nuclear/cytoplasmic fractionation and Western blot generated by Kevin Kelley.

Reduction of HdmX in tumor cell lines with wild-type p53, mutated Ras and high levels of HdmX triggers senescence.

It is known that HdmX over expression is found in many human tumors; however, the mechanisms leading to and outcomes of HdmX over expression have not been fully elucidated. It has also been indicated that many of the human tumors that over express HdmX maintain wild-type p53. Interestingly, 90% of pancreatic, 50% of colon and thyroid and 30% of all human tumors have mutated Ras (Saxena et al., 2008) which makes the tumor phenotype of mutant Ras, wild-type p53 and high levels of HdmX likely. Since HdmX can block oncogenic Ras induced senescence in untransformed human diploid fibroblasts (Figure 7), knocking down HdmX in tumor cells with high HdmX, mutant Ras and wild-type p53 may lead to tumor cell senescence.

To test this possibility, LNCaP cells, a prostate adenocarcinoma cell line with wild-type p53, mutant Ras and high HdmX were utilized (Ramos *et al*., 2001). These cells have been previously analyzed for their ability to senesce after various genetic manipulations making them an attractive cell line for use in this study (Obajimi et al., 2009; Baygi et al., 2010). Lentiviral short hairpin HdmX (shHdmX) and short hairpin LacZ (shLacZ) vectors were used since short hairpin RNA interference (shRNAi) technology is a highly efficient and specific method of silencing gene expression in cells.

Upon production of shHdmX and shLacZ lentivirus, LNCaP cells were infected and knock-down of HdmX confirmed by Western blotting (Figure 12A). This sh-HdmX construct was previously validated by Western blotting in our lab (K. Heminger, BMS Thesis). A slight reduction of HdmX protein was detected in all lanes infected with any

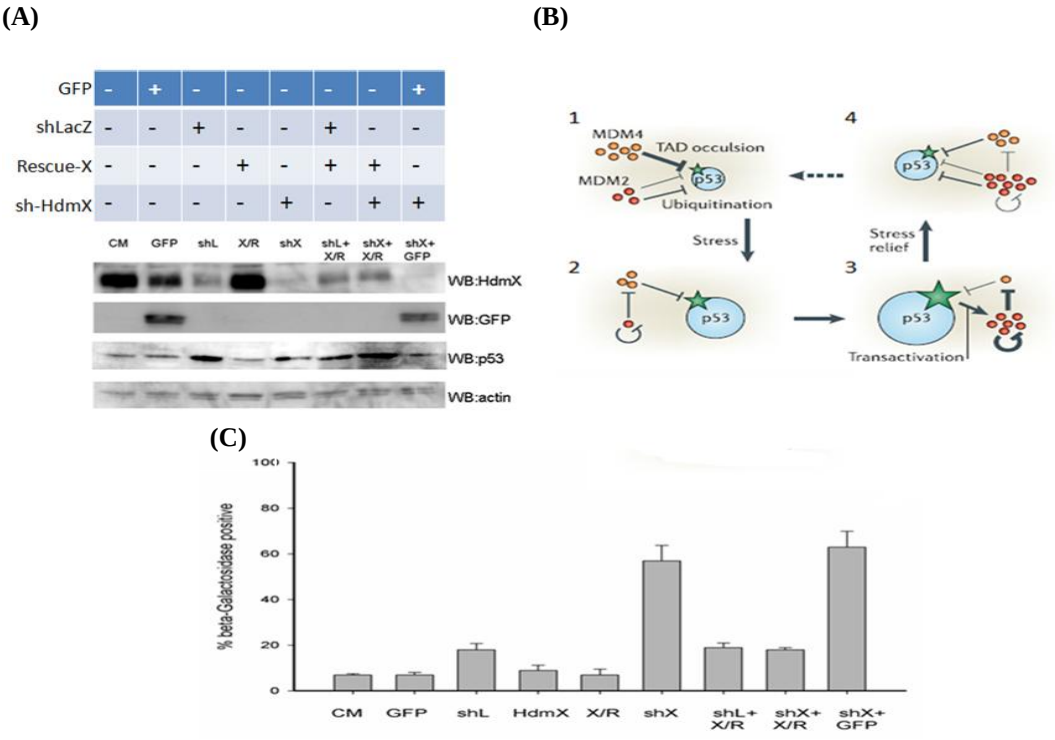

Figure 12: Loss of HdmX Induces β-Galactosidase Activity in LNCaPs. (A) LNCaP cells were transduced with no virus (CM), GFP, shLacZ (shL), HdmX/Rescue (X/R), sh-HdmX (shX), shL+X/R, shX+X/R or shX+GFP, selected and whole cell extracts were resolved by SDS-PAGE and subjected to Western blotting using antibodies indicated. (B) Diagram demonstrating modulation of Hdm2-HdmX-p53 axis in response to cellular stress (Toledo et al., 2006). 1. Unstressed conditions where p53 levels are kept low by Mdm2 (Hdm2) and Mdm4 (MdmX/HdmX). 2. Stress causes induction of p53 by ubiquitination and degradation of Mdm4 and Mdm2 by Mdm2. 3. p53 drives expression of Mdm2 to increase Mdm2 levels. 4. Mdm2, MdmX and p53 return to steady state levels. (C) Average % β-Galactosidase positive cells normalized to transduction efficiency +/- standard error of the mean is reported where >100 cells were counted per treatment condition (described in a) in three biological replicates.

short hairpin lentivirus, most likely due to a stress response and subsequent p53 activation in those cells leading to reduction of HdmX protein as a part of the p53-HdmX-Hdm2 loop (Figure 12B). The nearly complete elimination of HdmX protein was detected only in sh-HdmX infected cells. To confirm that any effect detected using sh-HdmX is a specific result of knock-down and not an off target effect from sh-HdmX infection, HdmX protein levels were rescued in LNCaP cell using a Lentivirus-HdmX expression vector harboring a silent mutation that makes the hdmX mRNA from this cDNA resistant to the hdmX short hairpin RNA, which was also confirmed by Western blot (Figure 12A).

LNCaP were infected with various lentivirus combinations as indicated in Figure 12 (C) followed by selection and incubation for approximately seven days. Cells were then stained for β-Galactosidase activity. Reducing HdmX in LNCaP cells led to an induction of senescence in approximately 58% of the cells and this level of senescence is higher than sh-LacZ infected (approximately 18%) or complete media (CM) treated (approximately 10%) cells (Figure 12C). Upon restoration of HdmX protein, there is a decrease in senescence levels similar to background senescence levels (Figure 12C, compare shLacZ to shX + HdmX/R, both approximately 18%). This finding supports that the induction of senescence in LNCaP cells when HdmX is reduced is specifically due to the decrease in HdmX protein.

To confirm that measurements of β-Galactosidase activity accurately represent cellular senescence, SAHF analysis was performed on LNCaP cells infected with sh-HdmX and none were detected in β-Galactosidase positive or negative LNCaP cells.

SAHF formation is a cell-type specific measurement of senescence induction; therefore, they do not appear in all senescent cells. It was recently shown that epithelial tumor cells treated with Nutlin-3a, and small molecule inhibitor of Mdm2, became β-Galactosidase positive; however, upon drug removal, these some cells resumed proliferation (Huang *et al*., 2009). So, it was important to determine if the β-Galactosidase staining that was detected in LNCaP cells upon HdmX reduction was reversible. To address this issue, an HdmX protein rescue/time course experiment was utilized.

LNCaP cells were infected with various lentiviral constructs as described in Figure 13 followed by incubation under selection for 7 days, at which time a second viral infection was completed to re-express HdmX protein levels in cells infected with sh-HdmX. After an additional 7 days of incubation under selection, all cells were subjected to β-Galactosidase staining as previously described. Approximately 70% of the LNCaP cells infected with only sh-HdmX were β-Galactosidase positive after 14 days which was similar to cells infected with sh-HdmX initially followed by Rescue-HdmX infection at day 7 (compare shX to shX : X/R in Figure 13A) suggesting that the increase in β-Galactosidase positive cells detected after infection with sh-HdmX is NOT reversible and represents a senescent state.

As in Figure 12C, shLacZ infection for 14 days induced senescence in about 20% of the cells slightly higher than the GFP infection control at about 10%. Importantly, cells initially infected with sh-HdmX and the rescue construct together only led to approximately 13% of the cells undergoing senescence after 14 days, while about 68% of the cells initially co-infected with sh-HdmX and GFP were induced to senesce. These

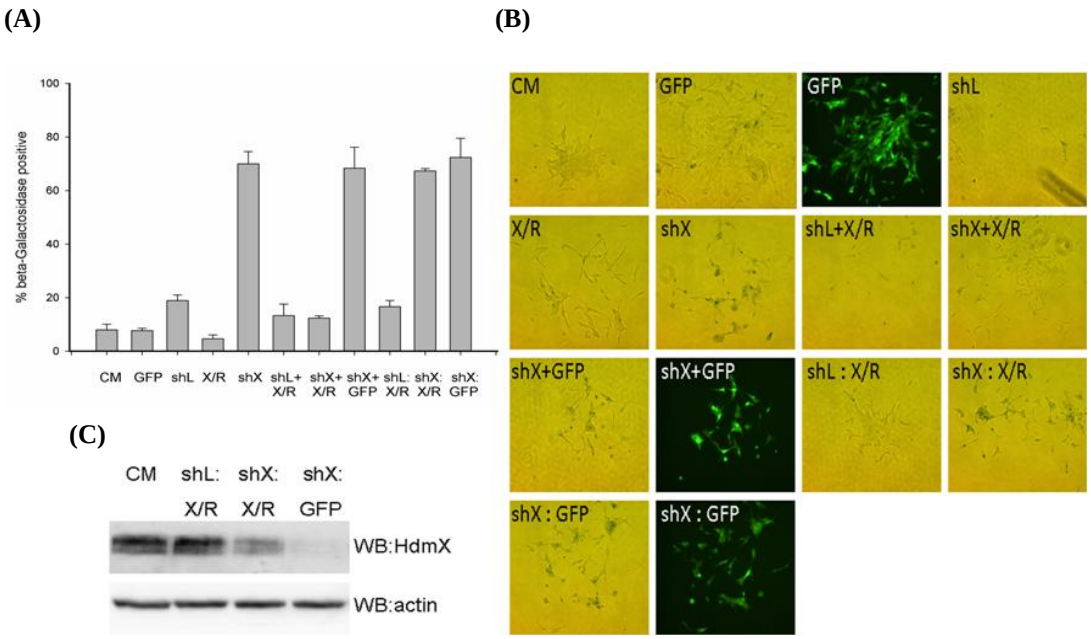

Figure 13: Loss of HdmX Induces an Irreversible Increase in β-Galactosidase Positive LNCaP Cells. (A) LNCaP cells were infected with no virus (CM), GFP, shLacZ (shL), HdmX/Rescue (X/R), sh-HdmX (shX), shL+X/R, shX+X/R, shX+GFP, shL, shX or shX and selection applied for 7 days. On day 7, shL infected cells were additionally infected with X/R (shL:X/R), shX infected cells with X/R (shX:X/R) and shX infected cells with GFP (shX:GFP) followed by an additional 7 days of incubation under selection. At day 14 all cells were subjected to beta-Galactosidase staining. Histogram represents average % β-Galactosidase positive cells normalized to transduction efficiency +/- standard error of the mean where >100 cells were counted for each treatment condition in three independent experiments. (B) Representative images of each treatment condition as described in (A). All images taken at 100X magnification and the same exposure time. (C) Western blot confirming HdmX protein rescue and knock-down in shX:X/R and shX:GFP treatment conditions, respectively.

results are similar to what is reported in Figure 12C for the 7 day time period. Initial co-infection of sh-LacZ and the rescue construct or sh-LacZ followed by the rescue protein was again confirmed via Western blotting (Figure 13C). Together this data provides evidence that targeting HdmX for cytoplasmic localization or reduction of total protein can induce an irreversible state of cellular senescence in human tumors. Understanding the dependency of mutant Ras and/or p53 on this induction of senescence will be a future direction for this project.

YPEL3 Induces Cellular Senescence.

The focus previously was on activation of p53 and now I will describe a downstream p53 target implicated in the senescence pathway. While much is known about p53 targets involved in apoptosis and cell cycle arrest, those critical to senescence induction are not as clearly defined. In studies where a cell cycle arrest of MCF7 cells was induced by activating p53 via silencing its negative regulators HdmX or Hdm2, novel p53 targets were discovered, one of which was YPEL3. YPEL3 was validated as a specific p53 target through RT-PCR and ChIP analysis (Kelley et al., 2010). Additionally, YPEL3 was reported to be growth suppressive potentially through the apoptotic pathway in murine myeloid precursor cells (Baker, 2003).

To further investigate the role of human YPEL3, full-length human YPEL3 was cloned from pCMV-SPORT6 vector (Open Biosystems) into the pLenti4/TO/V5/DEST vector, which contains a tetracycline responsive promoter (TetOn, Invitrogen) and a V5 tag. Lentivirus was then produced with this construct and used to transduce MCF7 (breast carcinoma) and U2OS (osteosarcoma) cells that were stably expressing the

Tetracycline Repressor protein (TetR). Colony formation assays were completed using the aforementioned cells treated with 1 microgram/mL of Tetracycline to induce YPEL3 compared to transduced cells without the addition of Tetracycline, both for approximately 14 days (Figure 14A/B). There was a clear reduction in the number of colonies formed when cells were treated with Tetracycline (approximately 50%) suggesting that YPEL3 is also growth suppressive in human cells (Figure 14A and B).

To further confirm that YPEL3 is growth suppressive in human cells, MCF7TetR and U2OSTetR expressing cells were infected with Tet-responsive YPEL3-V5 and stably selected. These stable pooled populations will be referred to as MCF7TetR/YPEL3 and U2OSTetR/YPEL3. Stable pools containing a Tet responsive LacZ expression vector were also created for use as a negative control. YPEL3 and LacZ expression upon Tetracycline induction was confirmed for U2OSTetR (Figure 15A) and MCF7TetR cell lines (data not shown). After confirmation of proper protein expression, a cell viability (MTT) assay was completed. U2OSTetR/YPEL3 cells induced with Tetracycline demonstrated a 50% reduction in cell viability compared to U2OSTetR/YPEL3 cells not treated with Tetracycline (Figure 15B). U2OSTetR/LacZ cells induced with Tetracycline as a negative control only demonstrated an approximately 18% reduction in viability. These results suggest that when expressed in human cells, YPEL3 is able to reduce cell viability.

To further confirm that YPEL3 induction leads to growth suppression, RNAi approaches were employed to knock down YPEL3 in MCF7 and U2OS cells (Figure 16). Knock down of YPEL3 using two separate lentiviral shYPEL3 constructs was confirmed

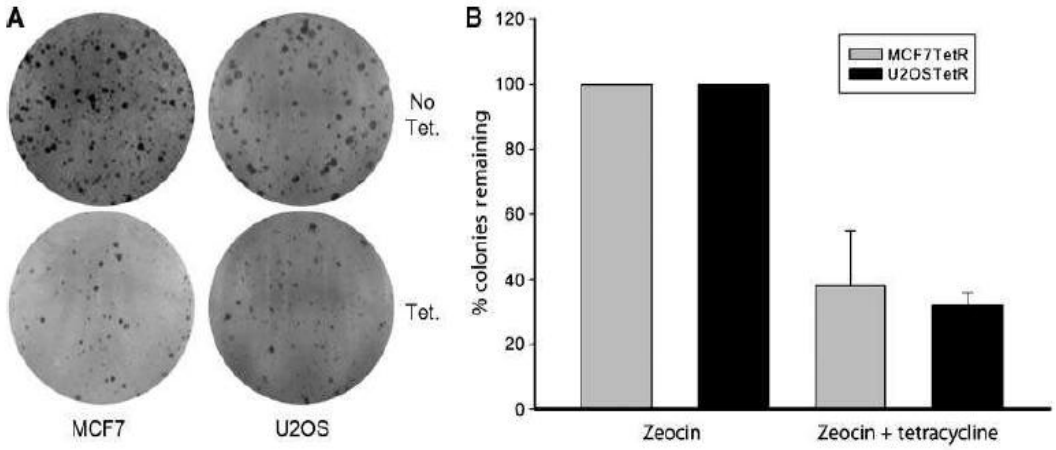

Figure 14: Induction of YPEL3 Leads to Growth Suppression in MCF7 and U2OS Cells. (A) Representative images of colony formation assays of MCF7TetR and U2OSTetR expressing cells transduced with Tet-inducible YPEL3-V5 (Zeocin resistant) and treated with or without 1 microgram/mL Tetracycline (Tet). (B) Percent colonies remaining +/- standard error of the mean in Tet treated cells described in (A) compared to non-Tet treated cells (set to 100%) (Kelley *et al*., 2010).

(A)

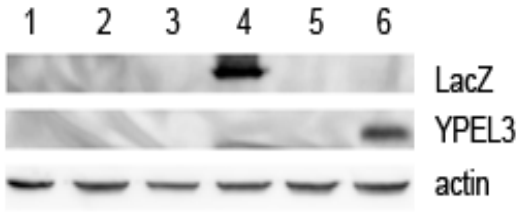

(B)

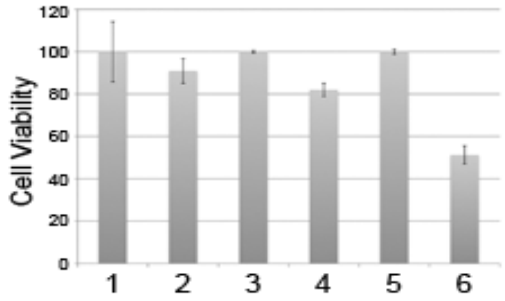

Figure 15: Induction of YPEL3 Causes Reduction in Cell Viability. (A) Western blot from whole cell lysates probed with anti-V5 antibody demonstrating YPEL3/V5 and LacZ/V5 protein expression in U2OSTetR parental (lanes 1,2); U2OSTetR/LacZ (lanes 3,4) and U2OSTetR/YPEL3 (lanes 5,6) cells treated with (lanes 2, 4, 6) and without (lanes 1, 3, 5) 1 µg/mL tetracycline. (B) MTT assay of cells as numbered and defined in (A) treated for 24 hours with or without tetracycline. Each condition was performed in quadruplicate with error bars representing standard error of the mean (MTT assay completed by Berberich, S.J.) (Kelley *et al*., 2010)

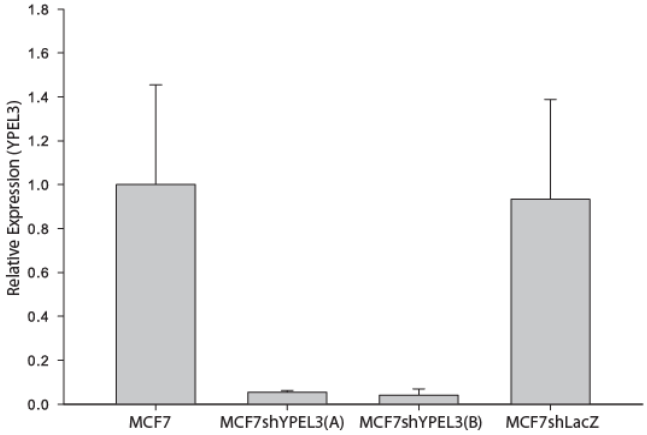

Figure 16: RT-PCR Confirmation of YPEL3 Knock-down by RNAi in MCF7 Cells. Relative expression of YPEL3 normalized to GAPDH in MCF7 parental, MCF7shYPEL3 (A), MCF7shYPEL3 (B) and MCF7shLacZ pooled stable cell lines. Error bars represent 95% confidence intervals.

by RT-PCR in MCF7 cells (Figure 16) and U2OS cells (with approximately 80% knock down, data not shown). Upon confirmation of YPEL3 knock-down, MCF7shLacZ and MCF7shYPEL3 (A) and (B) cells were plated at 50,000 cells per well in a six well dish. Cell counts from each cell type were obtained using the ViCell at days two, four, and six (Figure 17). MCF7shYPEL3 expressing cells grew at a faster rate than the shLacZ control cells, indicating that the reduction of YPEL3 conferred a growth advantage in MCF7 cells. Similar results were obtained using U2OS cells (data not shown). Together these results further support the role of YPEL3 in growth suppression.

Since YPEL3 was shown to be up regulated in apoptotic myeloid precursor cells and the induction of YPEL3 is associated with increase in Annexin V staining in these cells, we initially investigated whether human YPEL3 was growth suppressive through the apoptotic pathway in human cells. Interestingly, there was no indication that USOS, MCF7 or LNCaP cells induced to express YPEL3 were undergoing apoptotic programming as measured by PARP cleavage using doxorubicin treatment as a positive control (data not shown). Based on the inability to detect apoptosis in U2OS and MCF7 cells induced to express YPEL3 and the unique morphologic characteristics of these cells, I hypothesized that YPEL3 is growth suppressive through the cellular senescence pathway. To address this hypothesis, established U2OSTetR and MCF7TetR stable pooled cell lines were utilized and senescence was measured by β-Galactosidase staining and SAHF analysis, as previously described.

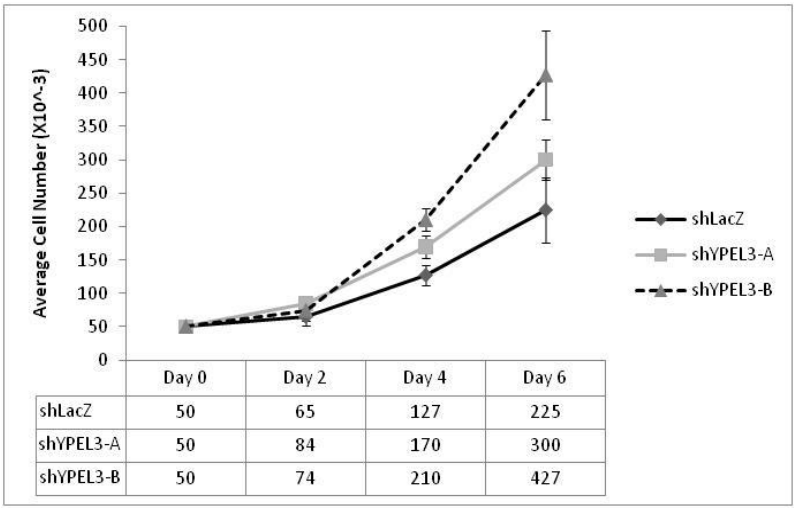

	Day 0	Day 2	Day 4	Day 6
shLacZ	50	65	127	225
shYPEL3-A	50	84	170	300
shYPEL3-B	50	74	210	427

Figure 17: RNAi Targeting YPEL3 Leads to Increased Cellular Proliferation. Pooled populations of MCF7 cells stably infected with either shLacZ (diamonds) or one of two shRNAs targeting YPEL3 (shYPEL3-A, squares; shYPEL3-B, triangle) were plated at 50,000 per 6 well dish. Two days later, 3 wells per cell line were separately counted using a ViCell cell viability counter (Day 2). Cell counts were repeated on days 4 and 6. Average cell number +/- standard deviation is reported for each cell type on each day counted. Experiment was repeated with similar results.

U2OSTetR/YPEL3, U2OSTetR/LacZ and U2OSTetR parental cells were plated in duplicate in six well dishes. For each cell type, one well was induced with Tetracycline at 1 μg/mL and the other with complete media. At the end of 6 days, the plate was subjected to β-Galactosidase staining as previously described. Images were taken of each treatment condition and representative images are shown in Figure 18A. Approximately 30% of the YPEL3 expressing U2OS cells were β-Galactosidase positive, as indicated by the blue positive staining (Figure 18B). This level of senescence was higher than the LacZ expressing control cells which were approximately 8% β-Galactosidase positive (Figure 18B). Together this suggests that YPEL3 induction triggers senescence in U2OS osteosarcoma cells.

To confirm that the senescence induction following an increase of YPEL3 was not specific to the U2OS cell type, MCF7 breast carcinoma cells were analyzed as described in Figure 18. MCF7 cells demonstrated the same phenotype where 25% of the YPEL3 expressing and only 8% of the LacZ expressing cells scored β-Galactosidase positive (Figure 19). Together these results suggest that the senescence induced by YPEL3 is not specific to only U2OS cells and that the growth suppression that occurs due to YPEL3 induction is likely occurring through the induction of senescence as measured by an increase in β-Galactosidase activity.

As mentioned previously, Huang and colleagues described a Nutlin-dependent cell cycle arrest that resulted in reversible increase in β-Galactosidase staining in

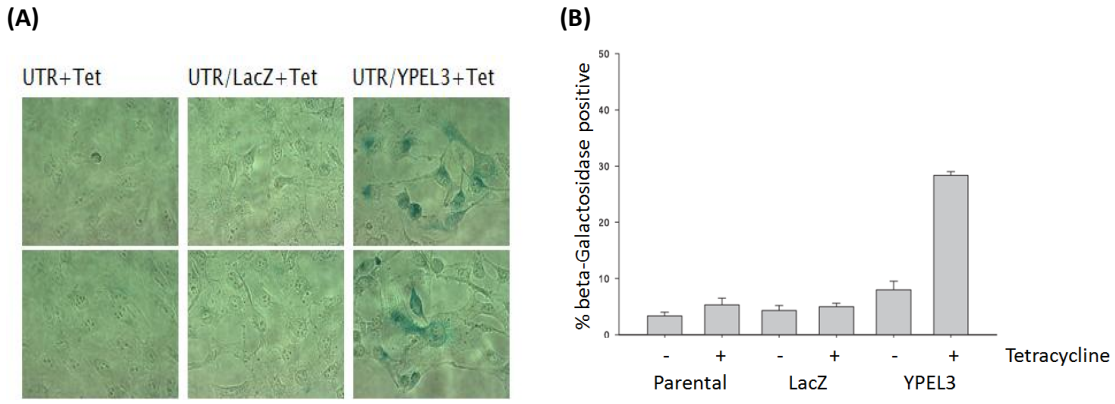

Figure 18: Increase of YPEL3 Triggers Cellular Senescence in U2OS Cells as Measured by β-Galactosidase Staining. (A) Representative images of U2OSTetR (UTR), U2OSTetR/LacZ (UTR/LacZ) and U2OSTetR/YPEL3 (UTR/YPEL3) cells induced with 1 µg/mL of Tetracycline for 6 days and subjected to beta-Galactosidase staining. Images taken at 100X magnification and same exposure time. (B) Histogram representing the average % β-Galactosidase positive cells per treatment condition +/- standard error of the mean of at least 100 cells counted per treatment condition in biological triplicate. (Kelley *et al*., 2010)

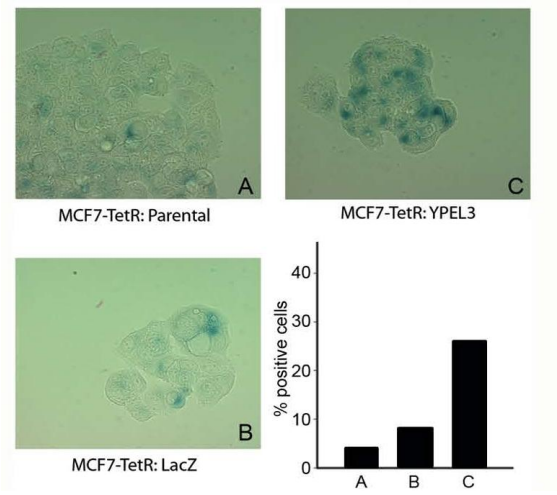

Figure 19: Induction of YPEL3 Triggers Senescence in MCF7 Cells as Measured by β-Galactosidase Staining. Representative images of MCF7TetR parental (A), MCF7TetR/LacZ (B) and MCF7TetR/YPEL3 (C) cells induced with 1 µg/mL Tetracycline for 6 days followed by β-Galactosidase staining. Images taken at 100X magnification and same exposure time. Histogram represents average % beta-Galactosidase positive of at least 100 cells scored per treatment condition. (Kelley *et al*., 2010)

epithelial tumor cells (Huang et al., 2009). Senescence, by definition, is an irreversible process; therefore, the use of β-Galactosidase staining as a sole measurement of senescence has been questioned. To ensure that the increase in β-Galactosidase staining seen with the induction of YPEL3 is in fact an indication of senescence in these cells, senescence associated heterochromatin formation (SAHF) was examined. SAHFs appear as permanent chromatin condensation occurs in senescent cells, as previously described (Figure 2).

U2OSTetR/YPEL3, U2OSTetR/LacZ and U2OSTetR parental cells treated as described in Figure 18 were subjected to Hoechst dye staining followed by fluorescence microscopy. Hoechst dye is a fluorescent stain used for labeling DNA and allows for the detection of punctuate foci within the nucleus upon SAHF formation. Representative images of this analysis are shown in Figure 20A. Notice the uniform staining of the DNA within the LacZ expressing control nuclei (left panels) and the punctuate foci within the nuclei of the YPEL3 expressing SAHF positive cells (right panels). The percentage of SAHF positive cells in YPEL3 expressing U2OS cells was similar to the percentage β-Galactosidase positive cells (approximately 28% and 30%, Figure 20B and 18B, respectively). SAHF detection provides further support that YPEL3 functions as a senescence inducer in human tumor cell lines. More importantly, the presence of SAHFs confirms that these cells are not reversibly β-Galactosidase positive since SAHF formation and associated silencing of E2F target genes do not occur in reversibly arrested cells (Narita et al., 2003).

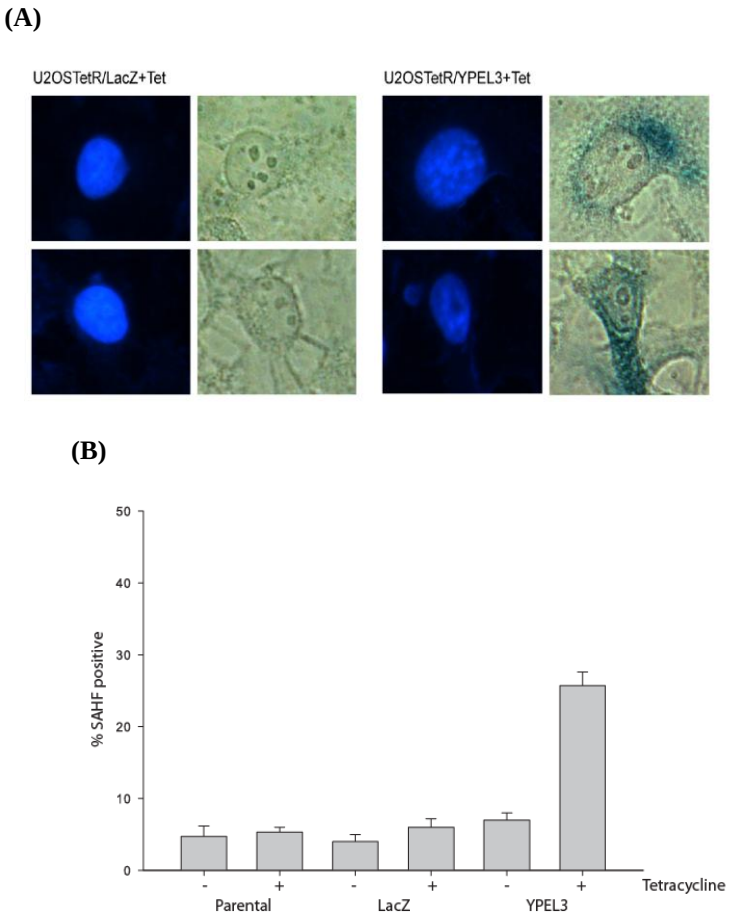

Figure 20: YPEL3 Induces Senescence in U2OS Cells as Measured by SAHFs. (A) Representative images of U2OSTetR/LacZ (left) and U2OSTetR/YPEL3 (right) cells incubated with 1 µg/mL Tetracycline for 6 days followed by Hoechst dye (images on left in set of 4) and beta-Galactosidase (images on right in set of 4) staining. Images taken at 400X magnification and same exposure time. (B) Histogram representing the average % SAHF positive cells per treatment condition +/- standard error of the mean of at least 100 cells counted per treatment condition in biological triplicate. (Kelley *et al*., 2010)

In order to confirm that the induction of senescence by YPEL3 was not unique to tumor cell lines, non-transformed human diploid fibroblasts (IMR90 cells) were utilized. As previously mentioned, oncogenic Ras is known to induce senescence in IMR90 cells and served as a positive control inducing senescence, as measured by β-Galactosidase activity and SAHF formation in approximately 75% of the cells (Figure 21B). GFP served as a negative control for viral infection and only about 18% of the cells scored positive for β-Galactosidase activity or SAHF formation. Approximately 45% and 65% of the IMR90 cells transduced with YPEL3 scored positive for β-Galactosidase staining and SAHF formation, respectively. Together these results suggests that elevated YPEL3 is sufficient to induce senescence in a non-transformed cell line and further supports the conclusion that human YPEL3 is growth suppressive through the induction of cellular senescence.

YPEL3 Functions Downstream of p53 During H-Ras^{G12V} Mediated Senescence.

As previously stated, oncogenic Ras-induced premature senescence requires functional p53. Yet, downstream targets of p53 that are necessary for senescence have been difficult to identify. Uncovering critical targets and regulatory proteins involved in the p53 pathway leading to senescence would provide useful targets for anti-cancer drug design. It is clear that YPEL3 is a p53 target and is sufficient to induce senescence in human diploid fibroblasts (Figure 21) along with human tumor cells lines, as described previously. However, it is unclear where YPEL3 fits within the senescence pathway. The induction of senescence in human diploid fibroblasts (IMR90 cells) by H-Ras^{G12V}

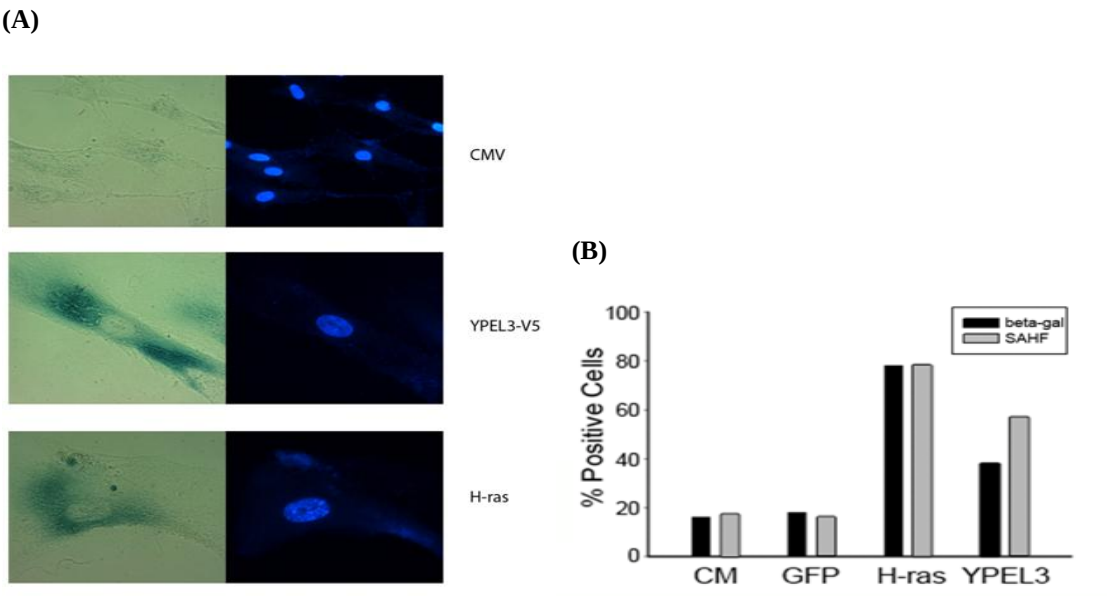

Figure 21: YPEL3 is Sufficient to Induce Senescence in Human Diploid Fibroblasts. (A) IMR90 cells transduced with empty virus (CMV), YPEL3-V5 or Ras (H-Ras^{G12V} = H-ras) were incubated for 7 days followed by β-Galactosidase (left panel) and Hoechst dye (right panel) staining. Brightfield and fluorescence images taken at 400X magnification and same exposure time for each. (B) Histogram represents % positive cells where over 100 cells were counted for each treatment condition described in (A) normalized to transduction efficiency based on GFP positive cells. (Kelley *et al*., 2010)

was used as a model system to begin to probe the location of YPEL3 within the senescence pathway.

First, to ensure that the use of oncogenic Ras mediated senescence in IMR90 cells was a good model system for the study of YPEL3, the expression profile of YPEL3 during H-Ras^{G12V} mediated senescence was investigated using RT-PCR analysis. This was achieved by following a time course protocol where H-Ras^{G12V} virus was transduced into IMR90 cells followed by daily RNA isolations and RT-PCR analysis for senescence associated genes as described by Mason and colleagues (2004). IMR90 cells were transduced with H-Ras^{G12V} virus following the time course described in Figure 22A. As previously reported, expression of p21, a known p53 target and senescence associated gene, was elevated at day 3 and again at day 6 post-infection (PI) (Mason et al., 2004). Interestingly, YPEL3 expression followed a similar pattern of induction at day 3 and day 6 PI. The feeding schedule was monitored and resulting increase in mitogenic activity correlating with fresh complete media addition was not the basis for this particular pattern of gene expression. Furthermore, the induction of senescence has also been described as a dynamic process (Young et al., 2009). The periodic induction of p21 as reported by Mason and colleagues along with YPEL3, described in this study, suggests that molecular targets of senescence may be transiently induced as the cell reprograms to an irreversibly arrested state (Mason et al., 2004; Kelley et al., 2010). These results supported the use of H-Ras^{G12V} mediated senescence as a tool for studying how YPEL3 induces senescence.

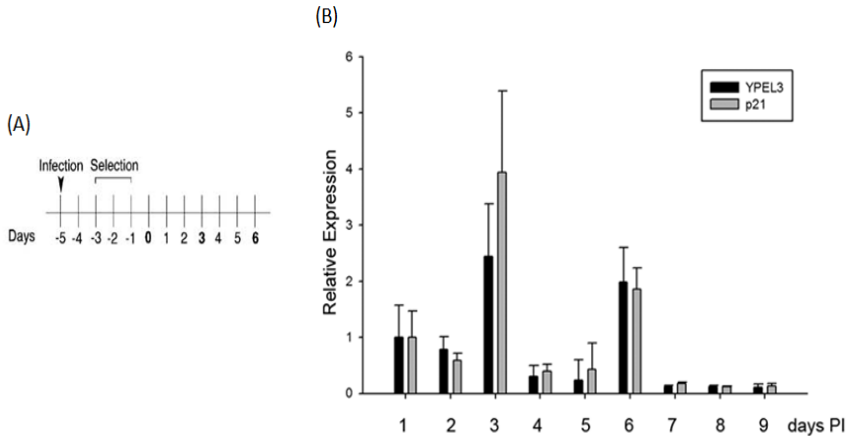

Figure 22: YPEL3 is Induced During H-Ras^{G12V} Mediated Senescence in IMR90s. (A) Schematic diagram representing infection and antibiotic (Blasticidin) selection schedule for IMR90 cells transduced with lentivirus expressing H-Ras^{G12V} (Mason *et al*., 2004). (B) RT-PCR analysis of YPEL3 and p21 expression normalized to GAPDH from cells described in (A) at time points indicated. Error bars represent 95% confidence intervals. (Kelley *et al*., 2010)

Previous data supports that YPEL3 is a p53-target and sufficient to induce senescence in IMR90 cells, but it is unclear whether YPEL3 is a critical p53 target required in IMR90 cells for H-Ras^{G12V} mediated senescence. To determine if YPEL3 expression is required for oncogene-induced senescence, the knock-down of YPEL3 using two different short-hairpin vectors (shYPEL3(A) and shYPEL3(B)) alone and in combination with H-Ras^{G12V} transduction were completed. β-Galactosidase staining and SAHF analysis were utilized to measure senescence, as described previously. Reduction of YPEL3 was confirmed at the mRNA level. Knock down in cells infected with shYPEL3 virus was confirmed by RT-PCR analysis (Figure 23). YPEL3 expression in shYPEL3 infected cells was only 30% that of IMR90 cells infected with shLacZ. Evaluation of endogenous YPEL3 protein level is difficult due to its rapid turnover through the ubiquitin-proteasome pathway (data not shown).

Upon confirmation of YPEL3 knock-down, IMR90 cells were transduced with H-Ras^{G12V} alone and in combination with shLacZ (negative control) or one of the YPEL3 short-hairpin viruses. Co-transduction of H-Ras^{G12V} and shLacZ produced senescence levels similar to H-Ras^{G12V} infection alone, demonstrating that infection with a short hairpin vector did not impact senescence (Figure 24). When endogenous YPEL3 levels are lowered using shYPEL3 (A) or shYPEL3 (B), H-Ras^{G12V} was only able to induce senescence in approximately 25% and 10% of the cells as measured by β-Galactosidase activity, respectively (Figure 24A). These levels are lower than control senescence levels of approximately 65% (H-Ras^{G12V} + shLacZ) suggesting that reducing YPEL3 blocks H-Ras^{G12V} mediated senescence in IMR90 cells. Results from the β-Galactosidase activity assay were supported by SAHF detection in cells transduced as described previously

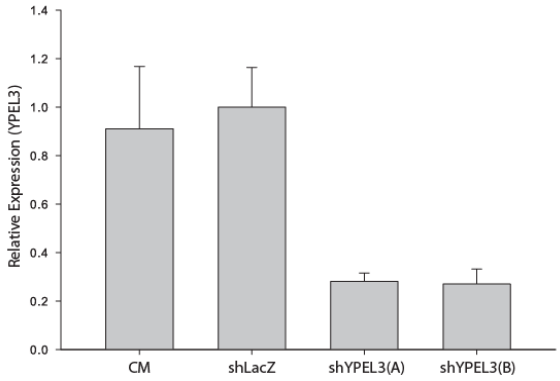

Figure 23: RT-PCR Confirmation of YPEL3 Knock-down by RNAi in IMR90 Cells. IMR90 cells uninfected (CM) or infected with shLacZ, shYPEL3 (A) or shYPEL3 (B) followed by selection were analyzed for YPEL3 mRNA levels normalized to GAPDH by RT-PCR. Error bars represent 95% confidence intervals (RT-PCR completed by Rebecca Tuttle, MD).

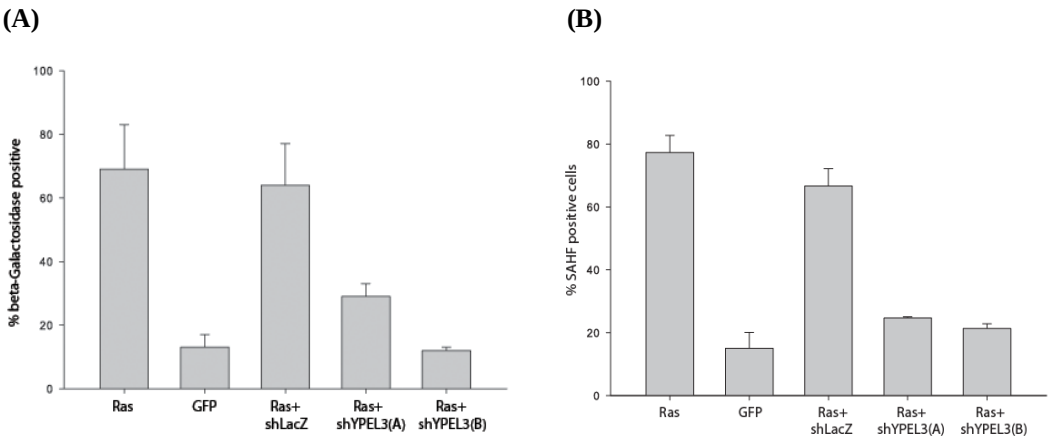

Figure 24: Loss of YPEL3 Blocks H-Ras^{G12V} Mediated Senescence in IMR90s. Histograms represent average % β-Galactosidase (A) or SAHF (B) positive cells where over 100 cells were counted for each transduction condition of IMR90 cells listed on X-axis (Ras=H-Ras^{G12V}). Averages normalized to transduction efficiency based on % GFP positive cells from three biological replicate experiments. Error bars represent standard error of the mean.

(Figure 24B), suggesting that YPEL3 is a critical downstream p53 target during H-Ras^{G12V} mediated senescence in IMR90 cells.

It is reported that p53 is required for oncogenic Ras induced senescence (Serrano et al., 1997) and that YPEL3 is a direct p53 target (Kelley et al., 2010). Combined with the result that YPEL3 is sufficient to induce senescence in IMR90 cells, I hypothesized that YPEL3 is functioning downstream of p53 during H-Ras^{G12V} mediated senescence. To address this issue, RNAi targeting p53 was used to block H-Ras^{G12V} mediated senescence combined with the addition of YPEL3 followed by senescence analysis as previously described. The use of shLacZ and GFP transductions were utilized as negative controls for shp53 and YPEL3, respectively. Knock-down of p53 was confirmed by Western blotting in IMR90 cells (Figure 25).

It is clear that transduction of IMR90 cells with oncogenic H-Ras^{G12V} (A) and YPEL3 (C) induces senescence in approximately 70% of the cells and this senescence level is higher than that achieved with the negative control GFP (B) at approximately 12% (Figure 26). The combination of H-Ras^{G12V} and GFP (D) served as a control for transduction of additional viruses with H-Ras^{G12V} and senescence levels for this treatment condition remain the same as H-Ras^{G12V} alone. Co-infection of H-Ras^{G12V} and YPEL3 (E) lead to senescence levels the same as H-Ras^{G12V} (A) suggesting that the two may be functioning through the same pathway or there is simply a threshold of senescence that is reached with H-Ras or YPEL3 alone, therefore, combining them does not provide a further increase in senescence level.

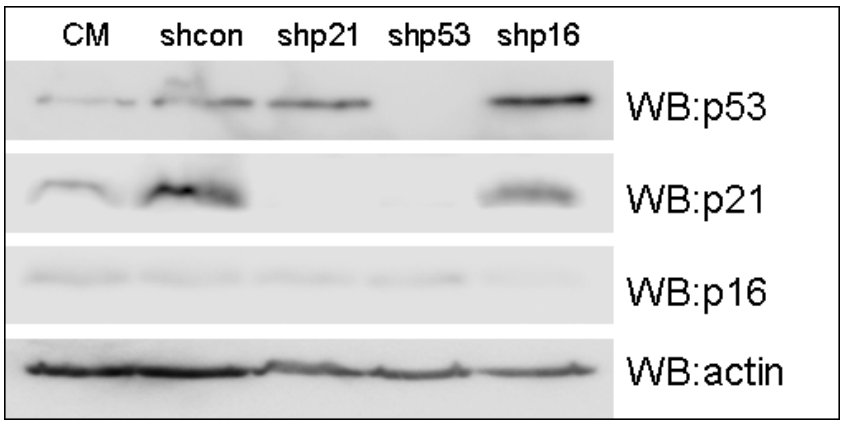

Figure 25: Western Blot Confirmation of p21, p53 and p16 Knock-down by RNAi in IMR90 Cells. IMR90 cells uninfected (CM) or infected with sh-control (shcon), shp21, shp53 or shp16 followed by selection were resolved by SDS-PAGE and subjected to Western blot analysis using antibodies indicated on right.

(A) **(B)**

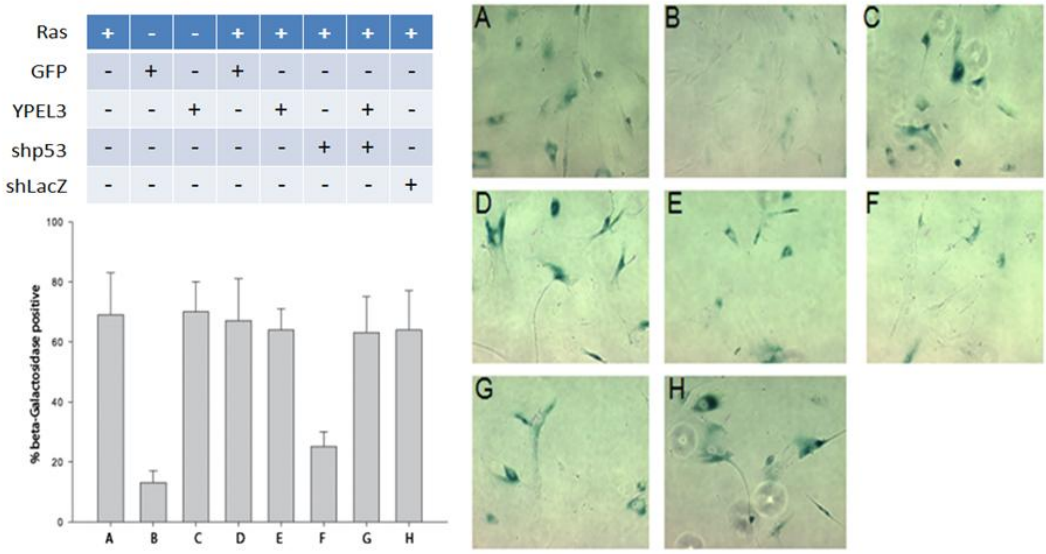

Figure 26: YPEL3 Functions Downstream of p53 During H-Ras^{G12V} Mediated Senescence in Human Diploid Fibroblasts as Measured by β-Galactosidase Staining. (A) Histogram represents average % β-Galactosidase positive cells where over 100 cells were counted for each transduction of IMR90 cells with (A) Ras (H-Ras^{G12V}) (B) GFP (C) YPEL3 (D) Ras+GFP (E) Ras+YPEL3 (F) Ras+shp53 (G) Ras+shp53+YPEL3 (H) Ras+shLacZ followed by incubation under selection for 7 days. Averages normalized to transduction efficiency based on % GFP positive cells (averaged from B and D) from three biological replicate experiments. Error bars represent standard error of the mean. (B) Representative images of treatment conditions described in (A) taken at same exposure time and 100X magnification. (Kelley *et al*., 2010)

When p53 levels were knocked down with H-Ras^{G12V} transduction (F), levels of senescence in IMR90 cells were lower (approximately 23%) than co-transduction of H-Ras^{G12V} and shLacZ (H) at approximately 68%, confirming that p53 is required for H-Ras^{G12V} mediated senescence in IMR90 cells. Interestingly, when YPEL3 is induced when p53 levels are knocked down with H-Ras^{G12V} infection (G), senescence levels return to levels similar to H-Ras^{G12V} infection alone. Together these results indicate that YPEL3 is functioning downstream of p53 in the induction of senescence in IMR90 cells by oncogenic Ras or parallel to p53 regardless of p53 levels.

To provide further support for the results obtained with the β-Galactosidase activity assay, SAHF analysis was completed under the same transduction conditions as described in Figure 26. As expected, the senescence levels measured by the percentage of SAHF positive cells (Figure 27) were similar to those observed using β-Galactosidase staining (Figure 26). This confirms that YPEL3 is functioning downstream of p53 in the H-Ras^{G12V} induced senescence pathway in non-transformed human fibroblasts. Additionally, the reduction of YPEL3 or p53 blocking H-Ras^{G12V} mediated senescence while YPEL3 rescues senescence blocked by reduction of p53 suggests that YPEL3 is a critical, downstream p53 target required for H-Ras^{G12V} mediated senescence.

To further investigate the mechanism through which YPEL3 is functioning as a senescence inducer, other key senescence related proteins, p16 and p21, were reduced in combination with H-Ras^{G12V}, YPEL3 or H-Ras^{G12V} and YPEL3 infection, followed by β-Galactosidase staining. p16 represents a direct link to the Rb arm of the senescence pathway and p21 is a link from the p53 pathway to the Rb pathway. p21 is a known p53

(A) **(B)**

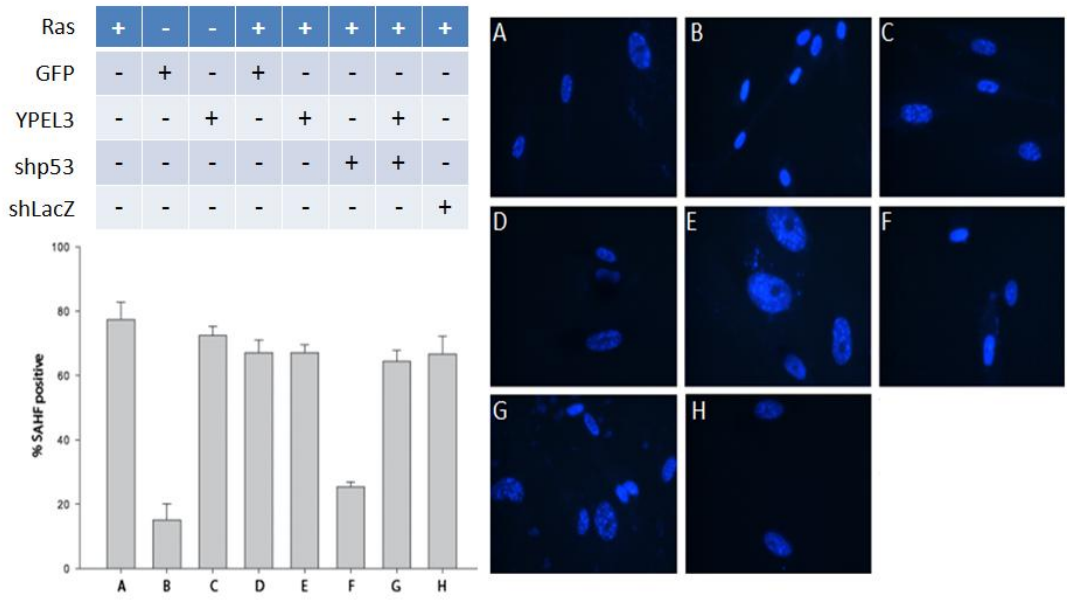

Figure 27: SAHF Analysis Confirms that YPEL3 Functions Downstream of p53 During H-Ras^{G12V} Mediated Premature Senescence. (A) Histogram represents average % SAHF positive cells where over 100 cells were counted for each transduction of IMR90 cells with (A) Ras (H-Ras^{G12V}) (B) GFP (C) YPEL3 (D) Ras+GFP (E) Ras+YPEL3 (F) Ras+shp53 (G) Ras+shp53+YPEL3 (H) Ras+shLacZ followed by incubation under selection for 7 days. Averages normalized to transduction efficiency based on % GFP positive cells (averaged from B and D) from three biological replicate experiments. Error bars represent standard error of the mean. (B) Representative images of treatment conditions described in (A) taken at same exposure time and 400X magnification. (Kelley *et al*., 2010)

target that is induced as cells undergo senescence and loss of p21 in human diploid fibroblasts allows them to bypass senescence programming (Brown et al., 1997). Additionally, loss of p16 allows for the block of oncogenic Ras mediated senescence in human diploid fibroblasts indicating the importance of the p16 arm of the senescence pathway in human cells (Brookes *et al*., 2002). Western blot analysis confirming knock-down of p16 and p21 using their respective short hairpin lentiviruses are demonstrated in Figure 25.

Infection of IMR90 cells with H-Ras^{G12V} induced senescence in approximately 55% of the cell and reducing levels of p16 or p21 blocked H-Ras^{G12V} mediated senescence as previously reported (Figure 28A). Interestingly, YPEL3 expression which is confirmed by RT-PCR (Figure 28B) rescued H-Ras^{G12V} mediated senescence blocked by reducing p16 but not p21. Future studies will be aimed at determining this discrepancy. H-Ras^{G12V} mediated senescence is carried out through complex signaling cascades and the inability of YPEL3 to rescue senescence blocked by lowering p21 may be explained through one of the many Ras mediated signaling cascades.

As previously indicated, YPEL3 induced senescence in IMR90 cells as measured by β-Galactosidase staining in approximately 58% of the cells (Figure 29A). When co-infected with shLacZ (control), shp16 or shp21, YPEL3 was still able to induce senescence in a similar percentage of IMR90 cells (approximately 57, 57 and 58%, respectively) while only 5-10% of the IMR90 cells scored β-Galactosidase positive when infected with no virus, GFP, shLacZ, shp16 or shp21 alone as controls. Validation of p16 and p21 knock down at the protein level in IMR90 cells using shp16 and shp21,

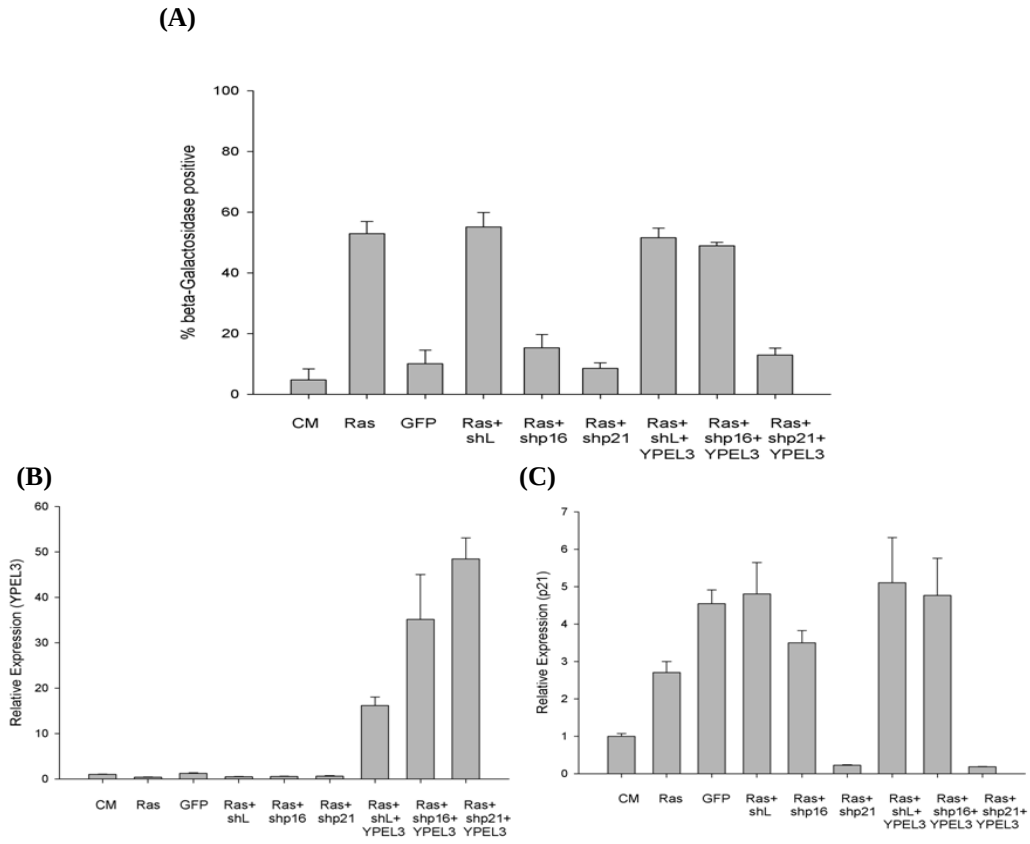

Figure 28: YPEL3 Rescues H-Ras^{G12V} Mediated Senescence Blocked by Decrease of p16 but Not p21. (A) Histogram represents average % β-Galactosidase positive cells where over 100 cells were counted for each transduction of IMR90 cells with no virus (CM), Ras (H-Ras^{G12V}), GFP, Ras+shL(shLacZ), Ras+shp16, Ras+shp21, Ras+shLacZ+YPEL3, Ras+shp16+YPEL3 or Ras+shp21+YPEL3 followed by incubation under selection for 7 days. Averages normalized to transduction efficiency based on % GFP positive cells from three biological replicate experiments. Error bars represent standard error of the mean. IMR90 cells uninfected (CM) or infected as in (A) were analyzed for YPEL3 (B) or p21 (C) mRNA levels normalized to GAPDH by RT-PCR. Error bars represent 95% confidence intervals (RT-PCR completed by Rebecca Tuttle, MD).

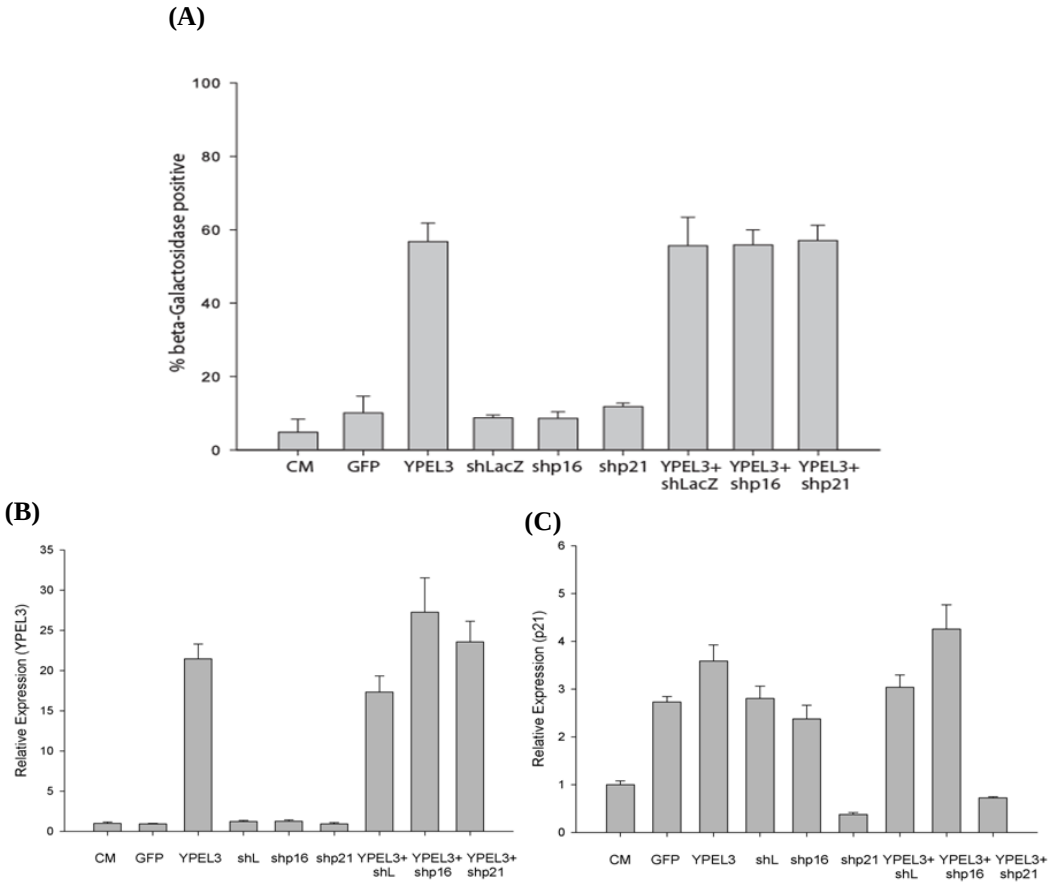

Figure 29: YPEL3 Functions Independent of p16 or p21 as a Senescence Inducer. (A) Histogram represents average % β-Galactosidase positive cells where over 100 cells were counted for each transduction of IMR90 cells with no virus (CM), GFP, YPEL3, shLacZ, shp16, shp21, YPEL3+shLacZ, YPEL3+shp16 or YPEL3+shp21 followed by incubation under selection for 7 days. Averages normalized to transduction efficiency based on % GFP positive cells from three biological replicate experiments. Error bars represent standard error of the mean. IMR90 cells uninfected (CM) or infected as in (A) were analyzed for YPEL3 (B) or p21 (C) mRNA levels normalized to GAPDH by RT-PCR. Error bars represent 95% confidence intervals (RT-PCR completed by Rebecca Tuttle, MD).

respectively, is shown in Figure 25. Expression of YPEL3 in treatment conditions where YPEL3 was infected is confirmed at the mRNA level by RT-PCR and is between 20 and 30 fold higher than control levels for each infection (Figure 29B). These results reinforce that expression of YPEL3 alone is sufficient to induce senescence in IMR90 cells and that this senescence is independent of p16 or p21 expression in these cells.

The addition of β-estradiol decreases YPEL3 expression in MCF7 Cells.

The estrogen receptor has been demonstrated to regulate p53 target genes through the presence of an estrogen response element next to a p53 response element (Menedez et al., 2007). Additionally, ERα was shown to bind directly to p53 and repress its function (Liu et al., 2006). YPEL3 has been described as a direct p53 target (Kelley et al., 2010), however, there is no predicted estrogen response element within the promoter region of YPEL3. It remains unknown whether ER signaling plays any role in regulation of YPEL3 gene expression, potentially through the interaction of p53 and ERα. Interestingly, a decrease in YPEL3 expression has been observed in breast tumor samples that contain ER negative status (personal communication R. Tuttle, MD). Taken together, this suggests that YPEL3 may be regulated through estrogen receptor signaling in a p53 dependent manner. Since YPEL3 is a direct p53 target, the hypothesis I tested is that expression of YPEL3 decreases in response to estrogen in ER+, wild-type p53 breast carcinoma cells.

To begin to investigate the role of the estrogen receptor in YPEL3 gene regulation, MCF7 breast carcinoma cells (ER+, wild-type p53) were incubated in complete media (CM) or charcoal stripped serum (CSS) for 48 hours followed by RNA

isolation and RT-PCR analysis (Figure 30). CSS is media that has been treated with activated carbon to remove non-polar materials such as certain growth factors, hormones and cytokines (purchased from Invitrogen) and served as a mechanism for estrogen removal. Expression of YPEL3 mRNA increased 4-fold accompanied by a corresponding increase in YPEL3 protein when MCF7 cells were treated with CSS compared to cells in CM suggesting that YPEL3 may at least indirectly be regulated by estrogen signaling (Figure 30). (RT-PCR analysis for the study of YPEL3 regulation by the estrogen receptor was completed by Rebecca Tuttle, MD).

To investigate the dependence of this increase in YPEL3 expression upon estrogen depletion, SKBr3 cells were utilized. These cells are ER- and have a gain-of function mutant p53. When incubated in CM or CSS for 48 hours there was no change detected in YPEL3 expression in these cells (Figure 31) supporting that it may in fact be estrogen receptor signaling that is responsible for the increase in YPEL3 expression after estrogen depletion. Since charcoal stripping serum removed all steroid hormones, adding back 17-β-estradiol (Sigma) to cells incubated in CSS allowed for the determination of gene expression modulation due specifically to estrogen removal. 17-β-estradiol (β-estradiol; beta-Estradiol; E_2) is the most potent, active form of the estrogen hormones. It serves as the most predominant sex hormone in females and is shown to induce transformation and tumorigenesis in human breast epithelial cells (Russo et al., 2006).

MCF7 cells were incubated in CSS for 24 hours prior to treatment with vehicle control (VC) or 17-β-estradiol (E2). The addition of 1nM β-estradiol to MCF7 cells reduced expression of YPEL3 approximately 50% compared to MCF7 cells incubated in

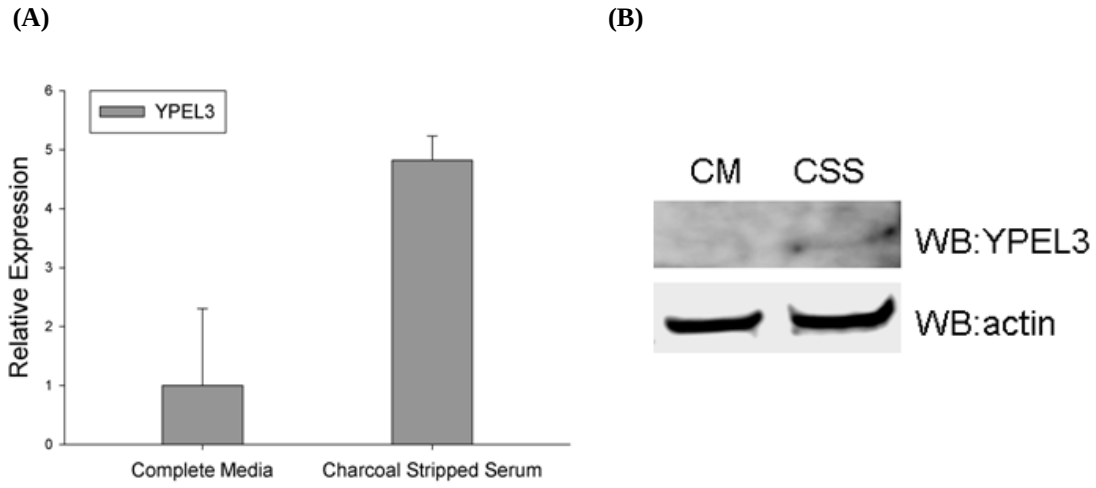

Figure 30: Expression of YPEL3 in MCF7 Cells Increases in Charcoal Stripped Serum. (A) RT-PCR analysis of YPEL3 expression normalized to GAPDH in MCF7 cells incubated in complete media (CM) or charcoal stripped media (CSS) for 48 hrs. Error bars represent 95% confidence intervals. (B) Protein was isolated from cells treated for 48 hours in CM or CSS followed by the addition of MG132 for the last 4 hours and resolved on a tricene gradient (low acrylamide concentration) gel followed by Western blotting. Antibodies used are indicated to the right of each image.

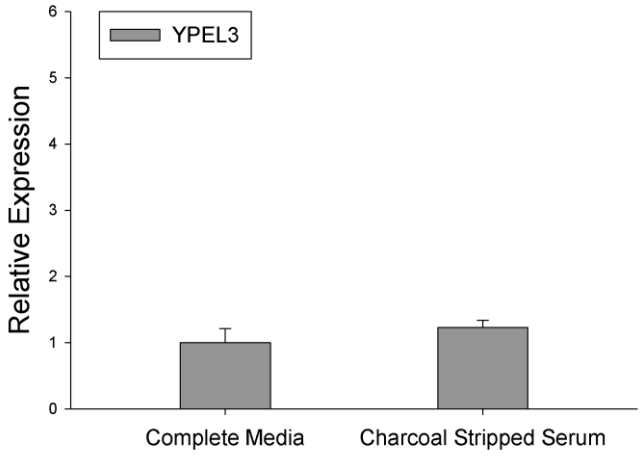

Figure 31: Expression of YPEL3 Is Unchanged in Charcoal Stripped Serum in an ER Negative Cell Line. RT-PCR analysis of YPEL3 expression normalized to GAPDH in SKBr3 cells incubated in complete media (CM) or charcoal stripped media (CSS) for 48 hrs. Error bars represent 95% confidence intervals.

CSS (Figure 32). This same concentration of β-estradiol produced a 2.5-fold increase in pS2 expression, which was used as a positive control in this experiment since pS2 is a known estrogen positively regulated gene. Increasing concentrations of β-estradiol did not further decrease the expression of YPEL3 or increase the expression of pS2 suggesting that 1 nM estradiol is a saturating dose for regulating gene expression of YPEL3 or pS2. This data supports the previous finding that YPEL3 may be regulated through the estrogen receptor and suggests that activation of the estrogen receptor by β-estradiol works to decrease YPEL3 expression in MCF7 cells.

Next, Tamoxifen was used to specifically block the interaction of estrogen with the estrogen receptor and further examine the regulation of YPEL3 expression. Tamoxifen is widely used clinically in the treatment of women with ER+ breast tumors for its ability to block the interaction of estrogen with the estrogen receptor (Osborne, 1998). MCF7 cells were incubated in CSS for 48 hours and showed a 3-fold increase in YPEL3 mRNA and a slight decrease in pS2 mRNA, as previously reported (Figure 32). The addition of 1 nM β-estradiol (E2) blocked the increase in YPEL3 or decrease in pS2 mRNA seen in CSS alone. More importantly, the further addition of 10 μM Tamoxifen to CSS+E2 reversed the E2 effects allowing a partial increase in YPEL3 and decrease in pS2 expression. Together, this data supports that YPEL3 gene expression is inhibited by estrogen, potentially through the estrogen receptor.

To address the p53 dependence of the increase of YPEL3 expression following estrogen removal, MCF7shp53 and MCF7shCON cell lines were generated. Knock down of p53 at the mRNA and protein level in the MCF7shp53 stable pools was

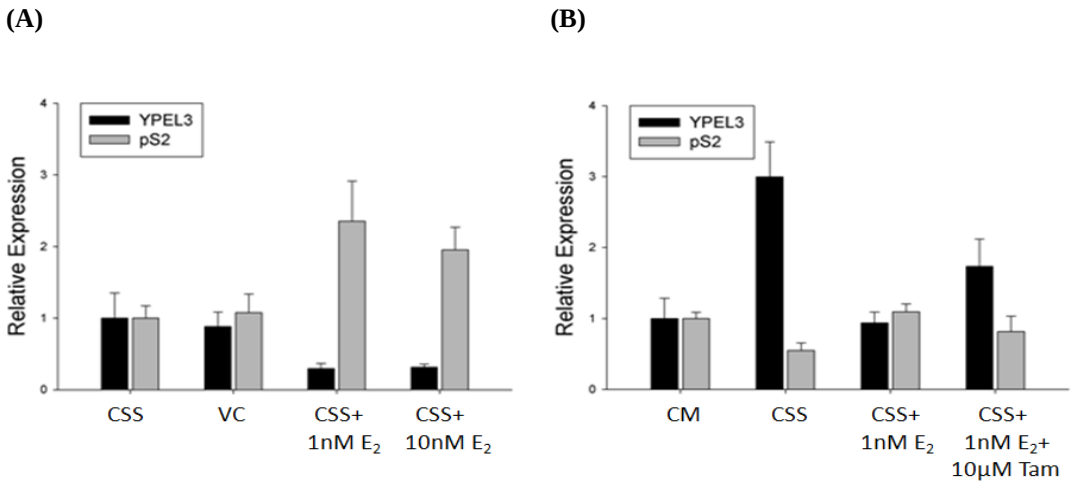

Figure 32: Decrease of YPEL3 Expression in MCF7 Cells Treated with β-estradiol is Partially Blocked by Tamoxifen. (A) RT-PCR analysis of YPEL3 and pS2 expression normalized to GAPDH in MCF7 cells incubated in charcoal stripped media (CSS) for 24 hrs followed by treatment with vehicle control (ethanol) or β-estradiol (Estradiol) for 24 hrs. Error bars represent 95% confidence intervals. 4.1 µl ethanol represents highest volume used for β-estradiol administration and is used for VC. (B) RT-PCR analysis of YPEL3 and pS2 expression normalized to GAPDH in MCF7 cells incubated in complete media (CM) or charcoal stripped media (CSS) for 24 hrs followed by treatment with indicated Tamoxifen (Tam; µM) and/or β-estradiol (E_2; nM) in CSS for 24 hrs. Error bars represent 95% confidence intervals.

confirmed via RT-PCR and Western blotting (Figure 33A/B). MCF7shp53 and MCF7shCON cells were grown in CM or CSS. There was a similar increase in YPEL3 expression, approximately 3 fold and 3.5 fold in MCF7shCON and MCF7shp53 cells, respectively, in cells grown in CSS for 48 hours (Figure 33C). The expression of p21 was also monitored to determine if CSS incubation was inducing a p53 stress response and p21 expression was not modulated by incubation in CSS in either cell line, supporting the p53 independence of the increase in YPEL3 expression upon estrogen depletion (Figure 33C). These findings suggest that the increase in YPEL3 expression upon estrogen depletion is independent of p53.

To determine if estrogen repression of YPEL3 was dependent on ERα signaling, a similar approach was utilized wherein ERα was knocked down using RNAi in MCF7 cells, followed by incubation in CM or CSS and RT-PCR analysis of YPEL3 expression. MCF7shERα stable pooled cells were unable to be maintained; therefore, MCF7 cells were infected in shCON or shERα lentivirus at an MOI of 5. MCF7 cells infected with shCON exhibited the same expression profile as seen with parental cells when incubated in CSS for 48 hours with an approximate 2.8-fold increase in YPEL3 mRNA and slight reduction of pS2 mRNA (Figure 34). MCF7 cells infected with shERα and grown in CM also demonstrated a 3-fold increase in YPEL3 mRNA. Therefore, cells grown in the absence of estrogen or ERα both demonstrate an elevation of YPEL3 mRNA, suggesting that it is the cooperation of estrogen with ERα that is allowing for the observed change in YPEL3 expression. Reduction of ERα was confirmed at the mRNA and protein levels (Figure 34).

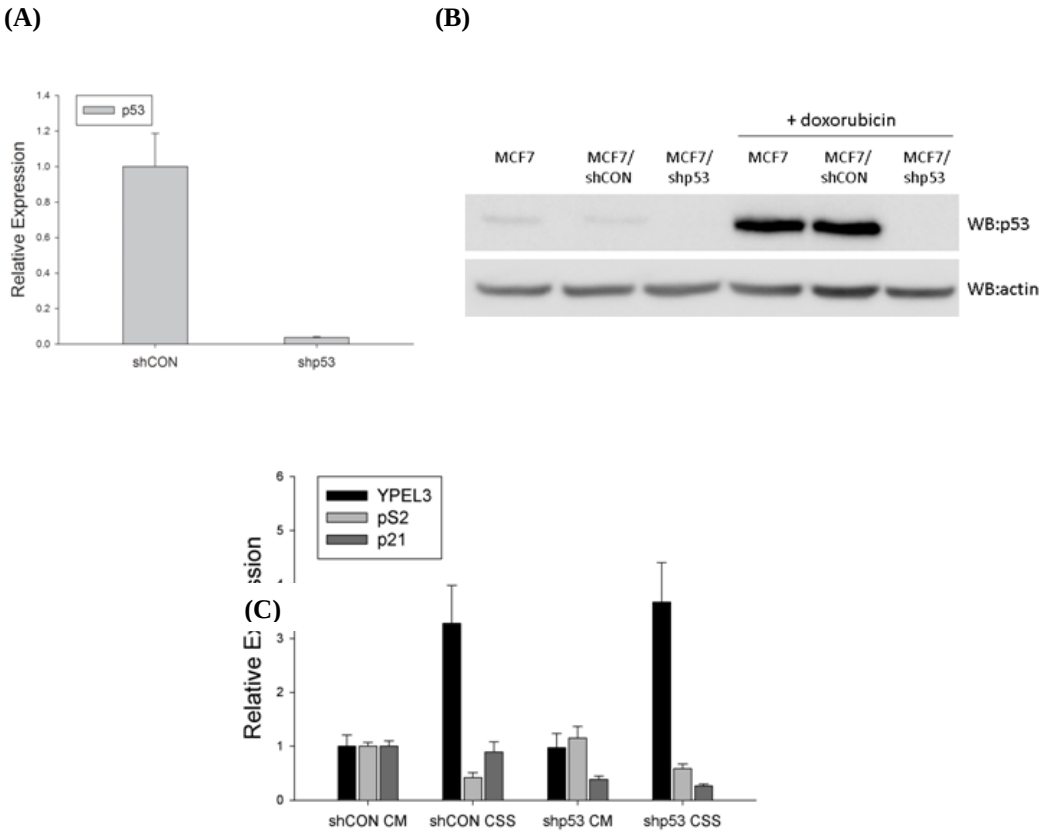

Figure 33: Increase in YPEL3 Expression Following Estrogen Depletion is Independent of p53. (A) RT-PCR analysis of p53 expression normalized to GAPDH in MCF7shCON and MCF7shp53 pooled, stable cells lines. Error bars represent 95% confidence intervals. (B) MCF7 parental, MCF7shCON and MCF7shp53 cells were treated without or with 0.5 μM doxorubicin overnight and whole cell extracts were resolved by SDS-PAGE and subjected to Western blotting. (C) RT-PCR analysis of YPEL3, pS2 and p21 expression normalized to GAPDH in MCF7shCON and MCF7shp53 cells incubated in CM or charcoal stripped media (CSS) for 48 hours. Error bars represent 95% confidence intervals.

(A) **(B)**

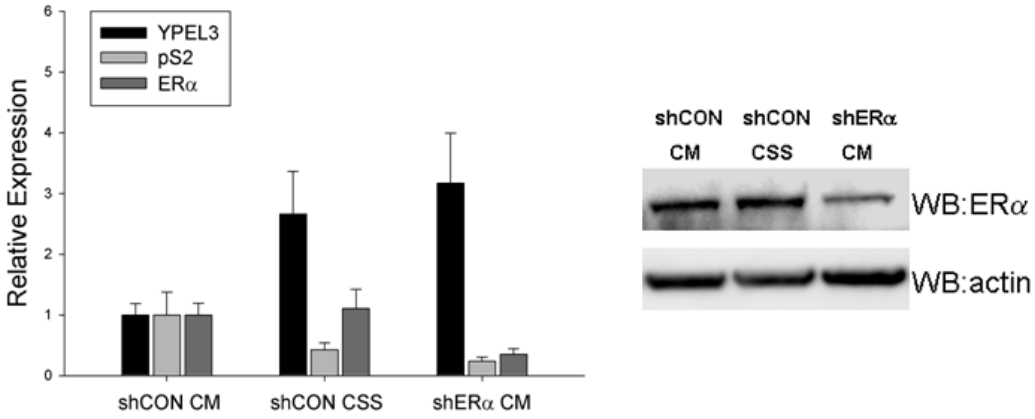

Figure 34: Increase in YPEL3 Expression Following Estrogen Depletion is Dependent on ERα. (A) RT-PCR analysis of YPEL3, pS2 and ERα expression normalized to GAPDH in MCF7 cells infected with shCON or shERα at an MOI of 5 and incubated in CM or CSS for 48 hours. Error bars represent 95% confidence intervals. (B) Whole cell extracts prepared from cells treated as in (A) were resolved by SDS-PAGE and subjected to Western blotting.

Removal of Estrogen Induces YPEL3-Dependent Senescence in MCF7 Cells.

Tamoxifen has been indicated to trigger a G_0/G_1 cell cycle arrest in ER+ breast tumors (Osborne, 1998). It has also been shown that the addition of estrogens can relieve the G_0/G_1 cell cycle block of MCF7 cells after treatment with Tamoxifen (Planas-Silva, et al., 1997). Additionally, over expression of YPEL3 was shown to induce senescence in MCF7 cells (Figure 19) and removal of estrogen by charcoal stripping the serum was shown to increase YPEL3 expression in MCF7 cells 4-fold compared to cells in complete media (Figure 30). Together this information led to the hypothesis that removal of estrogen from MCF7 cells would increase YPEL3-dependent senescence.

To address this hypothesis, wild-type MCF7 cells along with pooled stable populations of MCF7shLacZ and MCFshYPEL3 (A) and (B) cells characterized in Figure 16 were utilized. MCF7 cells were incubated in CM, CSS, or CSS plus 1 nM β-estradiol (E_2) for 6 days followed by β-Galactosidase staining (Figure 35A). Approximately 80% of the cells grown in CSS scored β-Galactosidase positive compared to approximately 12% of the cells in CM (Figure 35A). Since charcoal stripping the serum removes many hormones, growth factors and cytokines from the system, adding back of 1 nM estradiol allowed for investigation of the estrogen specific effects. When cells were incubated in CSS + 1 nM estradiol, the percentage of β-Galactosidase positive cells returned to approximately 35% indicating that the increase in β-Galactosidase staining upon treatment of cells in CSS was partially due to the removal of estrogen (Figure 35A). The addition of higher concentrations of estradiol (up to 100 nM) returned the percentage of β-Galactosidase positive cells to control level (Figure 35C).

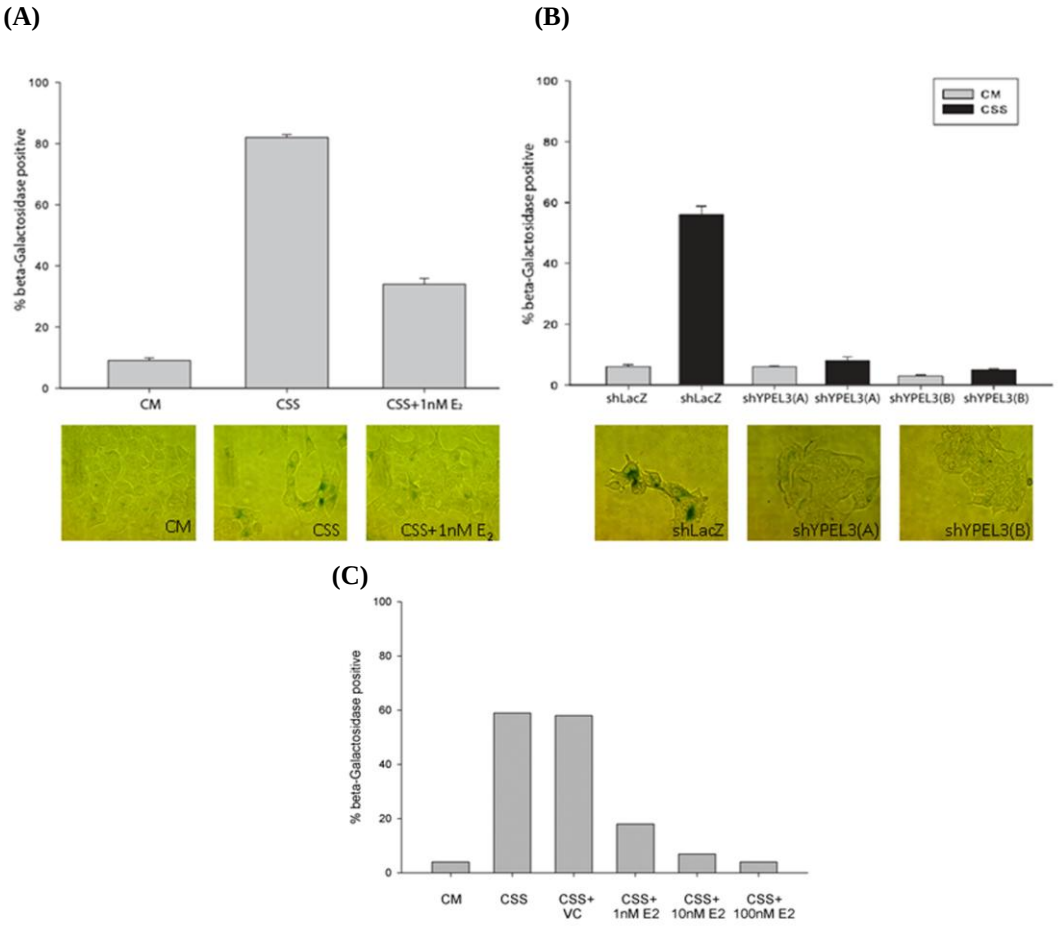

Figure 35: Removal of Estrogen Triggers YPEL3-Dependent Senescence in MCF7 Cells as Measured by β-Galactosidase Staining. (A and B) Top: Histogram representing the average % β-Galactosidase positive cells per treatment condition +/- standard error of the mean of at least 100 cells counted per treatment condition in biological triplicate. Cells were incubated for 6 days in indicated media. Bottom: Representative images of cells treated as in top histogram. Images taken at 100X magnification and same exposure time. (C) Histogram representing the average % β-Galactosidase positive cells per treatment condition of at least 100 cells counted per treatment condition. Cells were incubated for 6 days in indicated media.

Next, the role of YPEL3 in the induction of senescence of MCF7 cells upon estrogen depletion was investigated. MCF7shLacZ, MCF7shYPEL3(A) and MCF7shYPEL3(B) pooled, stable cell populations were incubated in CM or CSS for 6 days followed by β-Galactosidase staining as previously described for parental MCF7 cells. Approximately 58% of MCF7shLacZ expressing control cells scored β-Galactosidase positive when incubated in CSS for 6 days (Figure 35B). MCF7shYPEL3(A) and MCF7shYPEL3(B) expressing cells had baseline levels of β-Galactosidase staining when incubated in CSS for 6 days suggesting that the increase in senescence as measured by β-Galactosidase staining in MCF7 cells upon estrogen removal is dependent on YPEL3. The use of two separate shRNA constructs decreases the likelihood that the effect observed by silencing YPEL3 is the result of an off target effect, further confirming the specificity for the role of YPEL3 in estrogen removal mediated senescence.

Since the increase in YPEL3 expression in MCF7 cells following estrogen depletion was independent of p53 expression and dependent on ERα, I next investigated the role of p53 and ERα in CSS induced senescence of MCF7 cells. Incubation of MCF7shCON and MCF7shp53 cells (described in Figure 33) in CSS for 6 days led to an increase in β-Galactosidase positive cells, both at approximately 45% compared to CM incubated cells both with control β-Galactosidase positive percentages at 5% or below (Figure 36A). This finding supports the previous finding that the increase in YPEL3 expression and senescence induction of MCF7 cells following estrogen depletion is independent of p53.

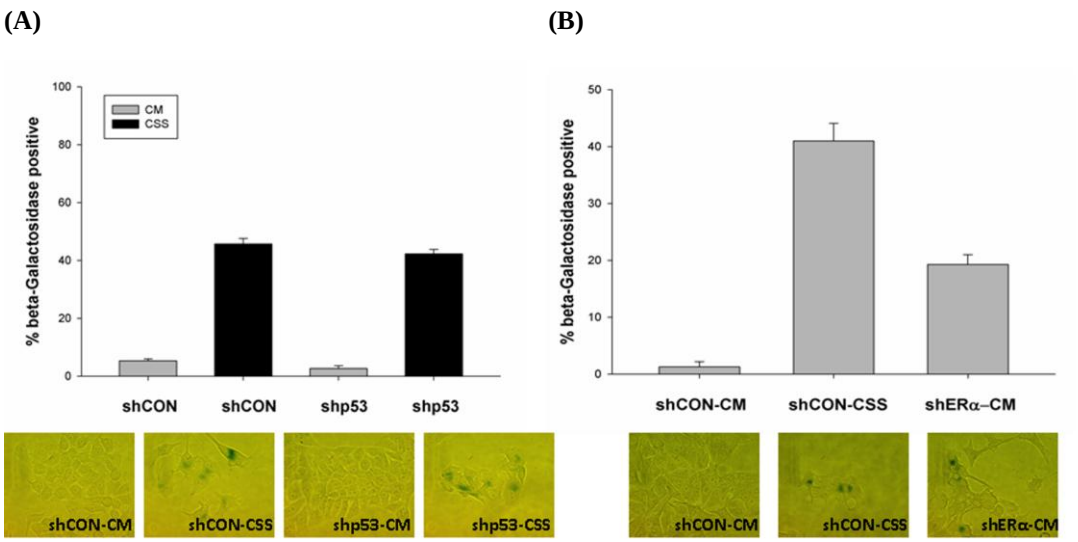

Figure 36: Removal of Estrogen Triggers ERα Dependent and p53 Independent Senescence in MCF7 Cells as Measured by β-Galactosidase Staining. (A) Top: Histogram representing the average % β-Galactosidase positive cells per treatment condition +/- standard error of the mean of at least 100 cells counted per treatment condition in biological triplicate. Cells were incubated for 6 days in indicated media. Bottom: Representative images of cells treated as in top histogram. Images taken at 100X magnification and same exposure time. (B) Top: Histogram representing the average % β-Galactosidase positive cells per treatment condition +/- standard error of the mean of at least 100 cells counted per treatment condition in biological triplicate. Cells were infected with shCON or shERa at an MOI of 5 incubated for 6 days in indicated media. Bottom: Representative images of cells treated as in top histogram. Images taken at 100X magnification and same exposure time.

Further evaluation of MCF7 cells infected with either shCON or shERα at an MOI of 5 followed by incubation in CSS for 6 days and β-Galactosidase staining revealed interesting results. In correlation with the expression of YPEL3 demonstrated in Figure 33, when ERα expression is reduced in MCF7 cells incubated in CM approximately 20% of the cells scored β-Galactosidase positive (Figure 36B). This increase in β-Galatosidase staining is not as high as the 40% of shCON infected cells incubated in CSS which is most likely due to the incomplete knock-down of ERα in these cells (see Figure34B) or that as stated previously, charcoal stripping serum removes more than estrogen. Together this data supports that the induction of senescence of MCF7 cells deprived of estrogen is dependent on ERα but independent of p53.

Tamoxifen is widely used clinically as an estrogen receptor blocker and has been demonstrated to reduce tumor burden in 50% of women with ER+ breast cancer (Osborne, 1998). It has also been shown to induce a G_0/G_1 cell cycle arrest in ER+ breast tumors, as mentioned previously. Therefore, I decided to evaluate Tamoxifen for its ability to induce YPEL3 expression and cellular senescence of MCF7 cells grown in CM (estrogen containing media). MCF7shLacZ cells treated with Tamoxifen compared to VC showed an increase in β-Galactosidase positive cells (35% and 5%, respectively) (Figure 37B) and YPEL3 mRNA (Figure 37A). While there was some induction of YPEL3 mRNA in shYPEL3 expressing MCF7 cells treated with Tamoxifen, these levels were insufficient to induce senescence. Only about 2% of the MCF7shYPEL3(A) vehicle control treated cells scored β-Galactosidase positive while approximately 5% of the MCF7shYPEL3(A) Tamoxifen treated cells scored β- Galactosidase positive (Figure

(A) **(B)**

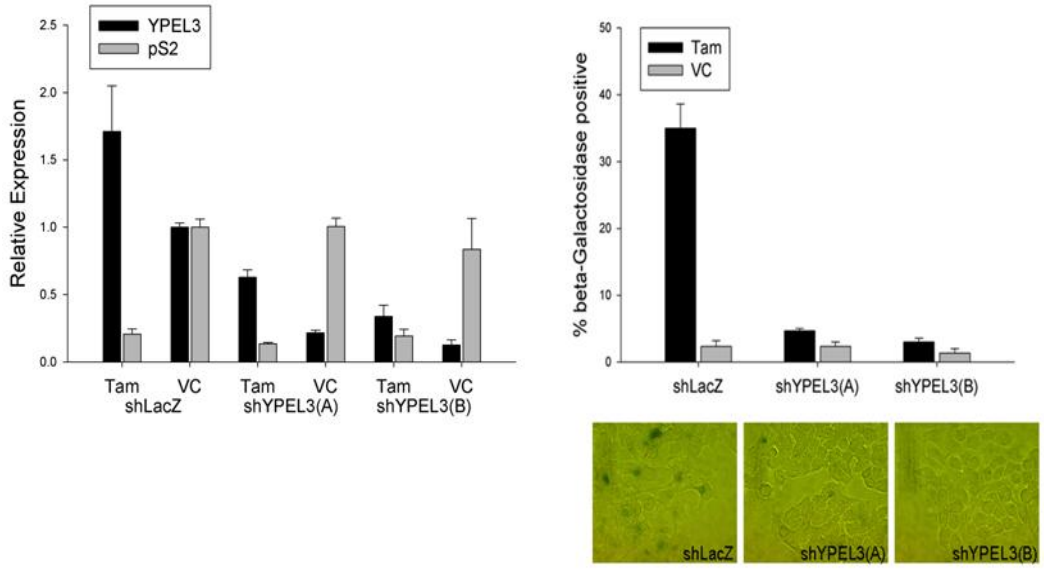

Figure 37: Tamoxifen Induces YPEL3 Dependent Senescence in MCF7 Cells.

(A) RT-PCR analysis of YPEL3 and pS2 expression normalized to GAPDH in MCF7shLacZ, MCF7shYPEL3(A) or MCF7shYPEL3(B) pooled, stable cell lines incubated in CM containing 0.5 μM Tamoxifen or vehicle control (VC) for 6 days. Error bars represent 95% confidence intervals. (B) Top: Histogram representing the average % β-Galactosidase positive cells per treatment condition +/- standard error of the mean of at least 100 cells counted per treatment condition in biological triplicate. Cells were treated as in (A). Bottom: Representative images of cells treated as in top histogram. Images taken at 100X magnification and same exposure time.

37B). These findings indicate that Tamoxifen can induce senescence in MCF7 cells and that this senescence is dependent on YPEL3 expression.

IV. Discussion

Uncovering the specific genes and regulatory mechanisms responsible for the induction and maintenance of tumor cell senescence is an active area of research which will hopefully lead to the development of new anti-cancer therapeutics, potential biomarkers for diagnostic or prognostic purposes and many other advances in the treatment of cancer. At the nexus of senescence induction is the p53 tumor suppressor protein. This study was designed to investigate the activation of p53 and its subsequent actions that lead to the induction of cellular senescence.

Reduction of HdmX Induces Cellular Senescence in Prostate Adenocarcinoma Cells

I first set out to investigate HdmX's contribution to the senescence pathway. Like MdmX in mouse embryonic fibroblasts, HdmX was demonstrated to block H-Ras^{G12V} mediated senescence in human diploid fibroblasts (Figure 7). To assess the role of HdmX interactions with p53 and Hdm2 on cellular senescence, point mutations were made in HdmX inhibiting its ability to bind p53 or Hdm2 (HdmXG57A and HdmXC437G, respectively). When substituted for wild-type HdmX in combination with H-Ras^{G12V}, neither mutant was able to block H-Ras^{G12V} mediated senescence suggesting that HdmX binding to p53 and Hdm2 are required to block oncogene induced senescence (Figure 10).

HdmX directly binding to p53 has been demonstrated to be required for its negative regulation of p53, which most likely explains why HdmXG57A cannot block H-Ras^{G12V} mediated senescence. Some of HdmX's activities have also been suggested via its direct interaction with Hdm2. For example, HdmX is shown to translocate to the nucleus by binding Hdm2 (Migliorini *et al*., 2002) and the heterodimer of HdmX:Hdm2 has been shown to be more stable than either protein alone (Tanimura *et al*., 1999). The nuclear cytoplasmic fractionation study in this thesis supported that HdmX binding to Hdm2 facilitates its nuclear localization where HdmX must bind to p53 to inhibit transactivation (Figure 11). The Western blots shown in Figures 8 and 11 also support that HdmX:Hdm2 heterodimer is the more stable form of the protein because HdmXC437G appeared less stable than wild-type HdmX or HdmXG57A when infected at the same MOI. Defining these required binding partners for HdmX's ability to block H-Ras^{G12V} mediated senescence may provide further direction for the development of effective small-molecules to trigger HdmX cytoplasmic localization.

Reports suggest that HdmX is over expressed in several tumors, most of which maintain wild-type p53 (Table 1; Wade *et al*., 2009). Interestingly, 90% of pancreatic, 50% of colon and thyroid and 30% of all human tumors have mutated Ras (Saxena *et al*., 2008) which makes the tumor phenotype of mutant Ras, wild-type p53 and high levels of HdmX likely. Since HdmX can block H-Ras^{G12V} induced senescence in untransformed human diploid fibroblasts as demonstrated in Figure 7, knocking down HdmX in tumor cells with mutant Ras, wild-type p53 and high levels of HdmX was hypothesized to induce senescence.

In fact, using shRNAi targeting HdmX induced senescence as indicated by an increase in beta-Galactosidase staining LNCaP cells (wild-type p53, mutant Ras, high HdmX). To demonstrate that the increase of beta-Galactosidase positive LNCaP cells upon sh-HdmX infection was specific to knocking down HdmX and not an off-target effect of the short-hairpin construct, HdmX protein levels were rescued in LNCaP cell using a Lentivirus-HdmX expression vector harboring a silent mutation that makes the hdmX mRNA from this cDNA resistant to the hdmX short hairpin RNA with an accompanied background level of senescence induction. These results support that the specific reduction of HdmX in LNCaP cells leads to tumor cell senescence as measured by beta-Galactosidase staining.

Huang and colleagues reported that epithelial tumor cells treated with Nutlin became beta-Galactosidase positive; however, upon drug removal, these beta-Galactosidase positive cells resumed proliferation (Huang *et al*., 2009). To confirm that the beta-Galactosidase positive cells detected in our study upon reduction of HdmX represented irreversible senescence, HdmX protein was added back after cells underwent senescence (day 7) followed by an additional 7 day incubation and beta-Galactosidase staining at day 14. In contrast to Nutlin treatment, reduction of HdmX protein in LNCaP cells did not change the percentage of beta-Galactosidase positive cells, supportive of irreversible senescence induction of these tumor cells.

As described, tumor cells have also been shown to undergo senescence following treatment with chemotherapeutic drugs, radiation or differentiating agents *in vitro* and *in vivo* (Roninson, 2003). The advantage of tumor cell senescence as an endpoint for anti-

cancer therapy has been supported by studies suggesting that senescent tumor cells are cleared by the immune system allowing for subsequent tumor regression (Xue et al., 2007; Ventura et al., 2007). These findings illustrate the potential clinical impact of the senescence observed in LNCaP cells after reduction of HdmX.

HdmX as a target for anti-cancer drug design has been supported by a number of studies. Treatment of tumors in mice that are over expressing MdmX with siMdmX has been shown by Gilkes and colleagues to reduce tumor volume through an unknown mechanism (Gilkes *et al*., 2006). Since the use of siRNA as a drug has had many clinical trial failures (Tiemann *et al*., 2009), there is a current push to develop small-molecule inhibitors that may have fewer off target effects. Once small molecule inhibitors of HdmX are developed through an intense screening process, they must be examined for their biological activity. While the findings discussed above outline a potential biological assay to examine novel HdmX small molecule inhibitors, they also suggest that targeting HdmX may lead to human tumor cell senescence.

The first small molecule inhibitor of MdmX, SJ-172550, was recently described (Reed *et al*., 2010). This inhibitor is described for its ability to block the MdmX : p53 interaction by binding to the p53 binding pocket of MdmX (Figure 38). This inhibitor was demonstrated to effectively kill MdmX overexpressing retinoblastoma cells. Interestingly, SJ-172550 was also demonstrated to function in an additive manner when combined with Mdm2 inhibitor, Nutlin-3a (Reed *et al*., 2010). Examining the effectiveness of these small molecule inhibitors on senescence induction of LNCaP cells along with other cell lines would provide further validation and mechanistic detail for

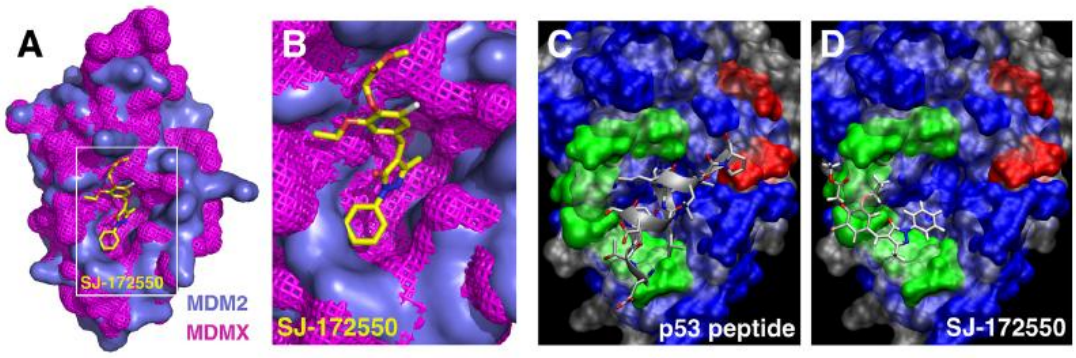

Figure 38: The First Small Molecule Inhibitor of MdmX. (A and B) Space filling model with overlaid Mdm2:Nutlin-3a (teal) with MdmX:SJ-172550 (pink) showing SJ-172550 bound to the p53 binding pocket of Mdm2/MdmX. (C) Position of the p53 peptide binding to MdmX based on the Mdm2/peptide crystal structure. Gray is the surface of Mdm2, blue/green/red is the surface of MdmX. (D) Primary docking pose of SJ-172550 to MdmX superimposed on the crystal structure of p53 peptide bound to Mdm2. Gray is the surface of Mdm2, blue/green/red is the surface of MdmX. (Reed *et al*., 2010).

their future testing in an animal model. Also, development of additional MdmX small molecule inhibitors targeting the MdmX : Mdm2 interaction may prove beneficial for use in combination with SJ-172550 based on the data generated in this study using HdmXC437G.

Expression of YPEL3 Induces Cellular Senescence

The re-activation of wild-type p53 by targeting HdmX in tumor cells, as described above, led to the induction of cellular senescence. While p53 signaling is critical to senescence induction, down-stream p53 targets required for the induction of cellular senescence have not been fully elucidated. Uncovering these players of the senescence pathway would represent potential drug targets useful in treating tumors containing mutant p53, where re-activation of p53 itself is not an option.

A microarray screen where p53 was activated by silencing its negative regulators, Hdm2 and HdmX, uncovered a potential p53 target, YPEL3 (Heminger *et al*., 2009). The validation of YPEL3 as a direct p53 target was completed by biochemical assays including ChIP analysis (Kelley *et al*., 2010); however, the biological role for human YPEL3 was unknown. This study provides evidence that YPEL3 is growth suppressive through the induction of cellular senescence in human tumor (MCF7 and U2OS) and non-transformed (IMR90) cell lines. Expression of YPEL3 reduced colony formation in MCF7 and U2OS human tumor cell lines and shYPEL3 expressing MCF7 cells demonstrated increased cellular proliferation compared to shLacZ expressing control cells supporting the growth suppressive activity of YPEL3. The induction of senescence

by YPEL3 was confirmed via beta-Galactosidase staining along with senescence associated heterochromatin formation (SAHF).

To begin to position YPEL3 within the senescence pathway, RNAi technology was utilized in IMR90 cells (human diploid fibroblasts), a cell line often used in the study of senescence due to its non-transformed nature and ability to undergo oncogenic Ras mediated and replicative senescence. Knocking down YPEL3 blocked H-Ras^{G12V} mediated senescence in IMR90 cells, suggesting that YPEL3 is a critical p53 target during H-Ras^{G12V} mediated senescence. Two separate short hairpin lentiviruses targeting YPEL3 were used in combination with H-Ras^{G12V} infection and both blocked senescence, suggesting that the specific reduction of YPEL3 is sufficient to block H-Ras^{G12V} mediated senescence. Furthermore, using RNAi targeting p53, it was demonstrated that YPEL3 is most likely functioning downstream of p53 in the Ras mediated senescence pathway.

Further probing of the senescence pathway using RNAi targeting p21 and p16 unveiled that YPEL3 is sufficient to induce senescence in human diploid fibroblasts and that this senescence induction is independent of p21 or p16 expression. p16 and p21 are known to play critical roles in non-transformed and tumor cell senescence (Shay *et al*., 2004). However, senescence induction has also been observed in non-transformed and tumor cell lines where p21 or p16 has been inactivated or is functionally absent, suggesting that other genes may mediate cellular senescence in these backgrounds. Therefore, YPEL3 may represent a novel cellular senescence mediator functioning

independent from p16 and p21. Additionally, results in Figure 29A suggest that neither p21 nor p16 are functioning downstream of YPEL3 during YPEL3 induced senescence.

Further evaluation of YPEL3's ability to rescue H-Ras^{G12V} mediated senescence blocked by reduction of p16 or p21 revealed intriguing results. While YPEL3 was able to rescue H-Ras^{G12V} mediated senescence blocked by reduction of p16, it could not rescue senescence in the presence of H-Ras^{G12V} and shp21. This finding will provide the foundation for a future project aimed at uncovering why YPEL3 is not sufficient to induce senescence in the presence of H-Ras^{G12V} and reduced p21. One possible explanation is that in the presence of H-Ras^{G12V} and reduced p21, YPEL3 may induce an apoptotic mechanism in IMR90 cells. This is supported by the observation that while H-Ras^{G12V}, shp21 and YPEL3 triple infected cells are not scoring β-Galactosidase positive they are also not proliferating like complete media or shLacZ infected control cells as indicated by the reduced number of cells in the H-Ras^{G12V}, shp21 and YPEL3 infected field compared to shLacZ infection control (Figure 39). Further investigation of this observation is required to make any conclusions about YPEL3's function in the presence of H-Ras^{G12V} and absence of p21.

This study of YPEL3's role in senescence has been limited to the H-Ras^{G12V} mediated senescence model using human diploid fibroblasts. There are many ways to induce tumor and non-transformed cells to senesce including, but not limited to, using agents that induce oxidative stress or DNA damage (Shay *et al*., 2004). For example, MCF7 breast carcinoma cells are shown to senesce in a p53-dependent manner after treatment with the DNA damaging agent Doxorubicin (Adriamycin) (Elmore *et al*., 2002). The modulation and dependence of YPEL3 gene expression can be evaluated

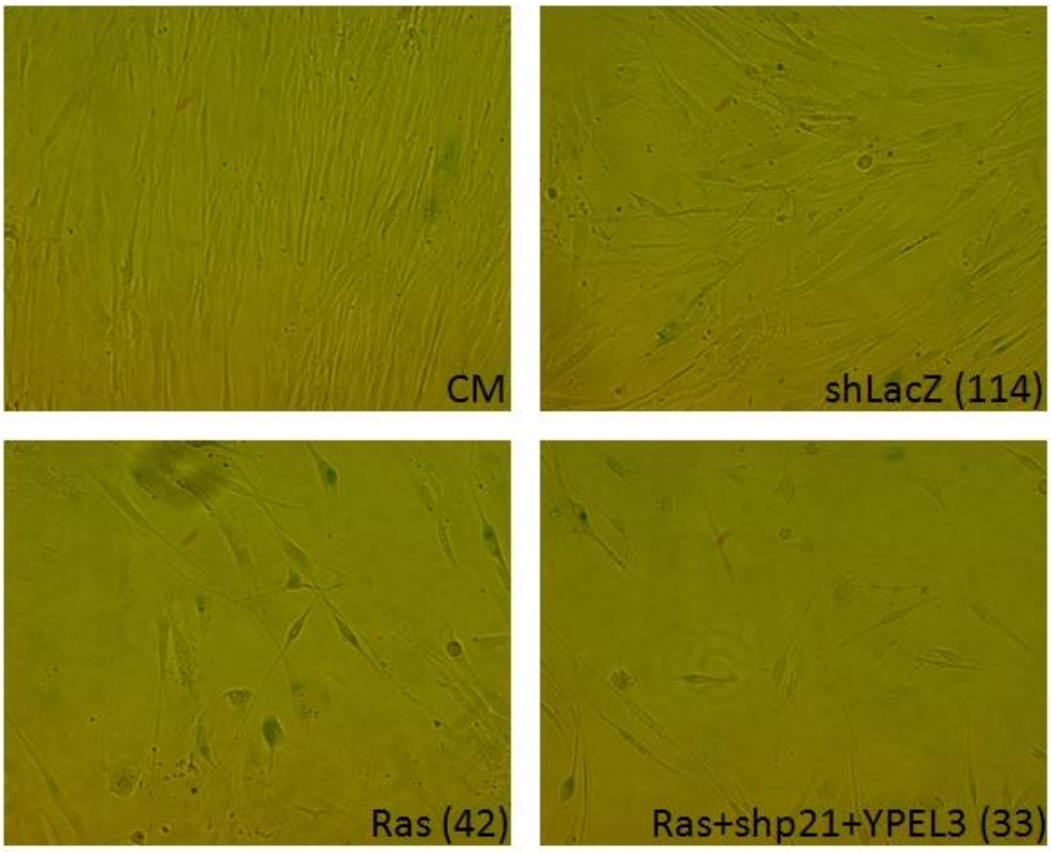

Figure 39: YPEL3 May Induce Apoptosis in the Presence of H-Ras^{G12V} and Absence of p21. Representative images of IMR90 cells infected as indicated at the bottom of the image, which was taken at 100X magnification and same exposure time. (Ras=H-Ras^{G12V}) Numbers listed for shLacZ, Ras and Ras+shp21+YPEL3 indicate approximate total number of cells present in image.

under this and other established cell culture conditions that induce senescence to further investigate the role of YPEL3 in senescence induction. Generation of this data will provide further mechanistic information describing how YPEL3 is involved in the senescence pathway and may strengthen the argument to target YPEL3 as an anti-cancer therapeutic.

YPEL3 is sufficient to induce accelerated senescence in human tumor and non-transformed cell lines, but it remains to be determined whether YPEL3 is involved in replicative senescence. Using aged IMR90 cells, the relative expression of YPEL3 can be monitored over passages to determine if YPEL3 mRNA increases as cells approach or enter replicative senescence. RNAi targeting YPEL3 and LacZ (control) can also be utilized to determine if knocking down YPEL3 is sufficient to block or delay replicative senescence in IMR90 cells. These types of experiments can be used to determine if YPEL3 has any role in replicative senescence, and if so, would further implicate YPEL3 as a tumor suppressor protein.

As previously mentioned, differences in the critical proteins involved in the senescence pathway in mouse and human cell culture systems have been noted. Future directions for this project include using a mouse model system, so I wanted to determine if YPEL3 was also sufficient to induce senescence in MEFs to begin to investigate both the mouse and human senescence pathways. Early data indicate that expression of YPEL3 is sufficient to induce senescence in MEFs, also (Figure 40). As in IMR90s, it will also be important to determine if YPEL3 has a role in replicative senescence in MEFs. If loss of YPEL3 does enable MEFs to escape replicative senescence, then

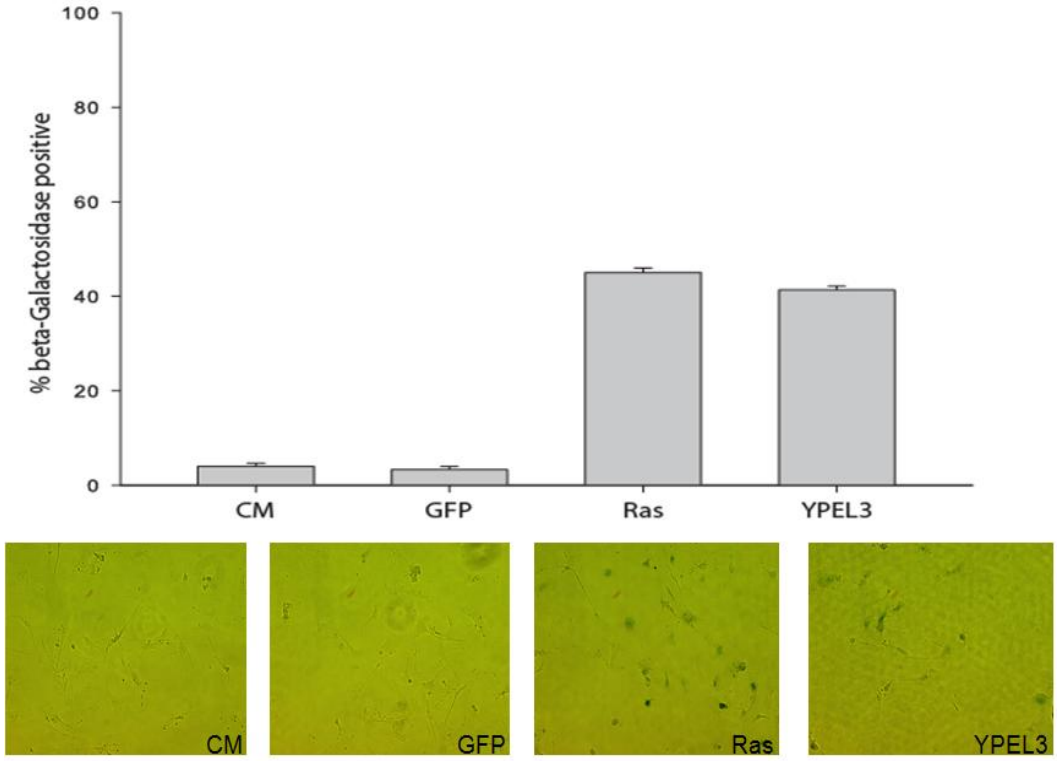

Figure 40: YPEL3 Is Sufficient to Induce Senescence in MEFs. MEFs infected with CM, GFP, Ras (H-Ras^{G12V}) or YPEL3 were incubated under selection for 7 days followed by β-Galactosidase staining. Histogram represents the average % β-Galactosidase positive cells from 3 independent experiments +/- SEM per treatment condition normalized to transduction efficiency determined by % GFP positive cells. (CM = complete media, Ras = H-Ras^{G12V}). Representative images from each treatment condition taken at 100X magnification and same exposure time are shown below.

cellular proliferation and transformation assays can be completed using MEFs to determine if YPEL3 is in fact functioning as a tumor suppressor protein, which is yet to be determined. More importantly, studies using MEFs may support knocking out YPEL3 in mice as a useful direction for the future study of YPEL3.

Further testing will be necessary to determine the mechanism through which YPEL3 is functioning to induce cellular senescence. Uncovering YPEL3 binding partners using either a yeast two-hybrid screening approach or co-immunoprecipitation followed by mass spectrometry may reveal binding partners of YPEL3 and provide direction for future mechanistic evaluation. Additionally, while a crystal structure of YPEL3 protein is not currently available, structural modeling programs have been used to determine a predicted structure from which correlations to function can be made (personal communication, Kevin Kelley). Together, these types of studies may assist in unveiling the detailed mechanism for YPEL3's ability to induce cellular senescence.

YPEL3 Expression Increases Following Estrogen Depletion Leading to Senescence

If YPEL3 is in fact functioning as a tumor suppressor protein, then YPEL3 expression may be reduced in human tumor tissue compared to normal control. To examine this hypothesis, eight different tumor types were screened for their mRNA expression of YPEL3 revealing that colon, lung and ovarian tumors contained statistically significant reductions of YPEL3 mRNA expression compared to normal controls (Kelley *et al*., 2010; personal communication Rebecca Tuttle). While examining this data, changes in YPEL3 expression were noted in breast tumor samples that appeared to correlate with ER status (personal communication R. Tuttle, MD). In a gene expression

profiling experiment where estrogen was added back to ER+ breast cancer cell lines, YPEL3 was uncovered in a list of down-regulated genes all lacking a defined estrogen response element (ERE) (Cicatiello *et al*., 2010). Therefore, we sought to examine whether YPEL3 is regulated through estrogen receptor signaling.

To begin to investigate the role of the estrogen receptor in YPEL3 gene regulation, MCF7 breast carcinoma cells (wild-type p53) were grown in charcoal stripped serum (CSS) to remove steroid hormones including estrogen. These cells demonstrated a 4-fold increase in YPEL3 gene expression and corresponding increase in YPEL3 protein compared to MCF7s grown in CM (Figure 30). No modulation of YPEL3 expression was detected in an ER- breast tumor cell line (SKBr3) grown in CM compared to CSS suggesting that the increase in YPEL3 upon estrogen removal occurs through the presence of an estrogen receptor (Figure 31). The add-back of 1 nM β-estradiol reduced YPEL3 mRNA compared to CSS alone while Tamoxifen blocked this reduction, further supporting that the increase of YPEL3 expression upon CSS treatment was specific to estrogen depletion and may be occurring through ER signaling.

YPEL3 was previously described as a direct p53-target gene (Kelley *et al*., 2010); therefore, the next step was to determine if the increase of YPEL3 expression upon estrogen depletion was dependent on p53. Using MCF7shp53 and MCF7shCON pooled, stable cell lines, estrogen removal was demonstrated to increase YPEL3 expression independent of p53. This finding was somewhat surprising and lead to the examination of the YPEL3 promoter region for an estrogen response element (ERE). Transfac (http://www.biobase-international.com/pages/index.php?id=transfac), a database

designed to investigate transcription factor binding sites, predicted no classic ERE contained within the YPEL3 promoter region, making the direct regulation of YPEL3 by the estrogen receptor unlikely. It was important at this point to determine if the increase of YPEL3 expression following estrogen removal was dependent on the presence of the estrogen receptor or if there was some indirect mechanism through which estrogen depletion was regulating YPEL3.

RNAi specifically targeting ERα in MCF7 cells was utilized to reveal that the increase in YPEL3 expression after estrogen depletion is in fact dependent on the presence of ERα. Together this data suggests that YPEL3 expression is inhibited by estrogen in breast cancer cells at least indirectly through the estrogen receptor. While examining the YPEL3 expression data was the first step, it was necessary to next determine if the increase of YPEL3 expression following estrogen depletion as described above translated to some biological activity. Since YPEL3 expression was demonstrated to induce senescence in MCF7 cells (Kelley *et al*., 2010), senescence induction of MCF7 cells depleted of estrogen was first evaluated.

The increase in YPEL3 gene expression in MCF7 cells after estrogen removal was accompanied by an increase in beta-Galactosidase positive cells, indicative of an increase in senescence. A senescence-associated gene, PAI-1, was also up-regulated in these beta-Galactosidase positive MCF7 cells, further supporting that these cells did in fact undergo senescence. MCF7 cells are p16-null, therefore examining SAHFs in these cells was not completed since SAHF formation has been shown to require functional p16 (Narita *et al*., 2006).

Silencing YPEL3 lead to complete block of senescence induced by estrogen removal in MCF7 cells suggesting that this senescence induction is YPEL3 dependent. However, upon add back of β-estradiol to CSS, there was only a partial rescue of cellular proliferation. Taken with the fact that when YPEL3 is silenced in MCF7 cells there in an increase in cell growth compared to shLacZ expressing control cells, it is possible that reduction of YPEL3 not only blocks senescence but allows for additional cellular proliferation. This data suggests that YPEL3 may be functioning as a tumor suppressor. Classic cellular transformation assays (as mentioned previously) will begin to address this question.

The exact mechanism through which the estrogen receptor down regulates YPEL3 expression has not been determined. Based on the absence of an ERE within the YPEL3 promoter region a direct regulation of YPEL3 expression by the estrogen receptor is unlikely. It has been observed that estrogen depletion of MCF7 cells led to an increase in luciferase activity using a luciferase reporter construct containing a region of the YPEL3 promoter, suggesting that the increase in YPEL3 upon estrogen depletion is, at least in part, due to increased transcription (personal communication Kevin Kelley). There are many known transcription factor binding partners of the estrogen receptor that can be investigated to determine through what indirect mechanism ERα is regulating YPEL3. For example, there are probable GATA1 transcription factor binding sites within the YPEL3 promoter which were uncovered using TFSEARCH (http://molsun1.cbrc.aist.go.jp/research/db/TFSEARCH.html) and ENCODE (http://genome.ucsc.edu/ENCODE/). The latter is a program designed to provide probable transcription factor binding sites as determined by chromatin immunoprecipitation followed by high throughput sequencing.

Reports suggest that bound ERα binds to and negatively regulates GATA1, providing a potential link from ERα to YPEL3 expression (Blobel *et al*., 1995).

Additionally, the increase in YPEL3 expression upon estrogen removal may be explained by the RNA stability of YPEL3 under these conditions. The use of cycloheximide to block translation can be used to begin to assess if RNA stability is the mechanism of increased YPEL3 expression under estrogen deprived conditions. These types of studies will provide the necessary information to begin to determine the exact mechanism through which YPEL3 is regulated by the estrogen receptor and will provide useful information for potential anti-cancer drug design.

The involvement of the estrogen receptor in MAPK signaling and Mdm2 function has been studied using the H-Ras^{G12V} mediated senescence model (Suga *et al*., 2007). It appears that ERα up regulates Mdm2 independent of p53, leading to suppression of p53 transcriptional activity (Phelps *et al*., 2003). This was further examined through use of MEK inhibitors with anti-estrogen (IC1182,780) therapy. When cells were treated with these two agents, the transcriptional activity of ERα was reduced followed by a reduction of Mdm2 levels, which was accompanied by increased p21 and reduced cell growth (Suga *et al*., 2007). The use of a MEK inhibitor, ER antagonist and PI3K inhibitor can be examined for their ability to increase YPEL3 expression leading to senescence. This type of data using a multidrug approach may provide support for designing anti-cancer therapies targeting YPEL3 for patients with ER+, wild-type p53 breast tumors.

Conclusion

This study was designed to identify critical upstream and downstream components of the p53 signaling pathway leading to cellular senescence. Beginning upstream, it was demonstrated that over expression of HdmX can block cellular senescence, which may, at least in part, explain how HdmX is contributing to tumor formation. Futhermore, reducing HdmX in a prostate adenocarcinoma cell line containing wild-type p53, mutant Ras and high levels of HdmX led to tumor cell senescence, suggesting that targeting HdmX in human tumors may be efficacious through induction of tumor cell senescence. Next, YPEL3, as a direct p53 target gene, was shown to function downstream of p53 and be required during H-Ras^{G12V} mediated senescence, making YPEL3 an interesting protein to further investigate for its role in cellular senescence.

The additional finding that expression of YPEL3 is increased in MCF7 cells (ER+, wild-type p53) after estrogen removal, which correlated with the induction of YPEL3-dependent, p53-independent senescence in these cells provided evidence that YPEL3 may be a viable therapeutic target in ER+ breast tumors. Together these three aims provide novel insights into the activation of p53 and one of its target genes that are both involved in senescence induction.

References

Ashcroft, M. and K.H. Vousden. (1999) *Regulation of p53 stability*. Oncogene. 18(53):7637-7643.

Baker, S.J., Fearon, E.R., Nigro, J.M., Hamilton, S.R., Persinger, A.C., Jessup, A.M., vanTuinen, P., Ledbetter, D.H., Barker, D.F., Nakamura, Y., White, R. and B. Vogelstein. (1989) *Chromosome 17 deletions and p53 gene mutations in colorectal carcinomas*. Science. 244(4901):217-221.

Baker, S.J. (2003) *Small unstable apoptotic protein, an apoptosis-associated protein, suppresses proliferation of myeloid cells*. Cancer Research. 63:705-712.

Balint, E. and K.H. Vousden. (2001) *Activation and activities of the p53 tumor suppressor protein*. British Journal of Cancer. 85(12):1813-1823.

Bartel, F., Schulz, J., Bohnke, A., Blumke, K., Kappler, M., Bache, M., Schmidt, H., Wurl, P., Taubert, H. and S. Hauptmann. (2005) *Significance of HDMX-S (or MDM4) mRNA splice variant over expression and HDMX gene amplification on primary soft tissue sarcoma prognosis.* International Journal of Cancer. 117:469-475.

Baygi, M.E., Soheili, Z.S., Schmitz, I., Sameie, S. and W.A. Schulz. (2010) *Snail regulates cell survival and inhibits cellular senescence in human metastatic prostate cancer cell lines*. Cell Biology and Toxicology. Online First™. April 16, 2010. 1573-6822.

Ben-Porath, I. and R.A. Weinberg. (2005) *The signals and pathways activating cellular senescence*. International Journal of Biochemistry and Cell Biology. 37:961-976.

Blobel, G.A., Sieff, C.A. and S.H. Orkin. (1995) *Ligand-dependent repression of the erythroid transcription factor GATA1 by the estrogen receptor*. Molecular and Cellular Biology. 15(6):3147-3153.

Brookes, S., Rowe, J., Ruas, M., Llanos, S., Clark, P.A., Lomax, M., James, M.C., Vatcheva, R., Bates, S., Vousden, K.H., Parry, D., Gruis, N., Smit, N., Bergman, W. and G. Peters. (2002) *INK4a-deficient human diploid fibroblasts are resistant to Ras-induced senescence*. The EMBO Journal. 21(12):2936-2945.

Brown, J.P., Wei, W. and J.M. Sedivy. (1997) *Bypass of senescence after disruption of* $p21^{CIP1/WAF1}$ *gene in normal diploid human fibroblasts*. Science. 277:831-834.

Carnero, A., Hudson, J.D., Price, C.M. and D.H. Beach. (2000) $p16^{INK4a}$ *and* $p19^{ARF}$ *act in overlapping pathways in cellular immortalization*. Nature Cell Biology. 2:148-155.

Cicatiello L., Mutarelli, M., Grober, O.M., Paris, O., Ferraro, L., Ravo, M., Tarallo, R., Luo, S., Schroth, G.P., Seifert, M., Zinser, C., Chiusano, M.L., Trainin, A., De Bortoli, M. and A. Weisz. (2010) *Estrogen receptor {alpha} controls a gene network in luminal-like breast cancer cells comprising multiple transcription factors and microRNAs*. American Journal of Pathology. 176(5):2113-2130.

Coppe, J.P., Patil, C.K., Rodier, F., Sun, Y., Munoz, D.P., Goldstein, J., Nelson, P.S., Desprez, P.Y. and J. Campisi. (2008) *Senescence-associated secretory phenotypes reveal cell-non-autonomous functions of oncogenic RAS and the p53 tumor suppressor*. PLoSBiology. 6(12):2853-2868.

Crawford, L.V., Pim, D.C., Gurney, E.G., Goodfellow, P. and J. Taylor-Papadimitriou. (1981) *Detection of a common feature in several human tumor cell lines-A 53 kDa protein.* Proceedings of the National Academy of Sciences. 78(1):41-45.

Danovi, D., Meulmeester, E., Pasini, D., Migliorini, D., Capra, M., Frenk, R., deGraaf. P., Francoz, S., Gasparini, P., Gobbi, A., Helin, K., Pelicci, P.G., Jochemsen, A.G. and J.C. Marine. (2004) *Amplification of Mdmx (or Mdm4) directly contributes to tumor formation by inhibiting p53 tumor suppressor activity*. Molecular and Cellular Biology. 24(13)5853-5843.

Deb, S.P. (2003) *Cell cycle regulatory functions of the human oncoprotein Mdm2*. Molecular Cancer Research. 1:1009-1016.

Dimri, G.P., Lee, X., Basile, G., Acosta, M., Scott, G., Roskelley, C., Medrano, E.E., Linksens, M., Rubelj, I., Pereira-Smith, O., Peacocke, M. and J. Campisi. (1995) *A biomarker that identifies senescent human cells in culture and in aging skin in vivo.* Proceedings of the National Academy of Sciences. 92:9363-9367.

Dirac, A.M.G. and R. Bernards. (2003) *Reversal of senescence in mouse fibroblasts through lentiviral suppression of p53*. The Journal of Biological Chemistry. 278(14):11731-11734.

Donehower, L.A., Harvey, M., Slagle, B.L., McArthur, M.J., Montgomery, C.A., Burtel, J.S. and A. Bradley. (1992) *Mice deficient for p53 are developmentally normal but susceptible to spontaneous tumors*. Nature. 356(6366):215-221.

Driscoll, M.D., Sathya, G., Muyan, M., Klinge, C.M., Hilf, R. and R.A. Bambara. (1998) *Sequence requirements for estrogen receptor binding to estrogen response elements*. The Journal of Biological Chemistry. 273(45):29321-29330.

Duan, J., Zhang, Z. and T. Tong. (2001) *Senescence delay of human diploid fibroblasts induced by anti-sense p16INK4a expression*. The Journal of Biological Chemistry. 276(51):48325-48331.

Elmore, L.W., Rehder, C.W., Di, X., McChesney, P.A., Jackson-Cook, C.K., Gewirtz, D.A. and S.E. Holt. (2002) *Adriamycin-induced senescence in breast tumor cells involves functional p53 and telomere dysfunction*. The Journal of Biological Chemistry. 277(38):35509-35515.

Farlie, P., Reid, C., Wilcox, S., Peeters, J., Reed, G. and D. Newgreen. (2001) *Ypel1: a novel nuclear protein that induces and epithelial like morphology in fibroblasts*. Genes to Cells. 6:619-629.

Ferbeyre, G., deStanchina, E., Lin, A.W., Querido, E., McCurrach, M.E., Hannon, G.J. and S.W. Lowe. (2002) *Oncogenic ras and p53 cooperate to induce cellular senescence.* Molecular and Cellular Biology. 22(10)3497-3508.

Finlay, C.A., Hinds, P.W. and A.J. Levine. (1989) *The p53 proto-oncogene can act as a suppressor of transformation.* Cell. 57(7):1083-1093.

Francoz, S., Froment, P., Bogaerts, S., DeClercq, S., Maetens, M., Doumont, G., Bellefroid, E. and J.C. Marine. (2006) *Mdm4 and Mdm2 cooperate to inhibit p53 activity in proliferating and quiescent cells in vivo*. Proceedings of the National Academy of Sciences. 103(9):3232-3237.

Fujita, K., Mondal, A.M., Horikawa, I., Nguyen, G.H., Kumamoto, K., Sohn, J.J., Bowman, E.D., Mathe, E.A., Schetter, A.J., Pine, S.R., Ji, H., Vojtesek, B., Bourdon, J.C., Lane, D.P. and C.C. Harris. (2009) *p53 isoforms Δ133p53 and*

p53β are endogenous regulators of replicative cellular senescence. Nature Cell Biology. 11(9):1135-1142.

Funayama, R. and F. Ishikawa. (2007) *Cellular senescence and chromatin structure*. Chromosoma. 116:431-440.

Giglio, S., Mancini, F., Gentiletti, F., Sparaco, G., Felicioni, L., Barassi, F., Martella, C., Prodosmo, A., Iacovelli, S., Buttitta, F., Farsetti, A., Soddu, S., Marchetti, A., Sacchi, A., Pontecorvi, A. and F. Moretti. (2005) *Identification of an aberrantly spliced form of HDMX in human tumors:a new mechanism for HDM2 stabilization.* Cancer Research. 65(21):9687-9693.

Gilkes, D.M., Chen, L. and J. Chen. (2006) *MDMX regulation of p53 response to ribosomal stress.* The EMBO Journal. 25:5614-5625.

Gilkes, D.M., Pan, Y., Coppola, D., Yeatman, T., Reuther, G.W. and J. Chen. (2008) *Regulation of MDMX expression by mitogenic signaling.* Molecular and Cellular Biology. 28(6):1999-2010.

Gjoerup, O., Wu, J., Chandler-Militello, D., Williams, G.L., Zhao, J., Schaffhausen, B., Jat, P.S. and T.M. Roberts. (2007) *Surveillance mechanism linking Bub1 loss to the p53 pathway*. Proceedings of the National Academy of Sciences. 104:8334-8339.

Grossman, S.R. (2001) *p300/CBP/p53 interaction and regulation of the p53 response*. European Journal of Biochemistry. 268:2773-2778.

Hayflick, L. (1965) *The limited in vitro lifetime of human diploid cell strains.* Experimental Cell Research. 37:614-636.

Heminger, K., Markey, M., Mpagi, M. and S.J. Berberich. (2009) *Alterations in gene expression and sensitivity to nongenotoxic stress following HdmX or Hdm2 knockdown in human tumor cells harboring wild-type p53*. Aging. 1(1):89-108.

Hosono, K., Sasaki, T., Minoshima, S. and N. Shimizu. (2004) *Identification and characterization of a novel gene family YPEL in a wide spectrum of eukaryotic species*. Gene. 340:31-43.

Hu, B., Gilkes, D.M., Farooqi, B., Sebti, S.M. and J. Chen. (2006) *MDMX overexpression prevents p53 activation by the MDM2 inhibitor nutlin*. Journal of Biological Chemistry. 281(44):33030-33035.

Hu, B., Gilkes, D.M. and J. Chen. (2007) *Efficient p53 activation and apoptosis by simultaneous disruption of binding to MDM2 and MDMX*. Cancer Research. 67(18):8810-8817.

Huang, B., Deo, D., Xia, M. and L.T. Vassilev. (2009) *Pharmacologic p53 activation blocks cell cycle progression but fails to induce senescence in epithelial cancer cells*. Molecular Cancer Research. 7(9)1497-1509.

Jackson, M.W., Lindstrom, M.S. and S.J. Berberich. (2001) *MdmX binding to ARF affects Mdm2 protein stability and p53 transactivation*. The Journal of Biological Chemistry. 276:25336-25341.

Jemal, A., Siegel, R., Ward, E., Hao, Y., Xu, J. and M.T. Thun. (2009) *Cancer Statistics, 2009*. CA A Journal for Physicians. 59:225-249.

Kelley, K.D., Miller, K.R., Todd, A., Kelley, A.R., Tuttle, R. and S.J. Berberich. (2010) *YPEL3, a p53 regulated gene that induces cellular senescence*. Cancer Research. 70(9):3566-3575.

Kidokoro, T., Tanikawa, C., Furukawa, Y., Katagiri, T., Nakamura, Y. and K. Matsuda. (2008) *CDC20, a potential cancer therapeutic target, is negatively regulated by p53.* Oncogene. 27:1562-2571.

Kortlever, R.M., Higgins, P.J. and R. Bernards. (2006) *Plasminogen activator inhibitor-1 is a critical downstream target of p53 in the induction of replicative senescence.* Nature Cell Biology. 8:878-884.

Kurz, D.J., Decary, S., Hong, Y. and J.D. Erusalimsky. (2000) *Senescence-associated β-galactosidase reflects an increase in lysosomal mass during replicative ageing of human endothelial cells*. Journal of Cell Science. 113:3613-3622.

Lane, D.P. and L.V. Crawford. (1979) *T antigen is bound to a host protein in SV40 – transformed cells*. Nature. 278(5701):261-263.

Laurie, N.A., Donovan, S.L., Shih, C.S., Zhang, J., Mills, N., Fuller, C., Teunisse, A., Lam, S., Ramos, Y., Mohan, A., Johnson, D., Wilson, M., Rodriquez-Galindo, C., Quarto, M., Francoz, S., Mendrysa, S.M., Guy, R.K., Marine, J.C., Jochemsen, A.G. and M.A. Dyer. (2006) *Inactivation of the p53 pathway in retinoblastoma.* Nature. 444:61-66.

Li, C., Lihong, C. and J. Chen. (2002) *DNA damage induces MDMX nuclear translocation by p53-dependent and –independent mechanisms.* Molecular and Cellular Biology. 22(21):7562-7571.

Linzer D.L. and A.J. Levine. (1979) *Characterization of a 54K Dalton cellular SV40 tumor antigen present in SV40 transformed cells and uninfected embryonal carcinoma cells*. Cell. 17(1):43-52.

Liu, W., Konduri, S.D., Bansal, S., Nayak, B.K., Rajasekaran, S.A., Karuppayil, S.M., Rajasekaran, A.K. and G.M. Das. (2006) *Estrogen receptor-α binds p53 tumor suppressor protein directly and represses its function*. The Journal of Biological Chemistry. 281(15):9837-9840.

Liu, W., Ip, M.M., Podgorsak, M.B. and G.M. Das. (2008) *Disruption of estrogen receptor α-p53 interaction in breast tumors: a novel mechanism underlying the anti-tumor effect of radiation therapy*. Breast Cancer Research and Treatment. 115:43-50.

Lopez-Pajares, V., Kim, M.M. and Z. Yuan. (2008) *Phosphorylation of MDMX mediated by Akt leads to stabilization and induces 14-3-3 binding*. The Journal of Biological Chemistry. 283(20):13707-13713.

Marine, J.C.W. and A.G. Jochemsen. (2005) *Mdmx as an essential regulator of p53 activity.* Biochemical and Biophysical Research Communications. 331(3):750-760.

Marine, J.C.W., Dyer, M.A. and A.G. Jochemsen. (2007) *MDMX: from bench to bedside.* Journal of Cell Science. 120:371-378.

Masiakowski, P., Breathnach, R., Block, J., Gannon, F., Krust, A. and P. Chambon. (1982) *Cloning of c-DNA sequences of hormone-regulated genes from the MCF-7 human breast cancer cell line*. Nucleic Acids Research. 10(24):7895-7903.

Mason, D.X., Jackson, T.J. and A.W. Lin. (2004) *Molecular signature of oncogenic ras-induced senescence*. Oncogene. 23:9238-9246.

Matijasevic, Z., Steinman, H.A., Hoover, K. and S.N. Jones. (2007) *MdmX promotes bipolar mitosis to suppress transformation and tumorigenesis in p53-deficient cells and mice.* Molecular and Cellular Biology. 28:1265-1273.

Matthews, J. and J. Gustafsson. (2003) *Estrogen signaling: a subtle balance between ERα and ERβ*. Molecular Interventions. 3(5):281-292.

Menendez, D., Inga, A., Snipe, J., Krysiak, O., Schonfelder, G. and M.A. Resnick. (2007) *A single-nucleotide polymorphism in a half-binding site creates p53 and estrogen receptor control of vascular endothelial growth factor receptor 1*. Molecular and Cellular Biology. 27(7):2590-2600.

Migliorini, D., Danovi, D., Colombo, E., Carbone, R., Pelicci, P.G. and J.C. Marine. (2002) *HdmX recruitment into the nucleus by Hdm2 is essential for its ability to regulate p53 stability and transactivation.* The Journal of Biological Chemistry. 277(9):7318-7323.

Momand, J., Wu, H.H. and G. Dasgupta. (2000) *MDM2 – master regulator of the p53 tumor suppressor protein.* Gene. 242:15-29.

Musgrove, E.A., Lilischkis, R., Cornish, A.L., Lee, C.S., Setlur, V., Seshadri, R. and R.L. Sutherland. (1995) *Expression of the cyclin-dependent kinase inhibitors p16INK4, p15INK4B, and p21WAF1/CIP1 in human breast cancer*. International Journal of Cancer. 63(4):584-591.

Narita, M., Nunez, S., Heard, E., Narita, M., Lin, A.W., Hearn, S.A., Spector, D.L., Hannon, G.J. and S.W. Lowe. (2003) *Rb-mediated heterochromatin formation and silencing of E2F target genes during cellular senescence*. Cell. 113:703-716.

Narita, M., Narita, M., Krizhanovsky, V., Nunez, S., Chicas, A., Hearn, S.A., Myers, M.P. and S.W. Lowe. (2006) *A novel role for High-Mobility Group A proteins in cellular senescence and heterochromatin formation*. Cell. 126:503-514.

Obajimi, O., Keen, J.C. and P.W. Melera. (2009) *Inhibition of de novo purine synthesis in human prostate cells results in ATP depletion, AMPK activation and induces senescence*. Prostate. 69:1206-1221.

Oliner, J.D., Kinzler, K.W., Meltzer, P.S., George, D.L. and B. Vogelstein. (1992) *Amplification of a gene encoding a p53-associated protein in human sarcomas*. Letters to Nature. 358:80-83.

Osborne, C.K. (1998) *Steroid hormone receptors in breast cancer management*. Breast Cancer Research and Treatment. 51:227-238.

Osborne, C.K. (1998) *Tamoxifen in the treatment of breast cancer*. New England Journal of Medicine. 339(22):1609-1618.

Pantoja, C. and M. Serrano. (1999) *Murine fibroblasts lacking p21 undergo senescence and are resistant to transformation by oncogenic ras*. Oncogene. 18:4974-4982.

Parrinello, S., Coppe, J.P., Krtolica, A. and J. Campisi. (2005) *Stromal-epithelial interactions in aging and cancer: senescent fibroblasts alter epithelial cell differentiation*. Journal of Cell Science. 118:485-496.

Phelps, M., Darley, M., Primrose, J.N. and J.P. Blaydes. (2003) *p53-independent activation of the hdm2-P2 promoter through multiple transcription factor response elements results in elevated hdm2 expression in estrogen receptor α-positive breast cancer cells*. Cancer Research. 63:2616-2623.

Planas-Silva, M.D. and R.A. Weinberg. (1997) *Estrogen-dependent cyclin E-cdk2 activation through p21 redistribution*. Molecular and Cellular Biology. 17(7):4059-4069.

Pomerantz, J., Schreiber-Agus, N., Liegeois, N.J., Silverman, A., Alland, L., Chin, L., Potes, J., Chen, K., Orlow, I., Lee, H.W., Cordon-Cardo, C. and R.A. DePinho. (1998) *The Ink4a tumor suppressor gene product, p19Arf, interacts with MDM2 and neutralizes MDM2's inhibition of p53*. Cell. 92(6):713-723.

Prives, C. and J. Manley. (2001) *Why is p53 acetylated?* Cell. 107:815-818.

Ramos, Y.F., Stad, R., Attema, J., Peltenburg, L.T., van der Eb, A.J. and A.G. Jochemsen. (2001) *Aberrant expression of HDMX proteins in tumor cells correlates with wild-type p53.* Cancer Research. 61:1839-1842.

Reed, D., Shen, Y., Shelat, A.A., Arnold, L.A., Ferreira, A.M., Zhu, F., Mills, N., Smithson, D.C., Regni, C.A., Bashford, D., Cicero, S.A., Schulman, B.A., Jochemsen, A.G., Guy, R.K. and M.A. Dyer. (2010) *Identification and characterization of the first small-molecule Inhibitor of MdmX*. The Journal of Biological Chemistry. 285(14)10786-10796.

Ring A. and M. Dowsett. (2004) *Mechanisms of tamoxifen resistance*. Endocrine Related Cancer. 11(4):643-658.

Roninson, I.B. (2002) *Oncogenic functions of tumour suppressor p21$^{Waf1/Cip1/Sdi1}$; association with cell senescence and tumour-promoting activities of stromal fibroblasts.* Cancer Letters. 179:1-14.

Roninson, I.B. (2003) *Tumor cell senescence in cancer treatment*. Cancer Research. 63:2705-2715.

Roxstrom-Lindquist K. and I. Faye. (2001) *The Drosophila gene Yipee reveals a novel family of putative zinc binding proteins highly conserved among eukaryotes*. Insect Molecular Biology. 10(1):77-86.

Russo, J., Fernandez, S.V., Russo, P.A., Fernbaugh, R., Sheriff, F.S., Lareef, H.M., Gerber, J. and I.H. Russo. (2006) *17-Beta-estradiol induces transformation and tumorigenesis in human breast epithelial cells*. The Federation of American Societies for Experimental Biology. 20:1622-1634.

Saporita, A.J., Maggi, L.B., Apicelli, A.J. and J.D. Weber. (2007) *Therapeutic targets in the ARF tumor suppressor pathway*. Current Medicinal Chemistry. 14:1815-1827.

Saxena, N., Lahiri, S.S., Hambarde, S. and R.P. Tripathi. (2008) *RAS: target for cancer therapy*. Cancer Investigation. 26:948-955.

Schwarze, S., Fu, V.X., Desotelle, J.A., Kenowski, M.L. and D.F. Jarrard. (2005) *The identification of senescence-specific genes during the induction of senescence in prostate cancer cells*. Neoplasia. 7(9):816-823.

Serrano, M., Lin, A.W., McCurrach, M.E., Beach, D. and S.W. Lowe. (1997) *Oncogenic ras provokes premature cell senescence associated with accumulation of p53 and* $p16^{INK4a}$. Cell. 88:593-602.

Sharp, D.A., Kratowicz, S.A., Sank, M.J. and D.L. George. (1999) *Stabilization of the MDM2 oncoprotein by interaction with the structurally related MDMX protein*. The Journal of Biological Chemistry. 274(53):38189-38196.

Shay, J.W. and I. B. Roninson. (2004) *Hallmarks of senescence in carcinogenesis and cancer therapy*. Oncogene. 23:2919-2933.

Shvarts, A., Steegenga, W.T., Riteco, N., van Laar, T., Dekker, P., Bazuine, M., van Ham, R.C., van der Houven van Oordt, W., Hateboer, G., van der Eb, A.J. and A.G. Jochemsen. (1996) *MDMX: a novel p53-binding protein with some functional properties of MDM2*. The EMBO Journal. 15(19):5349-5357.

Smogorzewska, A. and T. de Lange. (2002) *Different telomere damage signaling pathways in human and mouse cells*. The EMBO Journal. 21(16):4338-4348.

Suga, S., Kato, K., Ohgami, T., Yamayoshi, A., Adachi, S., Asanoma, K., Yamaguchi, S., Arima, T., Kinoshita, K. and N. Wake. (2007) *An inhibitory effect on cell proliferation by blockage of the MAPK/estrogen receptor/MDM2 signal pathway in gynecologic cancer*. Gynecologic Oncology. 105:341-350.

Tanimura, S., Ohtsuka, S., Mitsui, K., Shirouzu, K., Yoshimura, A. and M. Ohtsubo. (1999) *MDM2 interacts with MDMX through their RING finger domains*. FEBS Letters. 447:5-9.

Tiemann, K. and J.J. Rossi. (2009) *RNAi-based therapeutics – current status, challenges and prospects*. EMBO Molecular Medicine. 1:142-151.

Torre, E.A. and R.A. Fulco. (1995) *pS2 protein and breast cancer*. Minerva Ginecologica. 47(12):553-556.

Troester, M.A., Herschkowitz, J.I., Oh, D.S., He, X., Hoadley, K.A., Barbier, C.S. and C.M. Perou. (2006) *Gene expression patterns associated with p53 status in breast cancer*. Biomed Central Cancer. 6(276):1-13.

Vousden, K.H. and X. Lu. (2002) *Live or let die: the cell's response to p53*. Nature Reviews. 2:594-604.

Wade, M. and G.M. Wahl. (2009) *Targeting Mdm2 and Mdmx in cancer therapy: better living through medicinal chemistry*. Molecular Cancer Research. 7(1):1-10.

Wajapeyee, N., Serra, R.W., Zhu, X., Mahalingam, M. and M.R. Green. (2008) *Oncogenic BRAF induces senescence and apoptosis through pathways mediated by the secreted protein IGFBP7*. Cell. 132:363-374.

Walker, K. and A. Levine. (1996) *Identification of a novel p53 functional domain that is necessary for efficient growth suppression.* Proceedings of the National Academy of Sciences. 93:15335-15340.

Wang, X., Arooz, T., Siu, W.Y., Chiu, C.H., Lau, A., Yamashita, K. and R.Y. Poon. (2001) *MDM2 and MDMX can interact differently with ARF and members of the p53 family*. FEBS Letters. 490:202-208.

Wei, W., Hemmer, R.M. and J.M. Sedivy. (2001) *Role of $p14^{ARF}$ in replicative and induced senescence of human fibroblasts*. Molecular and Cellular Biology. 21(20):6748-6757.

Wei, W., Herbig, U., Wei, S., Dutriaux, A. and J.M. Sedivy. (2003) *Loss of retinoblastoma but not p16 function allows bypass of replicative senescence in human fibroblasts*. EMBO Reports. 4(11):1061-1066.

Weinberg, R.A. The Biology of Cancer. New York: Garland Science, Taylor and Francis Group, LLC, 2007.

Westley, B., May, F.E., Brown, A.M., Krust, A., Chambon, P., Lippman, M.E. and H. Rochefort. (1984) *Effects of antiestrogens on the estrogen-regulated pS2 RNA and the 52- and 160-kilodalton proteins in MCF7 cells and two tamoxifen-resistant sublines*. The Journal of Biological Chemistry. 259(16)10030-10035.

Xia, M., Knezevic, D., Trovar, C., Huang, B., Heimbrook, D.C. and L.T. Vassilev. (2008) *Elevated MDM2 boosts the apoptotic activity of p53-MDM2 binding inhibitors by facilitating MDMX degradation*. Cell Cycle. 7(11):1604-1612.

Xue, W., Zender, L., Miething, C., Dickins, R.A., Hernando, E., Krihanovsky, V., Cordon-Cardo, C. and S.W. Lowe. (2007) *Senescence and tumour clearance is triggered by p53 restoration in murine liver carcinomas*. Nature Letters. 445:656-660.

Young, A.R., Narita, M., Ferreira, M., Kirschner, K., Sadaie, M., Darot, J.F., Tavare, S., Arakawa, S., Shimizu, S., Watt, F.M. and M. Narita. (2009) *Autophagy mediates the mitotic senescence transition*. Genes and Development. 23:798-803.